INTERNATIONAL STANDARD

ISO 17282

First edition
2004-06-01

Plastics — Guide to the acquisition and presentation of design data

Plastiques — Lignes directrices pour l'acquisition et la présentation de caractéristiques de conception

Reference number
ISO 17282:2004(E)

ISO copyright office
Case postale 56 • CH-1211 Geneva 20
Tel. + 41 22 749 01 11
Fax + 41 22 749 09 47
E-mail copyright@iso.org
Web www.iso.org

Published in Switzerland

Contents

Page

Foreword ... iv

Introduction ... v

1 Scope ... 1

2 Normative references ... 1

3 Symbols ... 3
3.1 Test variables ... 3
3.2 Material properties for stress analysis (see Tables 2 and 3) ... 3
3.3 Failure properties (see Table 4) ... 4
3.4 Material properties for processing simulation (see Tables 3, 4 and 5) ... 5

4 Data needed for design ... 6
4.1 General ... 6
4.2 Design for thermomechanical performance ... 6
4.2.1 The design process ... 6
4.2.2 Design data for thermomechanical performance ... 7
4.3 Design for processing analysis ... 10
4.3.1 Processing simulation ... 10
4.3.2 Data for simulation of injection moulding ... 10
4.3.3 Data for simulation of extrusion ... 12
4.3.4 Data for simulation of blow moulding, blown film extrusion and thermoforming ... 12

5 Determination of design data ... 13
5.1 General ... 13
5.2 Data acquisition for design for mechanical performance ... 13
5.3 Data acquisition for design for processing ... 14

Annex A (informative) **Illustrations of the application of finite element analyses to plastics components** ... 19

Annex B (informative) **Application of processing simulation analysis for plastics** ... 48

Foreword

ISO (the International Organization for Standardization) is a worldwide federation of national standards bodies (ISO member bodies). The work of preparing International Standards is normally carried out through ISO technical committees. Each member body interested in a subject for which a technical committee has been established has the right to be represented on that committee. International organizations, governmental and non-governmental, in liaison with ISO, also take part in the work. ISO collaborates closely with the International Electrotechnical Commission (IEC) on all matters of electrotechnical standardization.

International Standards are drafted in accordance with the rules given in the ISO/IEC Directives, Part 2.

The main task of technical committees is to prepare International Standards. Draft International Standards adopted by the technical committees are circulated to the member bodies for voting. Publication as an International Standard requires approval by at least 75 % of the member bodies casting a vote.

Attention is drawn to the possibility that some of the elements of this document may be the subject of patent rights. ISO shall not be held responsible for identifying any or all such patent rights.

ISO 17282 was prepared by Technical Committee ISO/TC 61, *Plastics*, Subcommittee SC 2, *Mechanical properties*.

Introduction

Plastics and composites are increasingly being used in load-bearing applications where they compete with traditional materials such as steels and aluminium. In these applications, it is important to achieve a confident knowledge of the safe operating limits of the component through competent design. Computer methods for design are available, and are continually being improved, that enable predictions to be made of the performance of plastics under a variety of situations. These situations include mechanical performance under service loads and environments as well as a flow of the polymer melt during the manufacture of a component.

In order to design effectively with plastics in load-bearing applications, comprehensive data are generally needed which take into account the effects of time, temperature, rate and environment on properties. A number of International Standards have been developed that specify how certain data for plastics should be measured and presented. These are ISO 10350-1 and ISO 10350-2, and ISO 11403-1, ISO 11403-2 and ISO 11403-3.

The purpose of these standards is to enable comparable data to be measured on different materials from different sources to aid the process of materials selection. A substantial quantity of data is specified by these standards and, although not the primary purpose of the standards, some of these data are suitable for design. However, additional or alternative data will also be needed for many applications.

The purpose of this guide is to augment existing data presentation standards by identifying data that are needed specifically for design with plastics. The selection of these data is guided by the requirements of available computer methods for design. Preferred test methods, test specimens and test conditions are recommended in section 5 for determining these data. For some properties, ISO test methods or specimens are not yet available. Reference is then made in the Notes to Tables 6 and 7 to suitable procedures for data acquisition that may become standardised at a later stage.

It is intended that this guide assist the development of databases that will interface with computer methods for design so that the property data required by these methods can be readily accessed. For certain properties, some analysis and interpretation of data is needed in order to present information in the form required by the design analysis. Some procedures for data analysis are described in the annexes.

Plastics — Guide to the acquisition and presentation of design data

1 Scope

This International Standard gives guidelines for the acquisition and presentation of data that can be used for design with plastics. Emphasis is given to the acquisition of data needed by computerised methods for design. It includes data needed for the analysis of the flow of polymer melts during the manufacture of a component as well as data needed for the prediction of mechanical performance of the component in service. The data requirements cover design with unfilled plastics as well as filled, short-fibre reinforced and continuous-fibre reinforced materials.

2 Normative references

The following referenced documents are indispensable for the application of this document. For dated references, only the edition cited applies. For undated references, the latest edition of the referenced document (including any amendments) applies.

ISO 294-3, *Plastics — Injection moulding of test specimens of thermoplastics materials — Part 3: Small plates*

ISO 294-5, *Plastics — Injection moulding of test specimens of thermoplastics materials — Part 5: Preparation of standard specimens for investigating anisotropy*

ISO 527-2, *Plastics — Determination of tensile properties — Part 2: Test conditions for moulding and extrusion plastics*

ISO 527-4, *Plastics — Determination of tensile properties — Part 4: Test conditions for isotropic and orthotropic fibre-reinforced plastic composites*

ISO 527-5, *Plastics — Determination of tensile properties — Part 5: Test conditions for unidirectional fibre-reinforced plastic composites*

ISO 899-1, *Plastics — Determination of creep behaviour — Part 1: Tensile creep*

ISO 1183, *Plastics — Methods for determining the density and relative density of non-cellular plastics*

ISO 2577, *Plastics — Thermosetting moulding materials — Determination of shrinkage*

ISO 3167, *Plastics — Multipurpose test specimens*

ISO 6252, *Plastics — Determination of environmental stress cracking (ESC) — Constant-tensile-stress method*

ISO 6603-2, *Plastics — Determination of puncture impact behaviour of rigid plastics — Part 2: Instrumented impact test*

ISO 6721-2, *Plastics — Determination of dynamic mechanical properties — Part 2: Torsion-pendulum method*

ISO 6721-3, *Plastics — Determination of dynamic mechanical properties — Part 3: Flexural vibration — Resonance-curve method*

ISO 6721-4, *Plastics — Determination of dynamic mechanical properties — Part 4: Tensile vibration — Non-resonance method*

ISO 6721-5, *Plastics — Determination of dynamic mechanical properties — Part 5: Flexural vibration — Non-resonance method*

ISO 6721-7, *Plastics — Determination of dynamic mechanical properties — Part 7: Torsional vibration — Non-resonance method*

ISO 6721-8, *Plastics — Determination of dynamic mechanical properties — Part 8: Longitudinal and shear vibration — Wave propagation method*

ISO 6721-10, *Plastics — Determination of dynamic mechanical properties — Part 10: Complex shear viscosity using a parallel-plate oscillatory rheometer*

ISO 10350-1, *Plastics — Acquisition and presentation of comparable single-point data — Part 1: Moulding materials*

ISO 11357-2, *Plastics — Differential scanning calorimetry (DSC) — Part 2: Determination of glass transition temperature*

ISO 11357-3, *Plastics — Differential scanning calorimetry (DSC) — Part 3: Determination of temperature and enthalpy of melting and crystallization*

ISO 11357-4[1)], *Plastics — Differential scanning calorimetry (DSC) — Part 4: Determination of specific heat capacity*

ISO 11357-5, *Plastics — Differential scanning calorimetry (DSC) — Part 5: Determination of characteristic reaction-curve temperatures and times, enthalpy of reaction and degrees of conversion*

ISO 11357-7, *Plastics — Differential scanning calorimetry (DSC) — Part 7: Determination of crystallization kinetics*

ISO 11359-2, *Plastics — Thermomechanical analysis (TMA) — Part 2: Determination of coefficient of linear thermal expansion and glass transition temperature*

ISO 11403-1, *Plastics — Acquisition and presentation of comparable multipoint data — Part 1: Mechanical properties*

ISO 11403-2, *Plastics — Acquisition and presentation of comparable multipoint data — Part 2: Thermal and processing properties*

ISO 11443, *Plastics — Determination of the fluidity of plastics using capillary and slit-die rheometers*

ISO 15310, *Fibre-reinforced plastic composites — Determination of the in-plane shear modulus by the plate twist method*

ISO 17744, *Plastics — Determination of specific volume as a function of temperature and pressure (pVT diagram) — Piston apparatus method*

---

1) To be published.

3 Symbols

3.1 Test variables

ε tensile strain

NOTE Use of the true strain $\log_e (1 + \varepsilon)$ in place of the engineering strain is necessary when engineering strain values exceed about 0,1. Below a strain of 0,1, there is no significant difference between these quantities.

$\dot{\varepsilon}$ tensile strain rate

ε^p plastic component of the tensile strain

NOTE This is used in elastic–plastic models for describing non-linear behaviour.

γ shear strain

$\dot{\gamma}$ shear strain rate

γ^p plastic component of the shear strain

t time

σ stress

T temperature

f frequency

ch chemical environment

N number of cycles to failure in a fatigue test

R ratio of minimum to maximum stresses in a fatigue test

$\dot{T}$ rate of change of temperature

p pressure

p_{CH} cavity pressure at hold

t_H hold time

h specimen thickness

v_s slip velocity

3.2 Material properties for stress analysis (see Tables 2 and 3)

E tensile modulus obtained from a test at constant strain rate

E_p, E_n tensile moduli along and transverse to, respectively, the direction of preferred fibre or molecular orientation in a transversely isotropic material

G_p shear modulus of a transversely isotropic material for stress application in the direction of preferred orientation

D tensile creep compliance

E_R tensile stress relaxation modulus

D_p, D_n tensile creep compliances along and transverse to, respectively, the direction of preferred orientation in a transversely isotropic material

E', E'' tensile storage and loss moduli, respectively

G', G'' shear storage and loss moduli, respectively

σ_T true tensile yield stress (see Note 4 to Table 12)

λ hydrostatic stress sensitivity parameter (see Note 6 to Table 12)

σ_{Tp}, σ_{Tn} tensile yield stresses for loading along and transverse to, respectively, the direction of preferred orientation in a transversely isotropic material (see Notes 4 and 9 to Table 12)

σ_{Sp}, σ_{Sn} shear yield stresses for loading along and transverse to, respectively, the direction of preferred orientation in a transversely isotropic material (see Note 9 to Table 12)

ν Poisson's ratio

ν^e elastic component of the Poisson's ratio

ν^p plastic component of the Poisson's ratio equal to minus the ratio of the plastic component of the lateral strain to the plastic component of the axial strain in a specimen under a tensile stress (see Note 5 to Table 12)

ν_{pn} Poisson's ratio for an anisotropic material determined with the uniaxial stress applied along the direction of preferred orientation

ψ flow parameter

α coefficient of linear thermal expansion

α_p, α_n coefficients of linear thermal expansion parallel and normal to the direction of preferred orientation in a transversely isotropic material

c_p specific heat

3.3 Failure properties (see Table 4)

σ_u tensile strength obtained from a test at constant specimen deformation rate

σ_{up}, σ_{un} tensile strengths for loading along and transverse to, respectively, the direction of preferred orientation in a transversely isotropic material

ε_u strain at break obtained from a tensile test at constant specimen deformation rate

ε_{up}, ε_{un} strains at break for loading along and transverse to, respectively, the direction of preferred orientation in a transversely isotropic material

σ_c tensile creep rupture strength

σ_{cp}, σ_{cn} creep rupture strengths for loading along and transverse to, respectively, the direction of preferred orientation in a transversely isotropic material

σ_f tensile fatigue strength

σ_{fp}, σ_{fn} tensile fatigue strengths for loading along and transverse to, respectively, the direction of preferred orientation in a transversely isotropic material

3.4 Material properties for processing simulation (see Tables 3, 4 and 5)

η melt viscosity

η_{eu} uniaxial extensional viscosity

η_{eb} biaxial extensional viscosity

$\eta_{reactive}$ viscosity of the reactive system

N_1 first normal stress difference

ρ_B bulk density

ρ_m melt density

ρ_s density of the solid

$\rho_{reacted}$ density of reacted system

k thermal conductivity

k_m thermal conductivity of the polymer melt

c_p specific heat

c_{pm} specific heat of the polymer melt

T_s solidification temperature, a reference temperature defined by the mould filling simulation software

T_{ej} ejection temperature, a reference temperature defined by the mould filling simulation software

v specific volume

ΔH_r heat of reaction

t_{ind} isothermal induction time

α_{gel} gelation conversion

$\dot{R}$ reaction rate

μ_b, μ_s dynamic coefficients of friction between plastic and metal used for the barrel or screw respectively

T_m melting temperature

T_g glass transition temperature

T_c crystallisation temperature

ΔH_f enthalpy of melting

ΔH_c enthalpy of crystallization

X degree of crystallinity

$\dot{X}$ rate of crystallization

S_{Mp} moulding shrinkage parallel to the direction of preferred orientation

S_{Mn} moulding shrinkage normal to the direction of preferred orientation

ν_{pn} Poisson's ratio for a transversely isotropic material determined with the uniaxial stress applied along the direction of preferred orientation

ν_{np} Poisson's ratio for a transversely isotropic material determined with the applied stress along a direction normal to the direction of preferred orientation and the lateral strain measured in the preferred orientation direction

G_p shear modulus of a transversely isotropic material for stress application in the direction of preferred orientation

α_p coefficient of linear thermal expansion parallel to the direction of preferred orientation in an anisotropic material

α_n coefficient of linear thermal expansion normal to the direction of preferred orientation in an anisotropic material

4 Data needed for design

4.1 General

The design data identified here are grouped under two headings:

— Data for analysis of thermomechanical performance (section 4.2)

— Data for processing analysis (section 4.3)

4.2 Design for thermomechanical performance

4.2.1 The design process

The process of design for the mechanical performance of a component involves two operations. The first is an analysis of the stress and strain distributions in the component under service load. The second is a comparison of the maximum levels of stress, strain or displacement predicted by the analysis with maximum allowable values based on failure criteria for the material or operating conditions of the component. These operations are then repeated in order to select component dimensions and geometry whilst ensuring that safe limits are not exceeded. The data requirements for these two operations are different.

The data requirements for stress analysis are determined by the constitutive law that relates stress and strain under the appropriate service loading conditions. Choice of a valid constitutive relationship will depend upon the following factors.

— Mechanical behaviour, whether the material is isotropic or anisotropic or shows glassy or rubber-like behaviour.

— The level of induced strain. If this is small, then linear viscoelastic or linear elastic behaviour may be considered but, at higher strains, relationships between stress and strain will be non-linear.

— The history of the applied load or displacement and the temperature. Since plastics are viscoelastic, properties depend on time, frequency and strain rate and so their response to short-term loads such as impact will be very different from that under sustained load.

A finite element analysis (FEA) is a versatile method for calculating stress, strain and temperature distributions in a component of complex geometry. For this reason, the data requirements identified here for performing a stress analysis have been guided by available materials models that are suitable for plastics. An accurate calculation relies on the use of a materials model for the analysis which employs a realistic constitutive relationship.

The satisfactory operating limits of a component may be specific to the component or the plastics material from which it is made. Safe operating limits for the material are generally expressed in terms of ultimate values of stress or strain and will depend on many factors such as the temperature, the humidity, processing conditions, the presence of an aggressive environment and the history of the applied load. Where failure is caused by crack growth, additional property data may be needed.

4.2.2 Design data for thermomechanical performance

Data required for design for thermomechanical performance consist of data for carrying out a stress analysis and data for estimating material failure. In principle, these data requirements depend on the detailed materials characteristics exhibited by the material, and on the service conditions relevant to the application. However, in practice, the designer may adopt various simplifications by approximating materials behaviour or service conditions in order to make the design analysis technically tractable and financially viable. This influences data requirements and the practical use of data.

From the designer's point of view, the simplest form of materials behaviour is that of an isotropic, linear, temperature-insensitive, elastic material. However, as stated in section 4.2.1, plastics may exhibit aspects of anisotropy, nonlinearly, temperature-dependence, viscoelasticity or plasticity. Where a particular aspect is relevant to a design problem, the designer may decide to avoid a more complex analysis by assuming a simpler form of behaviour and compensate for this by use of "effective" material properties. Examples include use of a secant or tangent modulus to represent nonlinearity in a linear analysis, use of a long-time creep modulus to represent viscoelasticity in an elastic analysis, and use of "average" or "representative" property values to replace anisotropy and temperature-sensitivity. However, although a simpler (approximate) form of representation may be used, data for the more complex form of behaviour will generally be required in order to select appropriate "effective" properties.

Definition of the design problem involves specification of component geometry (shape, size, etc.) and service conditions (e.g. loads and other constraints). Although FEA packages can handle complex circumstances, the designer may idealise component geometry and may approximate service conditions in order to simplify the design calculations (e.g. by creating a "statically determinate" situation for which stresses and strains can be calculated separately, only the latter calculation requiring material properties). Similarly, the designer may use an approximate design calculation (e.g. assuming "pseudo-elasticity"). These idealisations and assumptions introduce inaccuracies into the design predictions which are not attributable to the quality of the design data, although appropriate data selection is required.

A crucial aspect of design analysis is the selection of suitable materials models. This selection determines consequent requirements for materials design data, and depends, in particular, on the nature of the service loads, for example:

— sustained loading, involving effects such as creep or stress relaxation, for which time under load is the important parameter;

— cyclic loading, for example in damped vibrations, for which frequency is the important parameter;

— high-rate loading, for example due to impact, for which strain rate is the important parameter.

Table 1 — Typical service conditions, materials behaviour and model types

Service conditions	Crucial parameter	Relevant types of materials behaviour	Model type(s) (see below)
Simpler conditions	—	Elastic	A, B
		Elastic–plastic	C
Sustained loading	Time	Viscoelastic or viscoplastic	C1, D1, E1
Cyclic loading	Frequency		C2, D2, E2
High-rate loading	Strain rate		C3, D3, E3

Model type:

a) Linear elasticity is the simplest and most commonly used materials model, at least for a first analysis.

b) A hypoelastic model enables approximate solutions to be obtained under strain levels where behaviour is non-linear. Hyperelastic models are available for elastomeric materials and are not considered in this International Standard.

c) Elastic–plastic models for metals are available in most FEA packages and are able to handle non-linear and three-dimensional stress conditions. Those based on von Mises yielding may have restricted suitability for plastics, and a more general form of the yield criterion with sensitivity to hydrostatic stress (the linear Drucker–Prager model) is considered here. Some versions of elastic–plastic models combine the effects of elasticity, plasticity and also time, frequency or rate. These latter types of model (C1, C2 and C3) are indicated in this table, but only C3 is considered in this International Standard.

d) Linear viscoelasticity is limited to small-strain behaviour, but data can be used in the three different forms (D1, D2, D3) depending on whether time, frequency or rate is the crucial service parameter.

e) Non-linear viscoelasticity models for general service conditions are not available in a useable form, but models exist for use under special conditions. These include a creep form (E1) based on isochronous curves, a finite-linear form (E2) for large amplitude vibrations and a rate-dependent form (E3): the last two are not discussed further in this International Standard.

As already noted, the stress analysis will also need to consider isotropic or anisotropic properties, linear or non-linear behaviour and the effects of temperature. It is therefore evident that there are many sets of conditions under which materials properties may be needed in principle, and it is necessary to focus on the most important cases. This is discussed now with reference to the model types indicated in Table 1.

Further consideration of these types leads to identification of the data required for design for thermomechanical performance. These data are summarised in Table 2 for isotropic materials. Anisotropic materials require additional data that describe the variation of properties with direction in the material. The simplest situation arises with the loading of parts in the form of a plate or panel where stresses are confined to a plane and stresses through the thickness direction are neglected. This is assumed in Table 3. Criteria for determining when material rupture will take place under multiaxial stress states and arbitrary loading histories have not been established for plastics. Ultimate values obtained from tensile tests under specific loading histories are indicated in Table 4. The symbols used in these tables are explained in Section 3.

When material behaviour is actually isotropic linear elastic, the data shown in Table 2 for model A are all that is required. When the behaviour is more complex, but an isotropic linear elastic analysis is performed, *data relevant to the other models may be needed in order to select appropriate "effective" properties.* For example, data for models D and E give effective properties to represent viscoelastic effects, data for models C and E can be used to select effective properties to handle nonlinearly, and data from Table 3 can be used to select effective properties to take account of the effects of anisotropy. When the design analysis takes these factors into account in full, then data for models C, D and E, and from Table 3, are required in their own right (but see Note to Table 3).

Table 2 — Data required for stress analysis (isotropic material)

Behaviour	Model type	Properties	Variable(s)
Linear elastic	A	E, ν	T
Non-linear elastic	B	E, ν,	T
		σ	ε, T
Non-linear (elastic–plastic)	C	E, ν^{e}	T
		σ_T	ε^{p}, T
		λ, ν^{p}, ψ	ε^{p}, T
Linear viscoelastic	D1	D, E_R, ν	t, T
	D2	E', E'' (or G', G''), ν	f, T
	D3	ρ	T
		E, ν	$\dot{\varepsilon}$, T
Non-linear viscoelastic	E1	D, ν	t, σ, T
		E_R, ν	t, ε, T
Rate-dependent, elastic–plastic	C3	E, ν^{e}	$\dot{\varepsilon}$, T
		σ_T	ε^{p}, $\dot{\varepsilon}^{p}$, T
		λ, ν^{p}, ψ	ε^{p}, $\dot{\varepsilon}^{p}$, T

Table 3 — Data required for stress analysis (anisotropic material)

Behaviour	Model Type	Properties	Variables
Linear elastic	A	E_p, E_n, ν_{pn}, G_p	T
Non-linear (Elastic–plastic)	C	E_p, E_n, ν_{pn}, G_p	T
		ε_{Tp}, σ_{Tn}	ε^{p}, T
		σ_{Sp}, σ_{Sn}	ε^{p}, T
Linear Viscoelastic	D1	D_p, D_n	t, T
Non-linear Viscoelastic	E1	D_p, D_n	t, σ, T
Rate-dependent, Elastic–plastic	C3	E_p, E_n, ν_{pn}, G_p	$\dot{\varepsilon}$, T
		σ_{Tp}, σ_{Tn}	ε^{p}, $\dot{\varepsilon}^{p}$, T
		σ_{Sp}, σ_{Sn}	ε^{p}, $\dot{\gamma}^{p}$, T
NOTE The above models and data requirements for anisotropic materials are clearly more complicated than those for isotropic materials and, except for the linear elastic case, are likely to be used very rarely except for the purpose of selecting effective properties.			

Under certain circumstances, property data will be required additional to those identified in Tables 2 and 3. If the analysis involves changes in temperature during loading, then the thermal expansion coefficient α (α_p and α_n for anisotropic materials) will be needed. If the loading generates high accelerations such that inertial forces are significant, then the density ρ of the material must be known. In situations where it is necessary to predict the effects of internal heating of the plastic material arising from large strain and high strain-rate loading, then data on the specific heat c_p will also be needed.

Furthermore, materials whose properties are sensitive to the concentration of absorbed water will need to have data supplied for material that has been conditioned at the relevant humidity for the application.

Table 4 — Ultimate values for stress and strain obtained from tensile tests with different loading histories

Service Conditions	Model type	Properties		Variables
		Isotropic	Anisotropic	
Simple conditions Constant elongation rate	A, B, C	σ_u, ε_u	σ_{up}, ε_{up}, σ_{un}, ε_{un}	T
Sustained loading	D1, E1	σ_c	σ_{cp}, σ_{cn}	t, ch, T
Cyclic loading	D2	σ_f	σ_{fp}, σ_{fn}	N, R, T
High-rate loading	C3	σ_u, ε_u	σ_{up}, ε_{up}, σ_{un}, ε_{un}	$\dot{\varepsilon}$, T

It should be noted that the failure properties of plastics are sensitive to long-term changes in the molecular or crystalline structure of the material brought about by various ageing processes. The most notable of these are physical ageing (relaxation of free volume), thermal ageing, brought about by exposure to elevated temperatures, and ultraviolet degradation caused by exposure to sunlight.

4.3 Design for processing analysis

4.3.1 Processing simulation

Among the various processing methods available for fabrication of plastics into useful parts, injection moulding is the most prevalent method in practice. As such, the CAE (computer aided engineering) tools for simulation of the injection moulding process are more advanced in terms of the number of programs available and their sophistication. Recently, more emphasis has been given to the development of CAE tools for simulation of other processing methods such as extrusion, blow moulding, and thermoforming.

4.3.2 Data for simulation of injection moulding

Simulation programs for injection moulding are available from a number of sources. In general, most of these programs provide a two-dimensional analysis incorporating temperature distribution through the third dimension. Enhancements to allow full three-dimensional simulation have only recently been introduced. Both of these simulation programs are rather complex in nature requiring rigorous definition of part geometry and utilising various viscosity models to describe the flow behaviour of polymer melts, and some expertise is required to use these programs. To overcome the need for such rigorous analysis, several simulation programs for simple two-dimensional simulation are currently on the market.

The main objective of these methods is to simulate the part-filling and post-filling steps in order to assess and optimize the manufacturability of the part. The three main types of analysis involved in injection moulding simulation are

— simple mould filling analysis to determine the ability to fill the mould cavity and to assess the pressure requirements,

— advanced mould filling, packing and cooling analysis, carried out to optimize the processing conditions or to evaluate part and mould design alternatives such as number of gates, proper gate size, its location, etc., and

— shrinkage and warpage analysis to satisfy tolerances and predict dimensional stability of the manufactured part.

The material properties needed for simple mould filling simulation are listed in Table 5.

Table 5 — Data needed for injection moulding simulation — Simple mould filling analysis of thermoplastics and thermoplastic elastomers

Property	Variables
η	$T,\ \dot{\gamma}$
ρ_m	—
$k_m,\ c_{pm}$	—
$T_s,\ T_{ej}$	—

Depending on the software package, reference is also made to the “no flow temperature” or the “transition temperature” in place of the solidification temperature T_s. The need for T_{ej} also depends on the software package. The material properties required for advanced filling, packing and cooling analysis are shown in Tables 6 and 7. The material property requirements are essentially the same for thermoplastics and thermoplastic elastomers. The main differences in the case of reactive materials, such as thermosets, are the inclusion of reaction kinetics data and use of reactive polymer viscosity data in place of melt viscosity data.

Table 6 — Data needed for injection moulding simulation — Advanced mould filling, packing and cooling analysis of thermoplastics and thermoplastic elastomers

Property	Variable(s)
η	$T,\ \dot{\gamma},\ p$
v	$p,\ T,\ \dot{T}$
$k,\ c_p$	T
T_s	$p,\ \dot{T}$
T_{ej}	—

When relevant data are not available, the pressure dependence of viscosity and the temperature dependence of thermal conductivity and specific heat are not included in the analysis.

Table 7 — Data needed for moulding simulation — Mould filling, packing and cooling analysis of reactive materials including thermosets

Property	Variable(s)
$\eta_{reactive}$	$T,\ t,\ \dot{\gamma}$
$\rho_{reacted}$	—
$k,\ c_p$	T
$\Delta H_r,\ \dot{R}$	$T,\ \dot{T}$
α_{gel}	—

The material properties required for shrinkage and warpage analysis are shown in Table 8.

Table 8 — Data needed for injection moulding simulation — Additional data for shrinkage & warpage analysis

Property	Variable(s)
S_{Mp}, S_{Mn}	h, p_{CH}
X (semicrystalline materials)	T
$\dot{X}$ (semicrystalline materials)	T, $\dot{T}$
E_p, E_n	T
ν_{pn}, ν_{np}, G_p	—
α_p, α_n	T

4.3.3 Data for simulation of extrusion

The simulation of extrusion generally includes consideration of the solids transport, the melting of the polymer in the barrel, flow of the melt in the die and the cooling of the extruded shape. Available CAE packages employ different viscosity models to describe the flow behaviour of the polymer melt (see Annex B) and make various simplifying assumptions. The simplifying assumptions typically relate to neglecting contributions from extensional flow, thereby avoiding the need for data on uniaxial extensional viscosity and the first normal stress difference.

The material properties needed for simulation of extrusion processes incorporating these analyses are listed in Table 9.

Table 9 — Material properties needed for simulation of extrusion

Type of analysis	Property	Variable(s)
Solids transport and melting of the polymer	T_m, ΔH_f (semicrystalline materials)	—
	T_g (amorphous materials)	—
	ρ_m, ρ_s	—
	μ_b, μ_s	p, T, v_s
	ρ_B	p
	k, c_p	T
Flow of melt in the die	ρ_m	
	k_m c_{pm}	T
	η, N_1	T, $\dot{\gamma}$
	η_{eu}	T, t, $\dot{\varepsilon}$
Cooling of the extrudate	T_c, ΔH_c (semicrystalline materials)	$\dot{T}$
	$\dot{X}$	T, $\dot{T}$

In practice, the temperature dependence of k and c_p is often ignored if the associated loss of accuracy is considered acceptable.

4.3.4 Data for simulation of blow moulding, blown film extrusion and thermoforming

Injection blow moulding and thermoforming processes involve deformation of a profile or a sheet in a softened state, while extrusion blow moulding and blown film extrusion processes involve deformation in the melt state. The material properties needed for these simulations are listed in Tables 10 and 11.

Table 10 — Material properties needed for simulation of injection blow moulding and thermoforming

Type of Analysis	Property	Variables
Reheating the preform or sheet	k, c_p	T
Deformation of softened material	k, c_p	T
	N_1	T, $\dot{\gamma}$
	η_{eb}	T, t, $\dot{\varepsilon}$
Solidification of the formed shape	T_s (amorphous materials)	$\dot{T}$, p
	T_c, ΔH_c (semicrystalline materials)	$\dot{T}$
	$\dot{X}$	T, $\dot{T}$

Table 11 — Material properties needed for simulation of extrusion blow moulding, and blown film extrusion

Type of Analysis	Property	Variables
Melting of polymer in the barrel	T_m, ΔH_f (semicrystalline materials)	
	T_g (amorphous materials)	
	ρ_m	
	μ_b, μ_s	p, T, v_s
	ρ_B	p
	k, c_p	T
Flow of melt in the die	ρ_m	
	k, c_p	T
	η, N_1	T, $\dot{\gamma}$
	η_{eu}, η_{eb}	T, t, $\dot{\varepsilon}$
Cooling of the extrudate	T_c, ΔH_c (semicrystalline materials)	$\dot{T}$
	$\dot{X}$	T, $\dot{T}$

5 Determination of design data

5.1 General

In this section, preferred test methods are identified for determining the properties shown in Tables 2 to 11. Standard test specimens and test conditions to be used for the acquisition of data are also recommended for each of the properties. Section 5.2 deals with data needed for design for mechanical performance and 5.3 with data needed for processing analysis.

For those properties for which ISO standards are not available for the measurement of data, reference is made, through the use of notes to the tables, to apparatus and specimens which have been used successfully. These methods may be subjects for future standards development.

5.2 Data acquisition for design for mechanical performance

Table 12 shows test methods recommended for determining the mechanical property data listed in Tables 2, 3 and 4.

The methods that are based on International Standards employ standard test specimens that are prepared under well-specified conditions. It should be noted that the material structure in these specimens will, in general, be different from that in the component to be designed. The influence that these structural differences will have on property values will depend upon the property, the processing method and conditions and the geometry of the component. Procedures for increasing the relevance of test specimen data for design are not yet recognised.

NOTE Working groups in ISO TC 61 are considering suitable mould designs for preparing additional standard test specimens in the form of a plate by injection moulding (ISO 294-5).

By testing specimens cut from the plate along and transverse to the direction of melt flow into the mould, it may be possible to obtain upper and lower bounds to properties arising from molecular or fibre orientation. Selection of appropriate property values within these bounds will require knowledge of the flow conditions in critical regions of the component.

Estimates of the anisotropy in tensile modulus of short-fibre reinforced plastics may also be obtained from flow simulation packages that calculate fibre orientation functions throughout a moulded product. A knowledge of fibre and matrix properties is required as well as certain other parameters. An important feature of this approach to the characterisation of elastic behaviour is that information is generated on the variation of properties through the thickness of the moulding. However, as with any predictive method, there will, in general, be some uncertainty in the accuracy of derived properties or performance values.

The precision with which specific test data can be used for design will also be restricted by batch-to-batch variations in material properties. The precision of data for design can then be increased by the statistical analysis of data from different batches.

Despite these limitations in test specimen data, the test methods in Table 12 are highly relevant for the acquisition of design data.

5.3 Data acquisition for design for processing

Table 13 shows recommendations for determining the data needed for processing simulations listed in Tables 5 to 11.

Table 12 — Preferred test methods for acquisition of data needed for design for mechanical performance

Property	Test method	Test specimen	Recommended test conditions	See Note
E	ISO 527-2	ISO 3167	ISO 11403-1	1
ν	ISO 527-2	ISO 3167	—	2
E_p E_n, ν_{pn}	ISO 527-2	Cut from ISO 294-5	ISO 11403-1	3
	ISO 527-4 or -6	See relevant part of ISO 527		
G_p	ISO 6721-7	Cut from ISO 294-3 or 5	ISO 11403-1	
	ISO 15310	150 mm square plate	Temperatures in ISO 11403-1	
σ_T	ISO 527-2	Waisted tensile specimen	ISO 11403-1	4
ν_p	ISO 527-2	ISO 3167	—	5
λ	Shear or compression test	—	—	6
D	ISO 899-1	ISO 3167	ISO 11403-1	
D_p, D_n	ISO 899-1	Cut from ISO 294-5	ISO 11403-1	3
E_s	No International Standard	—	—	7
E', E''	ISO 6721-4 or -5	Cut from ISO 294-3 or ISO 294-5	T ISO 11403 f 0,05, 0,5, 5, 50 Hz	8
G', G''	ISO 6721-7	Cut from ISO 294-3 or ISO 294-5	As above	8
σ_{T1}, σ_{T2}	ISO 527-2	Cut from ISO 294-5	ISO 11403-1	9, 4 and 3
σ_{S1}, σ_{S2}	No International Standard	—	—	10, 9
σ_u, ε_u	ISO 527-2	Waisted tensile specimen	ISO 11403-1	
σ_{up}, σ_{un}, ε_{up}, ε_{un}	ISO 527-2	Cut from ISO 294-5	ISO 11403-1	3
σ_c	ISO 6252	ISO 3167		
σ_{cp}, σ_{cn}	ISO 6252	Cut from ISO 294-5		3
σ_f	—	—	—	—

NOTE 1 ISO 11403-1 specifies the temperature values to be used if it is considered beneficial to present modulus values at standard temperatures so that data from different sources can be compared. Modulus values will increase with increasing strain rate and the rate-dependence will vary with temperature being greater the closer the temperature is to the centre of a relaxation region. The determination of the variation of modulus with rate is routine for strain rates in the range 1×10^{-5} to 1×10^{-1} s^{-1}. At higher rates, the measurement of strain is generally not possible using conventional extensometers (but see Note 4). Data acquisition at high rates is possible through correlations with measurements at lower temperature or with high frequency dynamic mechanical data.

For long-term loading applications (time under load greater than 0,5 h), creep modulus values should be used derived from tensile creep tests.

NOTE 2 The measurement of lateral strain for the determination of Poisson's ratio is not described in ISO standards. A transducer is needed for measuring the change in the width of the specimen under a uniaxial tensile stress. Lateral extensometers are available for this purpose. The Poisson's ratio varies with temperature and strain rate, and, as with modulus, the changes are most pronounced in a relaxation region. Poisson's ratio also varies with strain (see Note 5).

NOTE 3 Specimens of suitable geometry are cut from moulded sheet with specimen axes along and transverse to the direction of preferred orientation. For materials that can be injection moulded, properties will depend upon the processing conditions, the mould geometry and, possibly, the location in the mould. ISO 294-5 is concerned with standardising the dimensions and geometry of a mould in which plate specimens can be prepared having a high degree of anisotropy in properties. The optimum mould thickness for achieving high anisotropy is around 1 mm. The optimum length and width of the plate is then about 80 mm so that specimens having the geometry of the half-scaled, multipurpose test specimen (ISO 527-2 type 1BA) can be prepared by machining. Using this specimen geometry, failure properties can also be determined. Note also that if data only for strains well below failure are required, then measurements may be made on parallel-sided specimens cut from the standard 60 mm square plate (ISO 294-3) although, by virtue of the shorter specimen length, the accuracy of results is likely to be lower.

Table 12 (*continued*)

NOTE 4 In elastic–plastic materials models, non-linear behaviour is considered to be caused by plastic deformation. The lowest value of σ_T coincides with the onset of curvature (non-linearity) in the tensile stress/strain curve. The value of σ_T then varies with plastic strain and data are derived from measurements of stress/strain curves (see section A.4). Stress/strain data are generally needed over ranges of temperature and strain rate (see section A.5). Data at high strain rates are needed for the prediction of impact performance but the measurement of strain in high-speed tests has not been described in any standard. Strain values can be derived from measurement of cross-head displacement if corrections are applied for the machine compliance and the non-uniform strain in the specimen. For high-speed tests, use of a small tensile specimen is recommended.

There is also scope for obtaining data at high rates by extrapolation of measurements at moderate rates. Validated procedures for this are not yet available.

For long-term loading applications (time under load > 0,5 h), σ_T values should be obtained from isochronous stress/strain curves derived from tensile creep tests.

NOTE 5 The plastic component of Poisson's ratio ν_p is derived from simultaneous measurements of longitudinal and transverse strain in tensile tests taken to large strains where behaviour is non-linear. It is used to determine the flow parameter for elastic–plastic models. The transverse strain measurements are also used to derive true stress values from measurements of nominal (engineering) stress. Equations (A.8), (A.9), (A.7) and (A.6) relate relevant parameters.

NOTE 6 The quantity λ is used in the yield criterion in certain elastic–plastic materials models and is a measure of the influence of the hydrostatic component of stress on yield behaviour. It is equal to the ratio of yield stresses in uniaxial compression and uniaxial tension. It can be derived from measurements of compression or shear stress/strain curves in conjunction with tensile stress/strain data. The acquisition of data under compression requires elaborate apparatus to prevent buckling of the specimen. The use of this test with shorter thicker specimens to avoid buckling gives rise to lateral stresses in the specimen. The ISO standard ISO 604 is thus not adequate for this purpose. Shear stress/strain data can be obtained from tests on notched bars (Iosipescu) or notched plates (Arcan) loaded in simple shear. Shear strains can be measured in fibre-reinforced specimens using strain gauges, but a purpose-built extensometer is recommended for unreinforced plastics.

A proposed yield criterion for plastics (see section A.4) is

$$\sigma_T = \frac{\sqrt{3}(\lambda+1)}{2\lambda} J_{2D}^{1/2} + \frac{(\lambda-1)}{2\lambda} J_1$$

where J_1 and J_{2D} are stress invariants and are functions of the components of stress.

λ is then given by

$$\lambda = \frac{\sigma_C}{\sigma_T} = \frac{\sqrt{3}\sigma_S}{(2\sigma_T - \sqrt{3}\sigma_S)}$$

where

σ_C and σ_S are yield stresses in compression and shear at the same equivalent plastic strain as the tensile yield stress σ_T.

For those materials for which $\lambda = 1$, the above Equation reduces to the von Mises yield criterion.

NOTE 7 No ISO standard specifies the measurement of stress relaxation modulus. The specimen and extensometry are the same as those used to acquire creep data. A constant displacement is applied to the specimen and the reduction in load with time is recorded. The stress relaxation function $E_R(t)$ is given by the ratio of the time-dependent stress to the constant strain. The stress relaxation modulus at a particular time is approximately equal to the inverse of the creep compliance at the same time for times and temperatures remote from a relaxation region. More generally, the transformation of creep data to stress relaxation data requires a knowledge of the whole creep function.

NOTE 8 There are a number of commercial instruments that measure dynamic properties. These commonly employ small specimens so that a temperature scan can be completed relatively quickly. A small specimen can lead to significant errors in derived modulus values. The various parts of ISO 6721 should be consulted for information on sources of error in these tests and guidance on the application of corrections.

NOTE 9 These properties as a function of strain are only needed for the application of elastic–plastic models to anisotropic materials.

NOTE 10 Although no International Standard exists, the Iosipescu or Arcan test methods have been used to obtain stress/strain curves in shear for a variety of materials. For fibre reinforced plastics, strain gauges have been used to determine shear strains. For unreinforced plastics, the use of a purpose-built extensometer is recommended.

Table 13 — Preferred test methods for the acquisition of data needed for design for processing

Property	Variables	Test method	Test specimen	Recommended test conditions
η (thermoplastics)	$T,\ \dot{\gamma}\ , p$	ISO 11443	Raw material	See ISO 11403-2 and Note 1
η_{reactive} (thermosets)	$T, t,\ \dot{\gamma}$	See Notes 2 and 3	Raw material	—
η_{eu}	$T, t,\ \dot{\varepsilon}$	See Note 4	Raw material	—
η_{eb}	$T, t,\ \dot{\varepsilon}$	See Note 5	Raw material	—
N_1	$T,\ \dot{\gamma}$	See Note 6	Raw material	—
ρ_{m}	—	See Note 7	Raw material	—
ν	$p, T,\ \dot{T}$	ISO 17744	Injection-moulded specimen	See Notes 8 and 9
k	T	See Note 10	Raw material	—
c_{p}	T	ISO 11357-4	Raw material	Cooling scan at 10 °C/min (see ISO 11403-2)
T_{s}	$\dot{T}\ , p$	ISO 11357-3 see Note 11	Raw material	Cooling scans at 10 °C/min,50 °C/min, 100 °C/min and 200 °C/min (see Note 12)
T_{ej}	—	ISO 11357-3	Raw material	Cooling scan at 10 °C/min (see Note 12)
T_{m}	—	ISO 11357-3	Raw material	Heating scan at 10 °C/min
T_{g}	—	ISO 11357-2	Raw material	Cooling scan at 10 °C/min
T_{c}	$\dot{T}$	ISO 11357-3	Raw material	Cooling scans at 10 °C/min, 50 °C/min, 100 °C/min and 200 °C/min
ΔH_{f}	—	ISO 11357-3	Raw material	Heating scan at 10 °C/min
ΔH_{c}	$\dot{T}$	ISO 11357-3	Raw material	Cooling scans at 10 °C/min, 50 °C/min, 100 °C/min and 200 °C/min
X	T	ISO 11357-7	Raw material	Cooling scan at 10 °C/min
$\dot{X}$	$T,\ \dot{T}$	ISO 11357-7	Raw material	—
$\dot{R}$ (thermosets)	$T,\ \dot{T}$	ISO 11357-5	Uncured material	—
ΔH_{r} (thermosets)	$T,\ \dot{T}$	ISO 11357-5	Uncured material	—
α_{gel} (thermosets)	—	ISO 11357-5	Uncured material	Heating scan at 10 °C/min (see Note 13)
ρ_{reacted}	—	ISO 1183	cured material	—
α_{p} and α_{n}	T	ISO 11359-2	specimens cut from ISO 294-3 plate	See ISO 11403-2
S_{Mp} and S_{Mn} (thermoplastics)	h, p_{ch}	ISO 294-4	60 mm × 60 mm plate (ISO 294-3)	1, 1.5 and 2 mm thickness; cavity pressures of 25, 50 and 100 MPa
S_{Mp} and S_{Mn} (thermosets)	h, p_{ch}	ISO 2577	60 mm × 60 mm plate (See ISO 294-3)	1, 1,5 and 2 mm thickness; cavity pressures of 25, 50 and 100 MPa
E_{p} and E_{n}	T	ISO 527-2	specimens cut from ISO 294-5 plate	At 23 °C; 1 mm/min; 0,05 – 0,25 % strain range
ν_{pn} and ν_{np}	—	ISO 527-2	specimens cut from ISO 294-5 plate	At 23 °C; 1 mm/min; 0,1 – 0,5 % strain range (see Note 14)

Table 13 (*continued*)

Property	Variables	Test method	Test specimen	Recommended test conditions
G_p (moulding materials)	—	ISO 6721-2 OR ISO 6721-7	ISO 3167 or cut from ISO 294-5	See ISO 11403-1
G_p (fibre-reinforced plastics)	—	ISO 15310	150 mm square plate	—
μ_b, μ_s	p, T, v_s	See Note 15	—	—
ρ_B	p	See Note 16	—	—

NOTE 1 The pressure dependence of viscosity is relevant for moulding thin wall parts. However, the determination of the pressure dependence of viscosity is not addressed in any of the test standards for viscosity measurement. In most analyses, the pressure dependence of viscosity is therefore neglected.

NOTE 2 For the determination of viscosity of a reactive system, a slit die rheometer based on ISO 11443 is recommended. Alternatively, a parallel plate viscometer based on ISO 6721-10 may be used.

NOTE 3 To determine the dependence of viscosity on shear rate for a reactive system, a dynamic mechanical rheometer is recommended.

NOTE 4 No test standard existed at time of publication for measuring the uniaxial extensional viscosity of polymer melts. However, measurements can be made using Meissner's apparatus, the Göttfert Rheoten extensional rheometer or the Rosand Precision Ltd, Version 7 unit[2)]. It is recommended that uniaxial extensional viscosity be measured at 3 temperatures in the processing region.

NOTE 5 No test standard exists today for measuring the biaxial extensional viscosity of polymer melts, although development of new apparatus based on the use of film inflation has been reported by IKV. Alternatively, Meissner's apparatus has also been used for measuring biaxial extensional viscosity. It is recommended that biaxial extensional viscosity be measured at 3 temperatures in the processing region.

NOTE 6 For the determination of first normal stress difference at a limited range of shear rate, a parallel plate viscometer method based on ISO 6721-10 is recommended. The data need to be measured at the same conditions as in ISO 11403-2.

NOTE 7 Melt density can be obtained by the ratio of MFR and MVR, but more accurately from pvT data. It is recommended that melt density be measured at a temperature corresponding to the centre of the processing temperature range.

NOTE 8 It is recommended that measurements be made at a cooling rate of 2,5 °C/min at 40, 80, 120, 160 and 200 MPa with an estimation at 1 MPa.

NOTE 9 In the case of semicrystalline resins, the effect of cooling rate is apparent by shifts in both the crystallization temperature and the specific volume (or density). The corresponding shifts can be predicted by compensating for changes in crystallization temperature and degree of crystallinity estimated from DSC scans at fast cooling rates.

NOTE 10 For the determination of thermal conductivity, the transient line source method with cooling from the maximum recommended processing temperature to 23 °C is recommended.

NOTE 11 Pressure DSC can be used for the determination of the pressure dependence of solidification temperature but is currently not described by any test method standard.

NOTE 12 The solidification and ejection temperatures are reference temperatures which are obtained from the DSC scans as defined by the mould filling simulation software. The measurement of values as a function of pressure is currently not common practice (see Note 11).

NOTE 13 The gelation conversion is calculated using the Kamal model from the DSC characterisation of uncured material at several heating rates, in combination with slit die rheometer data using the Macasko model. α_{gel} is the conversion at which viscosity is infinite.

NOTE 14 Poisson's ratio ν_{pn} is measured in the linear portion of the stress-strain curve. Poisson's ratio ν_{np} can be calculated using $\nu_{np} = \nu_{pn} E_n/E_p$.

NOTE 15 No test standard currently exists to determine the dynamic coefficient of friction. Very often, the roughness of the barrel and screw surfaces are taken into consideration in assigning values for these parameters. For μ_b a common practice is to assign a value of 0.3 for a smooth barrel, 0.45 for a rough barrel and 1.0 for a grooved barrel. Similarly for μ_s, a value of 0.25 is assigned for a smooth screw surface and 0.35 for a corroded screw surface.

NOTE 16 No test standard currently exists to determine the bulk density of moulding materials. It may be possible to adapt the method ISO 61 intended for determination of the apparent density of moulding materials in powder form.

2) These are examples of products available commercially. This information is given for the convenience of users of this International Standard and does not constitute an endorsement by ISO of these products.

Annex A
(informative)

Illustrations of the application of finite element analyses to plastics components

A.1 Component geometry and loading arrangement

In this annex, the application of finite element methods is illustrated by calculations of stress and strain distributions in plastics components subjected to different loading situations. A range of types of material behaviour is considered. The aim is to show how the parameters required by various materials models used in FEA analysis can be derived from experimental data. Descriptions here are necessarily brief and reference should be made to technical literature and FEA user manuals for more detailed information.

The applications considered are shown in Table A.1.

Table A.1 — Applications of finite element analyses considered in this section

Section	Behaviour	Loading	Model type
A.2	Linear elastic	Static	A
A.3	Non-linear elastic	Static	B
A.4	Non-linear (elastic plastic)	Static	C
A.5	Non-linear (rate-dependent plasticity)	Impact	C3
A.6	Non-linear viscoelastic (time-dependent plasticity)	Creep	E1 or (C1)
A.7	Linear viscoelastic	Dynamic	D2
A.8	Anisotropic linear elastic	Static	A

In sections A.2 to A.6, the application of different materials models is considered to a single component geometry and loading arrangement. The component is a circular plate that is simply supported on a ring close to its circumference and loaded at its centre as shown in Figure A.1. The selected dimensions correspond closely with those used for puncture impact tests described in ISO 6603-2. Note that a specimen thickness of 3 mm has been chosen in place of the 2 mm thickness recommended in that International Standard. The element mesh for the specimen is shown in Figure A.2, where it can be seen that the loading device and the support are defined by a linear mesh which assumes that these parts are infinitely rigid compared with the plate.

A.2 Application of a linear elastic materials model

With this model, stress and strain components are considered to be linearly related at all levels of strain. However, geometric non-linearity, which allows for changes in the geometry of the plate brought about by large central displacements, is taken into account in the analysis. According to Table 2, the data requirements for this model are the tensile modulus E and Poisson's ratio ν. As indicated in Table 12, these can be determined from a tensile test following the procedure described in ISO 527-2. Any dependence of properties on the rate of loading or the time under load is not taken into consideration in the analysis but associated errors can be minimised by using data measured at strain rates or loading times appropriate to the application.

Results from a tensile test on a propylene copolymer are shown in Figure A.3 measured at a constant deformation rate of 10 mm/min. This corresponds to an elastic strain rate of $2 \times 10^{-3}\ s^{-1}$. Values for the tensile modulus of 1,6 GPa and for Poisson's ratio of 0,39 are obtained from the data in the strain range up to 0,01, which marks the limit of linear behaviour. Using these values, a finite element analysis has been used to obtain the variation of the force applied by the hemispherical contact with the central deflection of the plate. This is shown in Figure A.4 where it is compared with results derived from a non-linear analysis (see section A.4). Figure A.5 shows the distribution of the tensile component of strain in the radial direction at a central deflection of 4 mm. In certain regions of the plate, the strain magnitude is above the limit for linear behaviour and this is consistent with the observed departure of the predicted curve in Figure A.4 from the curve based on a model for non-linear behaviour.

Clearly the linear elastic analysis could be used to give closer agreement with the non-linear analysis at the higher deflections if an effective value for Young's modulus were chosen from the slope of the secant to the tensile stress/strain curve at an appropriate higher strain. A procedure for selecting the appropriate strain is, however, not clear, and the accuracy in predictions at the smaller central deflections would be reduced.

A.3 Application of a non-linear elastic materials model

Errors in the linear elastic analysis become progressively more significant at deflections where strain levels in the plate exceed the limit for linear behaviour. More accuracy in predictions can then be achieved using a hypoelastic model that allows for some non-linearity in the stress/strain curve in Figure A.3. The data requirements for this model are shown in Table A.2.

Table A.2 — Data requirements for a hypoelastic model derived from the data on the propylene copolymer shown in Figure A.3

ε	E_T	ν_T	I_1	I_2	I_3
–0,06	0,075	0,459	$-1{,}570 \times 10^{-2}$	$2{,}168 \times 10^{-3}$	$-2{,}944 \times 10^{-5}$
–0,04	0,252	0,457	$-6{,}032 \times 10^{-3}$	$1{,}070 \times 10^{-3}$	$-1{,}154 \times 10^{-5}$
–0,02	0,818	0,455	$-2{,}768 \times 10^{-3}$	$2{,}704 \times 10^{-4}$	$-1{,}485 \times 10^{-6}$
–0,01	1,200	0,433	$-1{,}754 \times 10^{-3}$	$6{,}546 \times 10^{-5}$	$-1{,}700 \times 10^{-7}$
0	1,600	0,390	0,0	0,0	0,0
0,01	1,200	0,433	$1{,}754 \times 10^{-3}$	$6{,}546 \times 10^{-5}$	$1{,}700 \times 10^{-7}$
0,02	0,818	0,455	$2{,}768 \times 10^{-3}$	$2{,}704 \times 10^{-4}$	$1{,}485 \times 10^{-6}$
0,04	0,252	0,327	$6{,}032 \times 10^{-3}$	$1{,}070 \times 10^{-3}$	$1{,}154 \times 10^{-5}$
0,06	0,075	0,221	$1{,}570 \times 10^{-2}$	$2{,}168 \times 10^{-3}$	$2{,}944 \times 10^{-5}$
0,08	0,013	0,176	$2{,}880 \times 10^{-2}$	$3{,}441 \times 10^{-3}$	$5{,}243 \times 10^{-5}$
0,1	0,003	0,157	$4{,}216 \times 10^{-2}$	$4{,}948 \times 10^{-3}$	$8{,}364 \times 10^{-5}$
0,2	0,001	0,122	$1{,}163 \times 10^{-1}$	$1{,}499 \times 10^{-2}$	$3{,}501 \times 10^{-4}$

E_T are values for the tangent tensile modulus obtained as a function of tensile strain ε and are equal to the gradient of the stress/strain curve at the strain ε, ν_T are values for the tangent Poisson's ratio and are equal to the gradient of the plot of lateral strain against longitudinal strain at the strain ε, and I_1, I_2 and I_3 are strain invariants and are related to the tensile strain ε as follows:

$$I_1 = (1 - 2\nu)\varepsilon$$

$$I_2 = \nu\varepsilon^2(2 - \nu) \qquad \text{(A.1)}$$

$$I_3 = \nu^2\varepsilon^3$$

at values of I_1, I_2 and I_3 where ε lies in the linear region of strain, E_T, and ν_T are the linear elastic values E and ν_e.

The force/deflection curve shown in Figure A.6 is predicted using this model. Figure A.7 shows contours of the tensile component of strain at a central deflection of 4 mm.

A.4 Application of elastic-plastic models

A.4.1 Elastic-plastic models and yield criteria

The limitations in the accuracy achievable with the hypoelastic model are not well understood but it seems that the model is unreliable under conditions of high strain and multiaxial stress. Elastic–plastic models are potentially more accurate under these conditions although it should be noted that they have been developed to describe deformation in metallic and certain other materials and their applicability to plastics is still a subject for further research. Non-linearity in a stress/strain curve is interpreted as due to plastic deformation, and the stress that marks the onset of curvature is considered as the first yield point. (Contrast this with the terminology used for plastics materials where non-linear deformation is largely recoverable and the yield point is the peak stress in the stress/ strain curve.) The subsequent increase of stress with strain is interpreted as strain hardening. In this region of strain, the total strain is considered to be comprised of both elastic and plastic components, the latter, according to the model, being non-recoverable. For this reason, elastic–plastic models would not be expected to apply to plastics in situations involving any reversal of the load.

In order to describe the contribution from plasticity to the total deformation, a knowledge is needed of parameters that characterise yielding and plastic strain hardening of the material. The yield parameters are defined by the yield criterion for the material and the shape of the tensile stress/strain curve determines the strain hardening behaviour.

With metals, yielding is commonly assumed to be dependent only upon the shear component of the applied stress. In this case the yield criterion is given by the von Mises Equation:

$$\sigma_T = \sqrt{3} J_{2D}^{1/2} \tag{A.2}$$

where J_{2D} is an effective shear stress and is a function of the components of the applied stress. In terms of components of principal stress σ_1, σ_2, σ_3

$$J_{2D} = \frac{1}{6}\left[(\sigma_1-\sigma_2)^2 + (\sigma_2-\sigma_3)^2 + (\sigma_3-\sigma_1)^2\right] \tag{A.3}$$

In Equation (A.2), σ_T is a yield stress in uniaxial tension and, for a strain hardening material, will increase with the plastic component of strain. Methods for determining σ_T and its dependence on plastic strain are explained in the next sub-section.

The von Mises yield criterion adequately describes the yield behaviour of only a limited number of plastics materials. In general, yielding is sensitive to both the shear and the hydrostatic components of stress and a modification to Equation (A.2) is more appropriate. The simplest modification considers the yield stress to be linearly related to the hydrostatic stress component J_1 so that Equation (A.2) becomes

$$\sigma_T = \frac{\sqrt{3}(\lambda+1)}{2\lambda} J_{2D}^{1/2} + \frac{(\lambda+1)}{2\lambda} J_1 \tag{A.4}$$

where

$$J_1 = \sigma_1 + \sigma_2 + \sigma_3 \tag{A.5}$$

The parameter λ is a measure of the sensitivity of yield behaviour to the hydrostatic component of stress. When λ = 1, Equation (A.4) reduces to Equation (A.2).

Equation (A.4) is identical to the linear Drucker–Prager model used is several FE packages and developed to describe slip in soil and related materials. Other models, with different forms for the hydrostatic stress sensitivity, are the Mohr–Coulomb and the exponent Drucker–Prager models.

A.4.2 Derivation of materials parameters

The data requirements for elastic–plastic materials models (type C) are listed in Table 2 and explained briefly in Notes 4, 5 and 6 to Table 12.

Values for Young's modulus E and Poisson's ratio ν_e at small strains are generally used to characterise elastic behaviour and to determine elastic components of strain. The shear modulus could be used in place of Poisson's ratio for this purpose but Poisson's ratio is recorded here because it can be measured in the tests used to determine E (see Table 12) and, if lateral strain measurements are extended into the non-linear region, these enable true stresses to be calculated from measured (engineering) values.

The finite element analysis requires data on the dependence of the true tensile yield stress against the true plastic strain. The determination of this function is illustrated in Figures A.3 and A.8. Figure A.3 shows a measured tensile stress/strain curve (referred to as the engineering stress) and the associated variation of Poisson's ratio with strain. In an elastic–plastic model, the limit of linear behaviour marks the onset of plastic deformation and hence the first yield stress. All stresses on the curve above this are engineering tensile yield stresses σ_Y. If the value of σ_Y corresponds to the strain ε at which Poisson's ratio is ν, then the true tensile yield stress at ε is given by

Error! Objects cannot be created from editing field codes. (A.6)

This function is also plotted in Figure A.3.

Equation (A.6) shows that true stress values should generally be used when strains exceed about 0,1.

In an elastic–plastic model, the strains ε corresponding to the non-linear region of Figure A.3 are considered to be the sum of elastic and plastic components. For arbitrary strain levels, these components must be true strains, so the true plastic strain $\log_e (1 + \varepsilon^p)$ is given by

Error! Objects cannot be created from editing field codes. (A.7)

where σ_T is the true yield stress at the engineering tensile strain ε. It can be seen that the use of true rather than engineering strains is generally necessary at strains above about 0,1.

Figure A.8 shows a plot of the true yield stress against the true plastic strain derived from the data in Figure A.3.

The remaining parameters in Table 2 for this model are λ, ν_p and Ψ. If the von Mises yield criterion is assumed to be valid then these parameters take the values

$\lambda = 1$

$\nu^p = 0{,}5$

$\Psi = 0$

and therefore do not need to be measured. The von Mises yield criterion is likely to be valid for those materials for which Poisson's ratio approaches a value of 0,5 with increasing tensile strain. Many plastics, especially multiphase systems, however, show a decrease in Poisson's ratio with strain which is probably associated with a plastic deformation mechanism that involves crazing or cavitation. The onset of this yield mechanism is indicated by a reduction in Poisson's ratio as shown in Figure A.3. The yielding of these materials is better described by a pressure sensitive criterion such as that given in Equation (A.4). Procedures

have been reported for determining λ from additional tests under a different stress state such as shear or compression.

An estimate for the flow parameter Ψ can be obtained from measurements of the plastic component of Poisson's ratio ν_p (see Figure A.8) using the equation

$$\tan \psi = \frac{3(1-2\nu^p)}{2(1+\nu^p)} \tag{A.8}$$

where ν_p is calculated from measurements of the lateral strain ε_t and is given by

$$\nu^p = -\left[\frac{\log_e(1+\varepsilon_t)+\frac{\nu^e\sigma_T}{E}}{\log_e(1+\varepsilon^p)}\right] \tag{A.9}$$

A.4.3 Comparison of FE analyses

Figures A.9 and A.10 show calculations of the force-deflection curve and strain distributions for the centrally loaded plate. Two materials models have been used. One is based on the von Mises criterion [Equation (A.2)] where the required materials parameters are Young's modulus, the elastic component of Poisson's ratio and the strain hardening function σ_T (ε_p) derived from the data shown in Figures A.3 and A.8. The other model has employed a hydrostatic stress sensitive yield criterion [Equation (A.4)] with the same tensile data as used in the von Mises model but with a value for λ = 1,5 and for Ψ = 30°. It can be seen that the strain patterns and the force/deflection curves are similar but the maximum strain levels predicted by each model are significantly different.

A.4.4 Summary of section A.4

A stress/strain curve in tension is the basic data requirement for an elastic–plastic analysis. From these data, a plot of tensile yield stress against plastic strain is derived. If this is the only material property information available, then a realistic value for Poisson's ratio at small strains must be estimated and von Mises yielding must be assumed.

If measurements of Poisson's ratio are also available to large strains, then true tensile yield stress values can be calculated. These values are only needed if strains exceeding about 0,1 are generated. In these situations, true plastic strain values should also be used.

A stress/strain curve under an additional stress state, such as compression or shear, is required to explore the need to use a yield criterion that is sensitive to the hydrostatic component of stress. Such yield criteria are employed in the Drucker–Prager and Mohr–Coulomb materials models. A hydrostatic stress sensitivity parameter for these models can be derived from the two stress/strain curves.

In the application considered here, the force-deflection curve calculated using a realistic yield criterion was similar to that obtained using the von Mises approximation. Values for the maximum strain in the plate were however significantly different. This difference might be important if the analysis were used in conjunction with a failure criterion based on a critical level of strain.

A.5 Application of an elastic-plastic model with strain rate-dependent materials properties

The deformation behaviour of plastics is sensitive to the rate of loading. Stress/strain data depend upon the strain rate, and hence cross-head speed, used to obtain the data. Some FE packages will carry out an elastic–plastic analysis with rate-dependent materials properties. The input data are then derived from stress/strain curves measured over a range of constant strain rates. Such data are shown in Figure A.11 for the propylene copolymer. Because waisted specimens are used, the strain rate increases by a factor of about 2 during the tests. The recorded values are plastic strain rates and are larger than the elastic strain rate corresponding to the initial stages of a test. Curves of yield stress against plastic strain [$\sigma_T(\varepsilon_p)$] were derived from these plots at each strain rate. A small variation of the tensile modulus with rate was also observed.

A dynamic analysis was used with these data to predict the force against deflection for the centrally loaded plate in Figure A.1 when deformed at different speeds. Values for the density of the plate and the impactor are also needed so that inertia contributions can be included. The pressure-sensitive yield criterion employed in section A.4 was used with values for λ = 1,5 and ψ = 30° assumed to be independent of strain rate. An explicit solver code was used for the analysis. Results for a range of loading speeds are shown in Figure A.12.

A.6 Application of a non-linear creep model

Creep in plastics is caused by relaxation processes in which time-dependent changes in the conformation of polymer molecules take place in response to an applied stress σ_0. The resulting creep deformation of the material is characterised by a time-dependent strain $\varepsilon(t)$ from which a creep compliance function

$$D(t) = \varepsilon(t)/\sigma_0 \tag{A.10}$$

is derived.

Creep behaviour is most commonly studied using tensile creep experiments in which case $D(t)$, $\varepsilon(t)$ and σ_0 are then associated with the tensile compliance, tensile strain and tensile stress respectively. A number of mathematical functions have been used to model experimental results. The function

$$D(t) = D_0 \exp(t/\tau)^n \tag{A.11}$$

has been used successfully for plastics at temperatures well below their glass transition temperature. The parameter τ is identified with a mean retardation time for the creep process which has a distribution of retardation times related to the magnitude of the parameter n. D_0 is the elastic compliance and is equal to the inverse of Young's modulus measured at an appropriate strain-rate.

Since the parameter τ in Equation (A.11) is assumed to be constant, the equation does not take account of physical ageing in the material. Physical ageing is associated with a slow reorganisation of the structure of the polymer following cooling from its processing temperature. These changes reduce the molecular mobility over a long period of time which gives rise to a progressive increase in the parameter τ with creep time. This produces a shift in the creep function at large creep times which can be modelled if the age and ageing rate of the material are known.

For small creep stresses, τ is independent of the stress magnitude and the creep behaviour is linear. At higher stresses, creep curves are observed to shift to shorter times as shown in Figure A.13 for experimental data obtained on PVC. This shift is interpreted as an increase in molecular mobility brought about by the application of elevated stresses that results in a reduction in the mean retardation time τ. It is this enhanced mobility that gives rise to non-linear creep behaviour. The increase in mobility is short-lived and, subsequent to load application, τ increases relatively quickly with time under load analogous to enhanced physical ageing. Modelling the stress and time dependence of τ and how they influence the creep deformation is still a subject for further research.

For the application considered here, the effects of physical ageing on the creep compliance will be neglected. For this situation, the creep data in Figure A.13 can be adequately modelled by a simple power law as follows

$$D(t) = D_o[1 + (t/\tau)^n] \quad \text{(A.12)}$$

Values for the parameters D_o, τ and n have been chosen to give the optimum fit to the experimental data. The fits are shown in Figure A.13. The values for D_o and m are the same for each curve. The parameter τ is different for each stress level but is assumed constant with creep time. This neglect of physical ageing is responsible for the inability of Equations (A.11) or (A.12) to accurately describe the shape of the experimental results. The dependence of τ on stress is adequately described by the following relationship, which is based on the Eyring equation for molecular transitions across a potential barrier whose height is changed by the applied stress:

$$\tau = \frac{A\,\sigma_o}{\sinh a\,\sigma_o} \quad \text{(A.13)}$$

where A and a are material parameters.

Values for the parameters in Equations (A.12) and (A.13) that were used to obtain the fits to the data in Figure A.13 are shown in Table A.3

Table A.3 — Values for the parameters in Equations (A.12) and (A.13) used to model creep in PVC

D_o GPa^{-1}	n	A s·MPa^{-1}	a MPa^{-1}
0,305	0,28	$4{,}2 \times 10^6$	0,3

It is worth noting that the values for A and a in Table A.3, and hence the retardation times τ, depend on the physical age of the material when the load was applied. For the PVC data shown in Figure A.13, creep stresses were applied 240 h after specimens had been quenched from the glass transition temperature for PVC. At low stresses (6 MPa and below), the specimen will age significantly during the test, and this has led to the departure of Equation (A.12) from creep data. If the specimen had been much older when the creep test was started, then the parameter τ would have been larger but would change less during the test. Equation (A.12) would then give a better fit to experimental data as long as the appropriate larger τ value was used. The effect of elevated stresses on the older material would still be to reduce the τ value at load application but τ will increase again subsequently with creep time. This will lead to similar departures of Equation (A.12) from creep data as illustrated in Figure A.13.

Equations (A.12) and (A.13) described creep under a uniaxial tensile stress. However, Equation (A.12) can be generalised to apply to multiaxial creep stress states as follows

$$\varepsilon_{ij}(t) = S_{ijkl}\,\sigma_{kl}\left[1 + (t/\tau)^n\right] \quad \text{(A.14)}$$

$$\tau = \frac{A\,\bar{\sigma}}{\sinh a \times \bar{\sigma}} \quad \text{(A.15)}$$

The tensor Equation (A.14) relates components of the time-dependent strain $\varepsilon_{ij}(t)$ to components of applied stress σ_{kl} through the elastic compliance tensor S_{ijkl}. For an isotropic material, the components of the compliance tensor can be expressed in terms of two material properties, usually the tensile modulus and Poisson's ratio, as shown later in Equation (A.20).

The parameter $\bar{\sigma}$ is an effective stress and accounts for the observation that the reduction of τ with stress depends on the stress state as well as the stress magnitude. This is demonstrated through an analysis of creep tests under uniaxial compression where the reduction of τ for a given stress level is observed to be significantly less than that obtained under the same uniaxial tensile stress. This suggests that it is the shear component of stress that is mainly responsible for reducing τ, but this reduction is also influenced by the

hydrostatic component. By analogy with the influence of hydrostatic stress on yielding in plastics given by Equation (A.4), an expression for $\bar{\sigma}$ of the following form has been considered:

$$\bar{\sigma} = \frac{\sqrt{3}(\beta+1)}{2\beta} J_{2D}{}^{1/2} + \frac{(\beta-1)}{2\beta} J_1 \tag{A.16}$$

J_1 and J_{2D} are invariants of the creep stress matrix and are defined by Equations (A.3) and (A.5). From analyses of non-linear creep data for PVC under tension and compression, a value for β = 2 was derived.

The creep function given by Equation (A.14) with (A.15) treats creep as time-dependent elasticity. Since the time dependent term is also influenced by the stress magnitude, then non-linear behaviour is modelled. Non-linear creep in finite element packages is generally modelled by time-dependent plasticity. These models are widely applicable to creep in metallic materials but require some evaluation before they can be used to represent the behaviour observed with plastics and described by Equation (A.14).

In time-dependent plasticity models, the total strain is the sum of elastic and plastic components and it is the plastic component that is responsible for time-dependence and hence creep. A general form for the creep strain rate is considered to be the sum of contributions arising from shear and swelling (volumetric) deformation mechanisms. The strain rates of the tensor components of creep strain ε_{ij} are then represented by

$$\dot{\varepsilon}_{ij}(t) = \dot{\varepsilon}_{\mathrm{s}} \left(\frac{\partial q}{\partial \sigma_{ij}} \right) + \dot{\varepsilon}_{\mathrm{sw}} \delta_{ij} \tag{A.17}$$

where $\dot{\varepsilon}_{\mathrm{s}}$ and $\dot{\varepsilon}_{\mathrm{sw}}$ are the contributions to the strain rate arising from shear and volumetric deformations. The parameter q is used in place of $\sqrt{3}\, J_{2D}{}^{1/2}$ [see Equation (A.3)] and is an effective stress and δ_{ij} = 1 for $i = j$ and 0 for $I \neq j$.

It can be shown that

$$\frac{\partial q}{\partial \sigma_{ij}} = \frac{3}{2q} \left(\sigma_{ij} - \sigma_m \delta_{ij} \right) \tag{A.18}$$

where σ_{m} is the mean stress and is equal to $J_1/3$ [see Equation (A.5)].

Equation (A.17) can therefore be written as

$$\dot{\varepsilon}_{ij}(t) = \dot{\varepsilon}_{\mathrm{s}} \frac{3\sigma_{ij}}{2q} + \left(\dot{\varepsilon}_{\mathrm{sw}} - \frac{3\sigma_{\mathrm{m}}}{2q} \dot{\varepsilon}_{\mathrm{s}} \right) \delta_{ij} \tag{A.19}$$

Returning now to the creep function for PVC, Equation (A.14) can be written in the form

$$\varepsilon_{ij}(t) = \left[(1+\nu) D_{\mathrm{o}} \;\; \sigma_{ij} - 3\nu D_{\mathrm{o}} \;\; \sigma_{\mathrm{m}} \;\; \delta_{ij} \right] \;\; \left[1 + (t/\tau)^n \right] \tag{A.20}$$

where ν is Poisson's ratio and is assumed to be constant with creep time.

When differentiated, this gives

$$\dot{\varepsilon}_{ij}(t) = \frac{n}{\tau^n} \left[(1+\nu) D_{\mathrm{o}} \;\; \sigma_{ij} - 3\nu D_{\mathrm{o}} \;\; \sigma_{\mathrm{m}} \;\; \delta_{ij} \right] \; t^{n-1} \tag{A.21}$$

This can be identified with Equation (A.19) if

$$\dot{\varepsilon}_{\mathrm{s}} = \frac{2q}{3} \cdot \frac{n}{\tau^{n}} \; (1+\nu) D_{\mathrm{o}} \; t^{\,n-1}$$

and

$$\dot{\varepsilon}_{\mathrm{sw}} = \frac{n\sigma_{\mathrm{m}}}{\tau^{n}} \cdot \left(1-2\nu\right) D_{\mathrm{o}} \cdot t^{\,n-1} \tag{A.22}$$

Furthermore, in the notation used here to refer to the stress invariants q and σ_{m}, Equation (A.16) becomes

$$\bar{\sigma} = \frac{(\beta+1)q}{2\beta} + \frac{3(\beta-1)\sigma_{\mathrm{m}}}{2\beta} \tag{A.23}$$

Thus $\dot{\varepsilon}_{\mathrm{s}}$ and $\dot{\varepsilon}_{\mathrm{sw}}$ in the time-dependent plasticity model (Equation (A.17)) can be determined from a knowledge of materials parameters n, τ, ν and D_{o} and the creep stress identified by q and σ_{m}.

A creep model based on Equations (A.19) and (A.22) has been used here with a finite element package to determine the deformation under creep loading of the plate specimen illustrated in Figure A.1. The material was taken to be PVC whose creep behaviour is characterised by Equations (A.20) and (A.23). Values for the materials parameters in these Equations are listed in Table A.3 together with $\beta = 2$ and $\nu = 0{,}35$. A force of 200 N was applied to the hemispherical contact. Calculations of the central deflection with time under load are shown in Figure A.14. Also shown in that figure are contours of maximum principal stress near the beginning and at the end of the creep analysis. It is seen that the distribution of stress within the specimen changes with time and the stress level relaxes in regions of high stress. Accompanying this, calculations of strain distributions show a general increase in strain level with time under load.

For comparison, an analysis was also undertaken for *linear* viscoelastic behaviour. Here the relaxation time τ was assumed to be constant at a value of 4×10^{6} s which is approximately that given by the curve for 12 MPa in Figure A.13. With this analysis, the modulus of all regions within the plate will decrease at the same rate independent of the magnitude or state of the stress. This analysis gave strain distributions that increased with time but, in contrast to the non-linear creep analysis, the stress distribution remained constant. The calculated variation of the central displacement and strain distributions with time under load were also significantly different from those obtained with the non-linear analysis.

A.7 Application of a linear viscoelastic materials model

In this illustration, a finite element analysis is used to calculate the response of a simple component to cyclic loading that excites resonant vibrations in the component. The frequencies and relative amplitudes of the lower frequency resonant modes are determined. For the application considered here, the driving force is assumed to have a constant amplitude of 10 kN over the frequency range of interest, although the response to an arbitrary distribution of forcing frequencies could be calculated if the force distribution is known.

The component in this application is a thin-walled, hemispherical shell that is fixed at its circumference to a very stiff foundation. The dimensions of the shell and the mesh used in the analysis are shown in Figure A.15. The cyclic force is applied to the component through the foundation, and the direction of the force is considered to be normal to the foundation plane. The force is assumed to be sufficiently small that the strains in the shell are at all times within the linear viscoelastic range for the material.

The minimum data requirements for the analysis (see Table 2) are values for the storage and loss components of the dynamic tensile modulus, E' and E'', Poisson's ratio ν and the density ρ of the polymer. Strictly, Poisson's ratio is a complex quantity but a negligible loss of accuracy will generally result from assuming this to be a real number. The simplest analysis requires data for E' and E'' at a single frequency and the appropriate temperature and assumes properties are independent of frequency. When the vibration

frequencies are within a relaxation region for the polymer, more accurate predictions will be obtained using data measured over the relevant frequency range.

Figure A.16 shows comprehensive dynamic property values for a polypropylene homopolymer. Values for E' and tan $\delta_E = E''/E'$ are shown over a wide frequency range and at discrete temperatures between -10 °C and 50 °C. These results were obtained using a variety of dynamic mechanical test methods. Data at low frequencies up to 100 Hz were determined using the tensile forced non-resonance method (see ISO 6721-4). Between 100 Hz and 5 kHz, the flexural resonance method was used (see ISO 6721-3). A modification of this method, in which the specimen was forced to vibrate in a longitudinal resonance mode, enabled data up to 10 kHz to be measured. An ultrasonic wave propagation method (see ISO 6721-8) was used to determine properties in the range 1 MHz to 5 MHz.

Calculations are shown in Figure A.17 of resonant mode frequencies and amplitudes of the polypropylene shell at a temperature of 20 °C. Curve (a) in Figure A.17 was obtained using values for E' and E'' measured at a single frequency of 10 Hz. The assumption here is that properties do not depend on frequency. For comparison, curve (b) shows the response predicted when data for E' and E'' over the frequency range between 0,1 Hz and 100 kHz are employed taken from the curves at 20 °C in Figure A.16.

The measurement of the comprehensive data set in Figure A.16 requires a variety of test methods, but data like these are often derived from a much smaller quantity of measured values by assuming equivalence in the frequency and temperature dependence of properties. In this way, data over a wide frequency range are obtained by superposition of E' vs. frequency data measured over a narrow frequency range but covering a wide span of temperature. The relaxation mechanism in Figure A.16 is assigned to the glass-to-rubber transition in the amorphous phase of the polymer and the kinetics of this transition are generally described by the WLF equation for time-temperature superposition. Indeed, the frequencies of the peaks in tan δ_E satisfy the WLF equation for the temperature dependence of mean relaxation times. However, the breadth of the loss factor curves in Figure A.16 becomes more narrow as the temperature is raised. This implies that the distribution of relaxation times in this relaxation process changes with temperature. As a consequence, the shape of the E' against frequency curve will change with temperature, and this will limit the accuracy of property values predicted using time-temperature superposition.

A.8 Application of an anisotropic elastic model

An anisotropic linear elastic analysis is used here to derive the stress distribution around a hole in the centre of a laminate under a uniaxial tensile stress. The laminate consists of 8 layers of a unidirectional, continuous-fibre reinforced plastic. Coordinate axes and laminate dimensions are shown in Figure A.18. The x-axis is in the direction of applied stress. The fibre orientation in each layer is identified by the angle that the fibre axis makes with the x-axis and is shown in the enlarged section. Coordinate axes for each layer are defined such that the 1-axis is along the direction of fibre orientation. Properties in the plane transverse to this axis are assumed to be isotropic. The 3-axis is taken to coincide with the through-thickness direction (z-axis) of the laminate.

In the analysis, constraints associated with load introduction are assumed to be localised at each end of the plate so that the material around the hole can be considered to be in a state of plane stress. This implies that there are no components of stress in the laminate along the thickness direction (z-axis).

Because of the assumption of transverse isotropy, 5 independent materials parameters are needed to characterise the elastic anisotropy of a single layer. Table A.4 lists 5 properties that are commonly used for this purpose. E_1 and E_2 are tensile moduli along and transverse to the direction of fibre orientation, respectively. G_{12} and G_{23} are shear moduli in a plane containing the fibre axis and in the plane normal to this axis, respectively and ν_{12} is Poisson's ratio for an applied stress along the fibre axis. In Table A.4, these parameters are identified with properties E_p, E_n, G_p and ν_pn, which were introduced in Table 3 and section 3.2.

Table A.4 also gives measured values for a carbon-fibre-reinforced epoxy. Properties were determined using specimens cut from a compression moulded plate in which the fibres were aligned in a single direction. Tensile properties and Poisson's ratio were measured using ISO 527-5, and the shear modulus G_{12} was determined using ISO 15310. A knowledge of the transverse shear modulus G_{23} is not needed for this analysis since a state of plane stress exists in the laminate and in each layer. It may be worth noting that

these properties can also be determined using ultrasonic wave propagation methods described in ISO 6721-8. The current version of that standard deals with isotropic materials, and the data analysis required for anisotropic materials is not described.

Table A.4 — Materials properties for a transversely isotropic carbon fibre reinforced epoxy

$E_1 = E_p$ (GPa)	$E_2 = E_n$ (GPa)	$G_{12} = G_p$ (GPa)	$\nu_{12} = \nu_{pn}$	G_{23}
135	10	5,3	0,3	—

A finite element analysis has been used to calculate the distribution of the maximum principal stress in each layer produced by an applied stress of 140 MPa. Contours of maximum principal stress are shown in Figure A.19. The maximum values of these stresses have been used to explore the validity of using multiaxial failure criteria for an individual layer to predict the onset of failure in the laminate.

Dimensions in millimetres

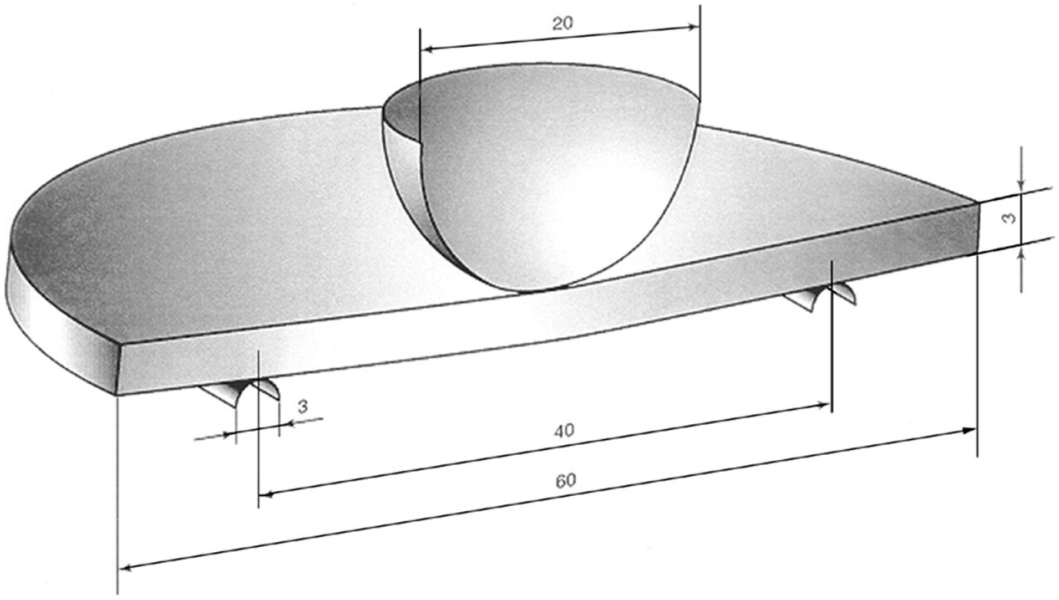

Figure A.1 — Circular plate specimen and loading arrangement used to illustrate application of different materials models with finite element analyses

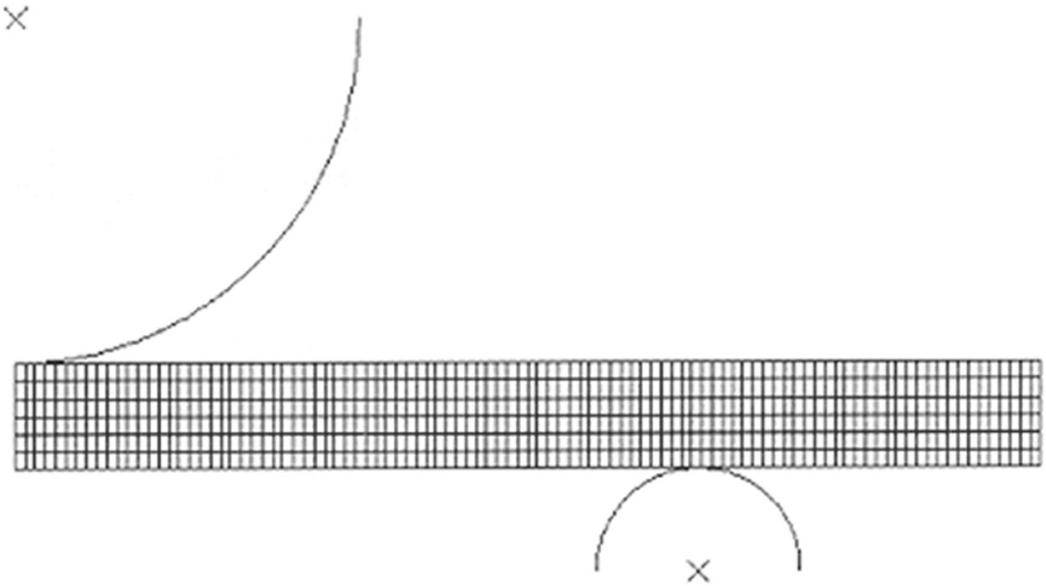

Figure A.2 — Diagram of meshes used for finite element analyses

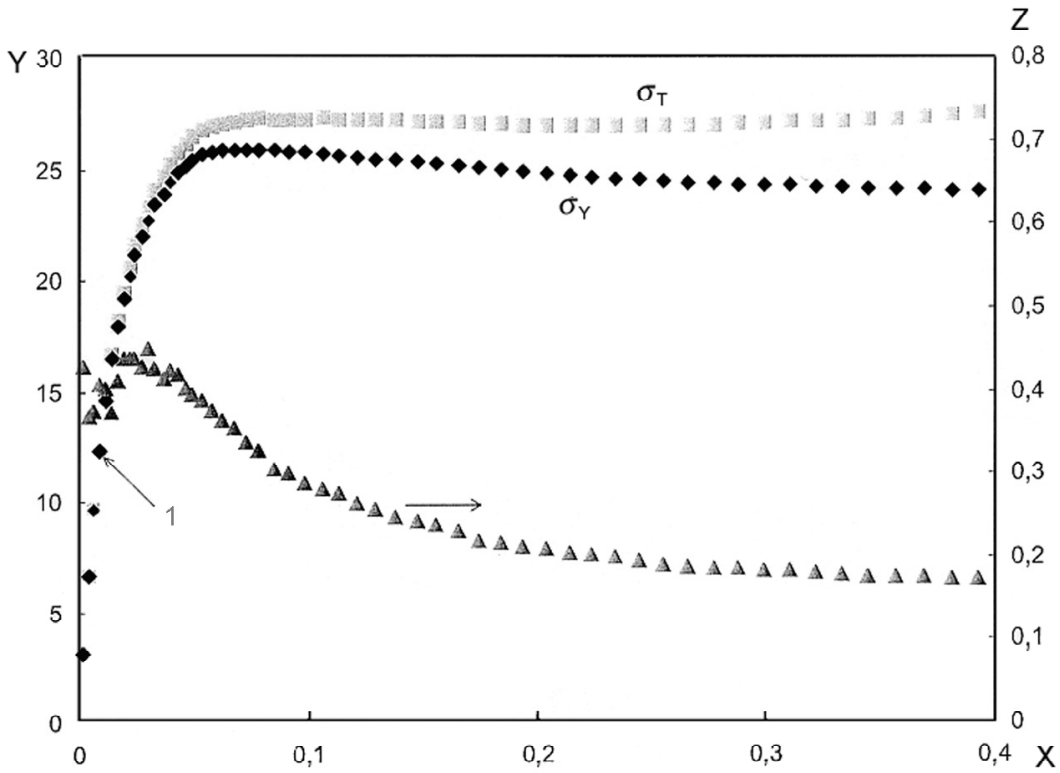

Key

X true strain
Y stress, MPa
Z Poisson's ratio
σ_T true stress
σ_Y engineering stress
1 first yield point

NOTE The true tensile stress has been calculated from these results using Equation (A.6).

Figure A.3 — Measured values of engineering tensile stress and Poisson's ratio with tensile strain for propylene-ethylene copolymer

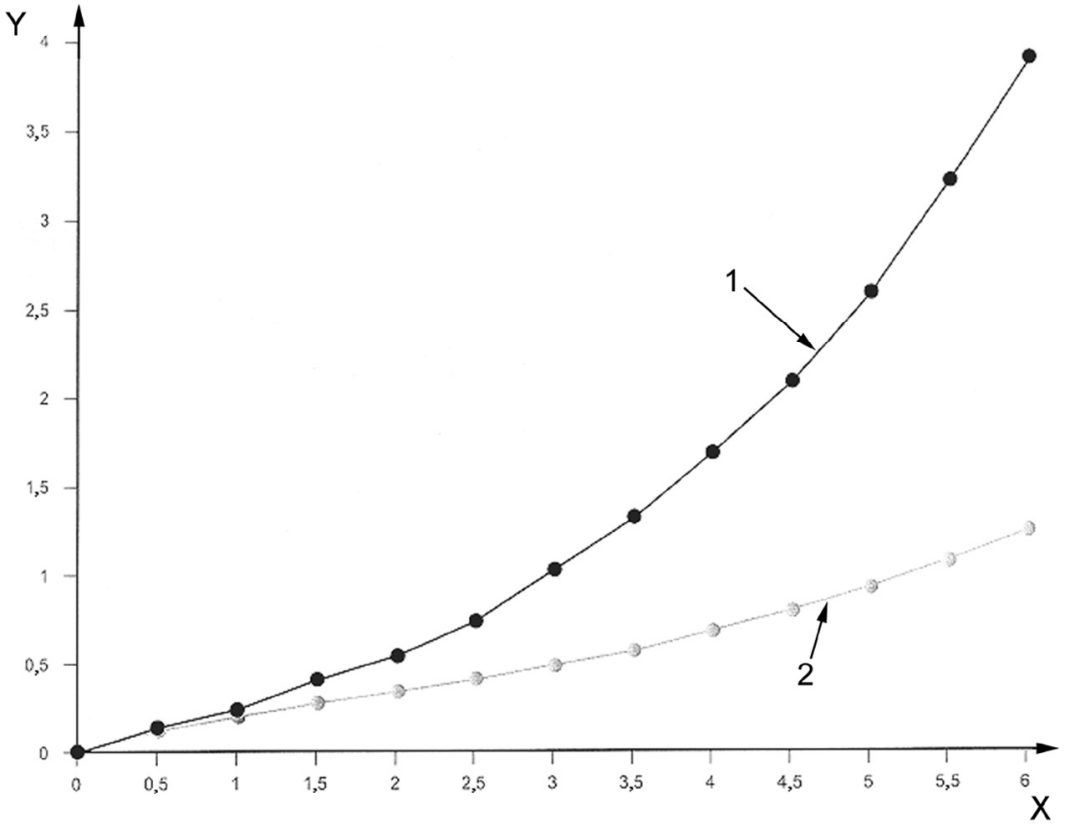

Key

X displacement, mm

Y force, kN

1 elastic analysis

2 von Mises and Drucker–Prager analysis

Figure A.4 — Calculated variation of force with central deflection obtained with linear elastic analysis — Comparison made with calculations based on non-linear analysis (see Figure A.9)

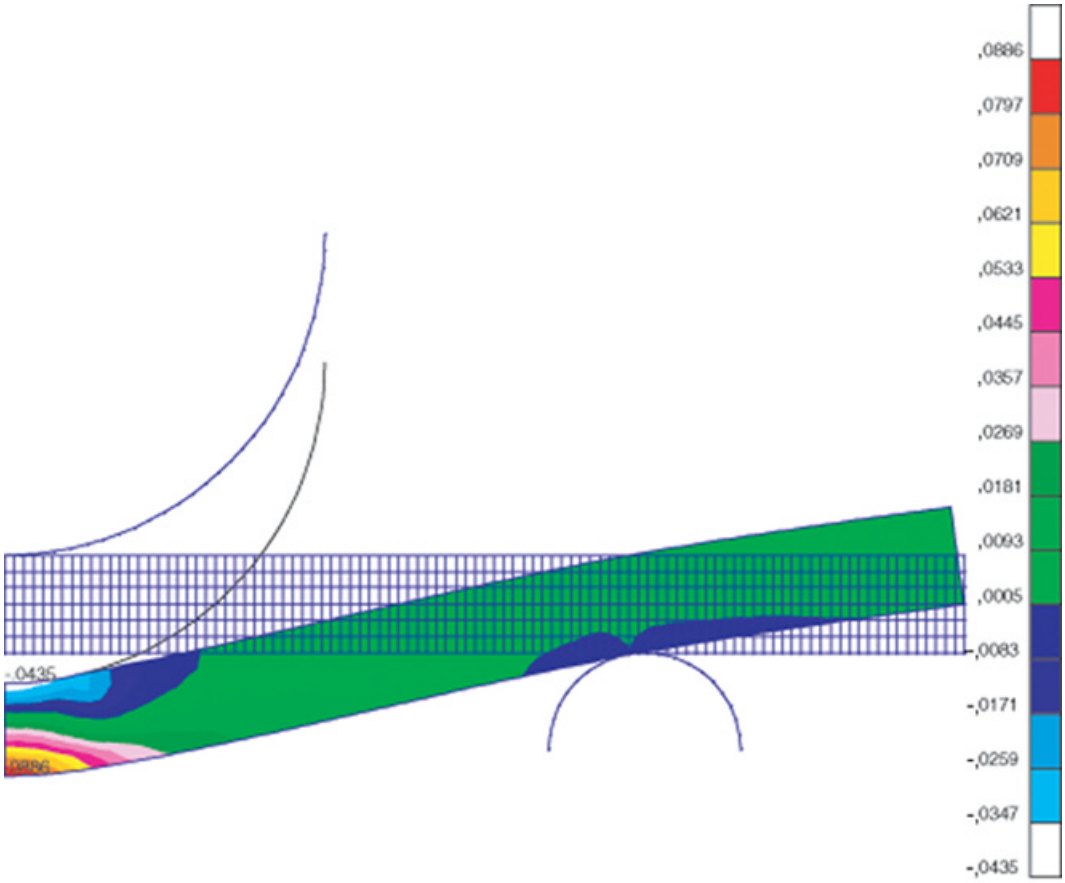

Figure A.5 — Contours of tensile strain in radial direction at central deflection of 4 mm predicted using linear elastic analysis

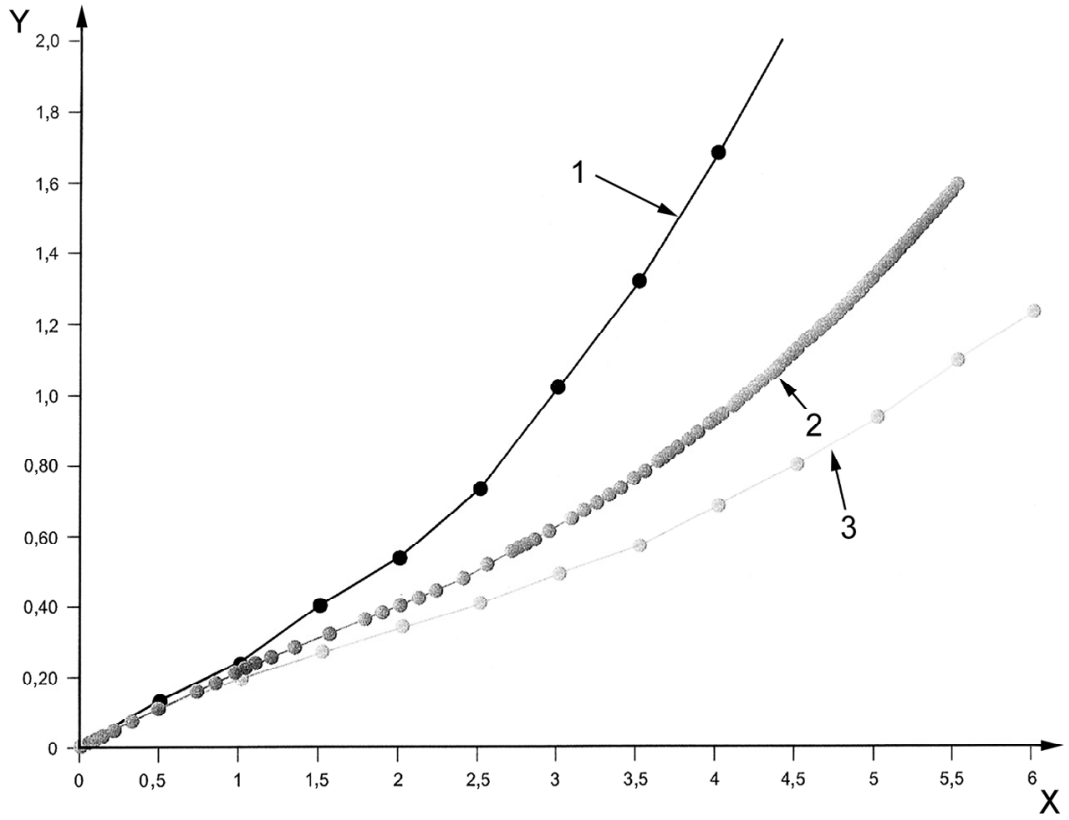

Key

X displacement, mm
Y force, kN
1 elastic
2 hypoelastic
3 von Mises

Figure A.6 — Variation of force with central deflection predicted using non-linear, elastic analysis

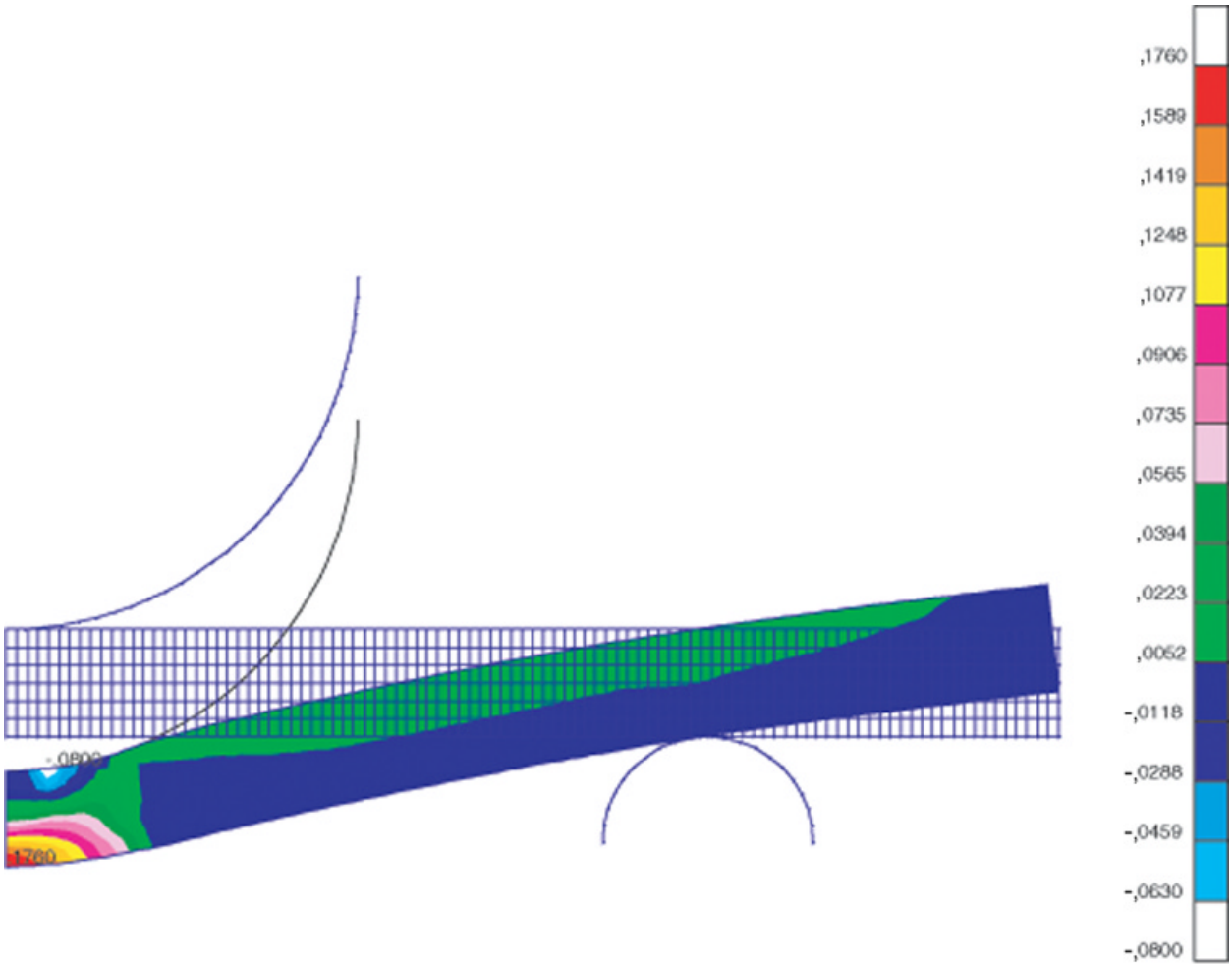

Figure A.7 — Contours of tensile strain in radial direction at central deflection of 4 mm predicted using non-linear elastic analysis

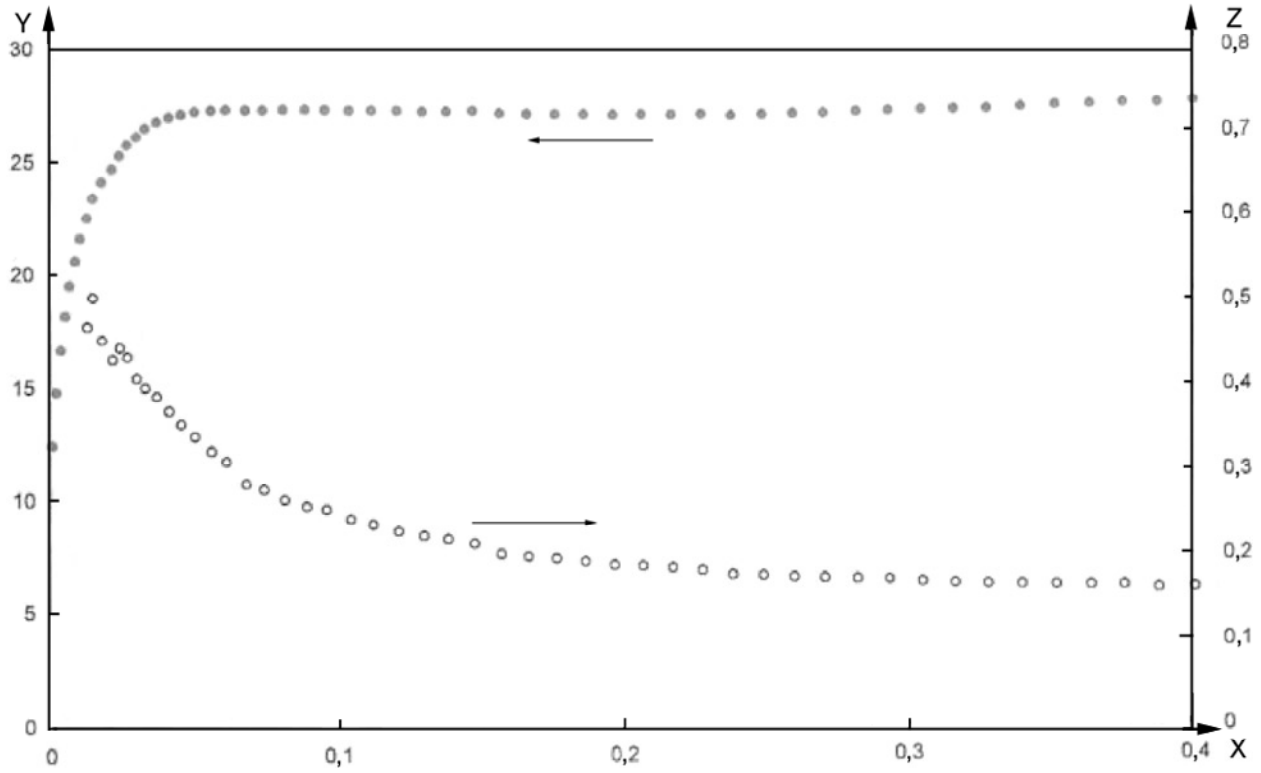

Key

X true plastic strain

Y true yield stress, MPa

Z true plastic Poisson's ratio

Figure A.8 — True yield stress and plastic component of Poisson's ratio with true plastic component of strain for propylene-ethylene copolymer derived from data in Figure A.3
[see Equations (A.7) and (A.9)]

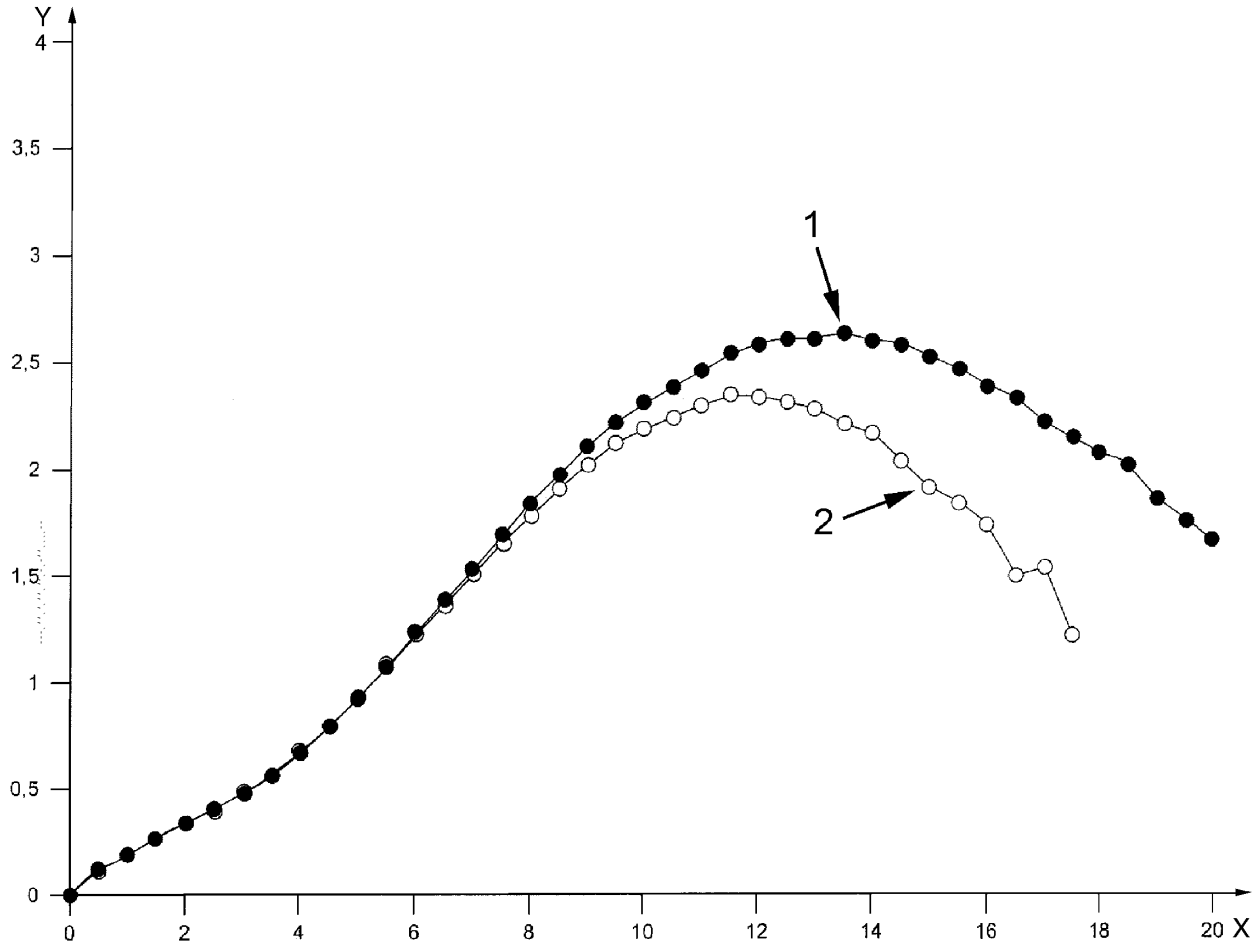

Key

X displacement, mm
Y force, kN
1 Drucker–Prager analysis
2 von Mises analysis

Figure A.9 — Force/deflection curves calculated using von Mises and linear Drucker–Prager models

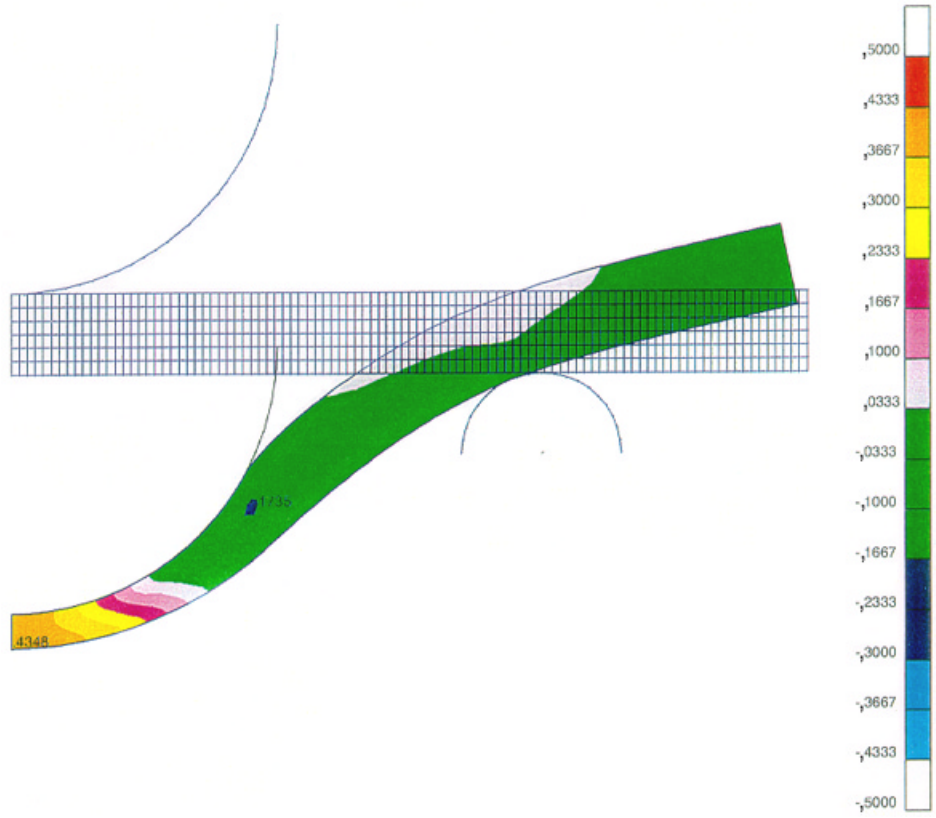

a)

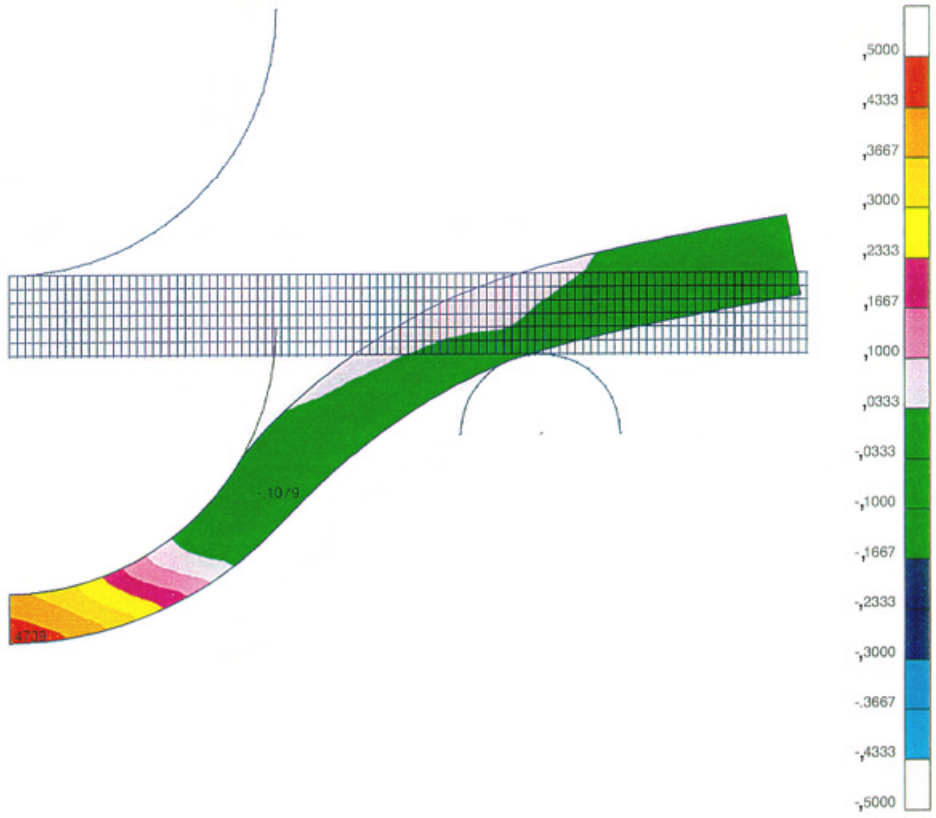

b)

Figure A.10 — Contours of tensile strain in radial direction at central deflection of 12 mm calculated using a) von Mises model and b) linear Drucker–Prager model

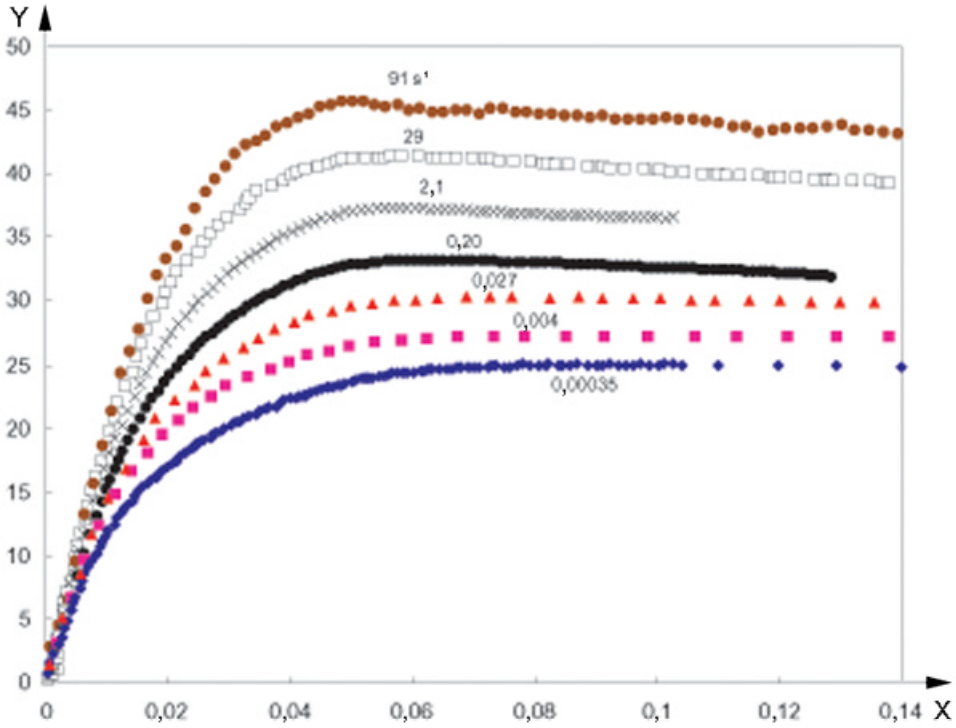

Key

X strain

Y stress, MPa

The values indicated with each curve are values for the plastic strain rate.

Figure A.11 — True stress/true strain curves for a propylene-ethylene copolymer measured at different strain rates, 23 °C tension

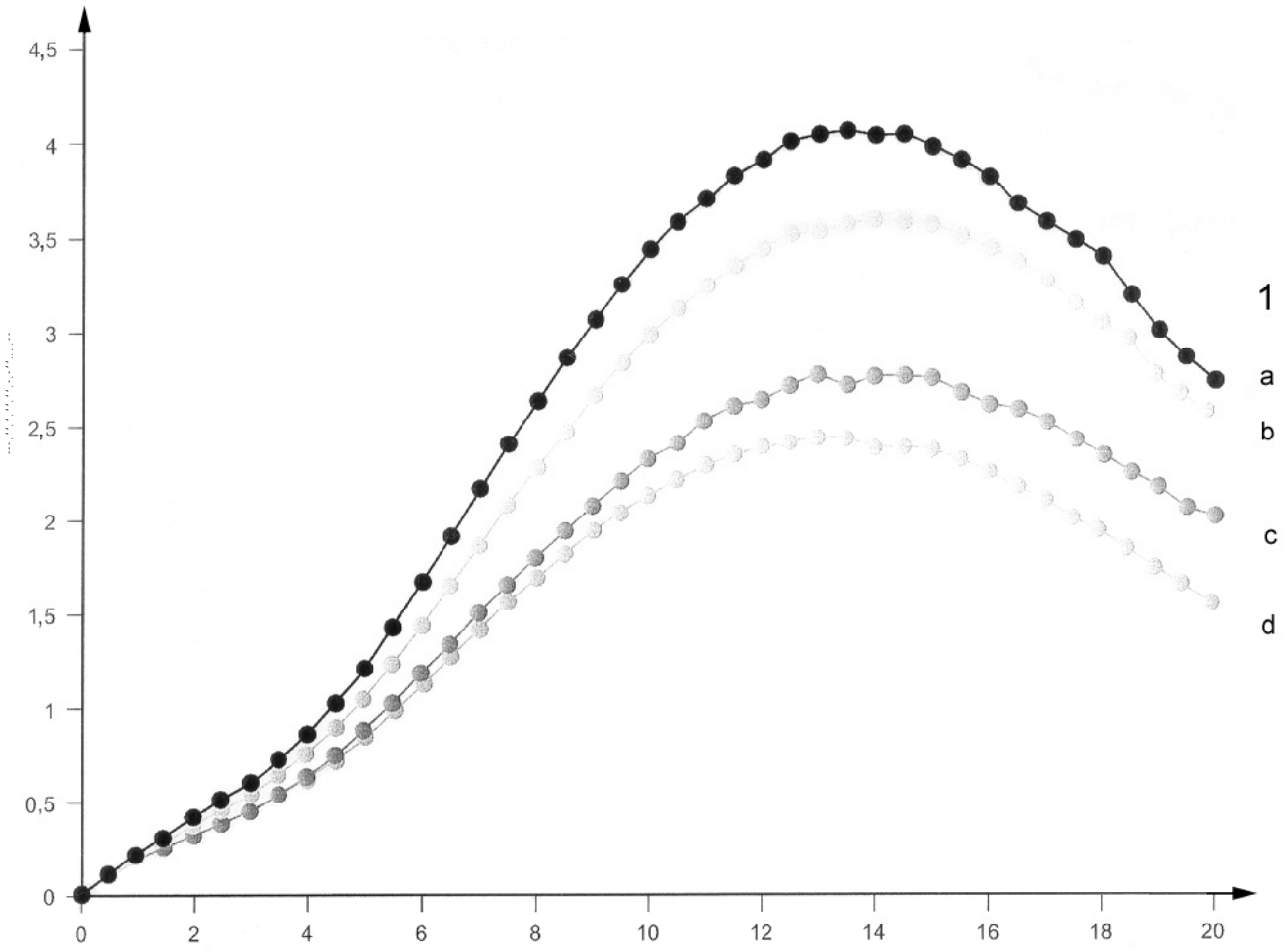

Key

X displacement, mm

Y force, kN

1 testing speed

a 1 m/s

b 0,1 m/s

c 0,01 m/s

d 1 mm/s

Figure A.12 — Force/deflection curves calculated for range of loading speeds using rate-dependent material properties shown in Figure A.11 and linear Drucker–Prager model

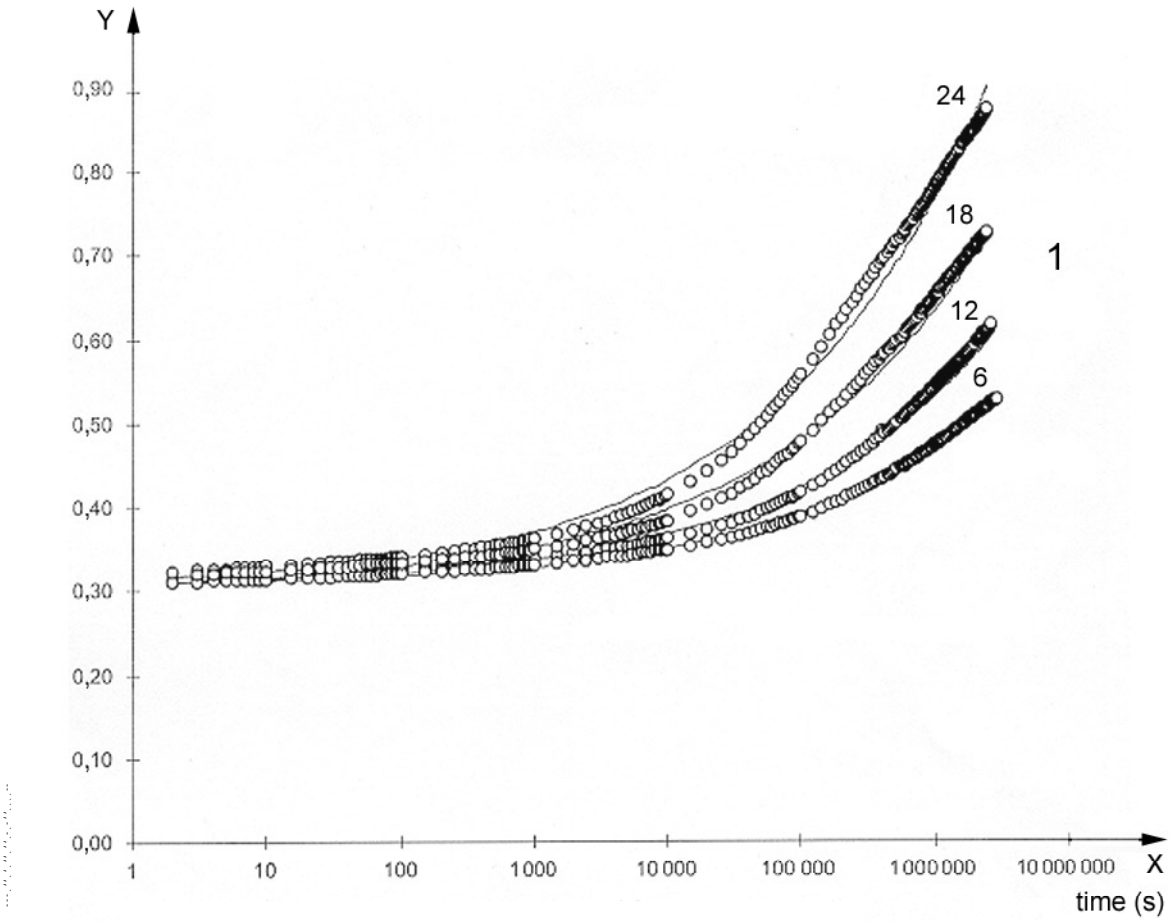

Key

X time, s

Y tensile compliance, GPa^{-1}

1 applied stress, MPa

NOTE Creep behaviour is modelled using Equations (A.12) and (A.13) in which the effects of physical ageing have been neglected.

Figure A.13 — Tensile creep compliance curves for PVC at different levels of applied stress

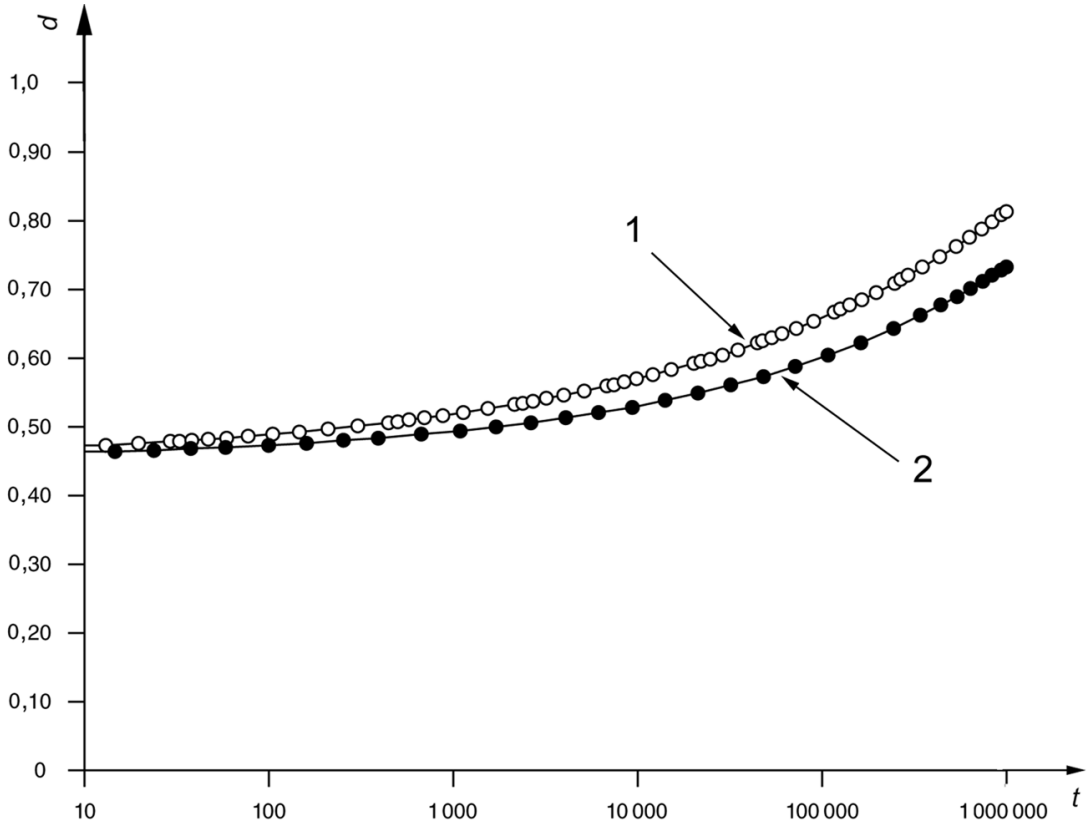

a)

Key

t time, s

d deflection, mm

1 non-linear analysis

2 linear analysis, $\tau = 4 \times 10^6$ s

Figure A.14 — Calculated increase in central deflection d of plate with creep time t (a) and change in the distribution of the maximum principal stress with creep time (b)

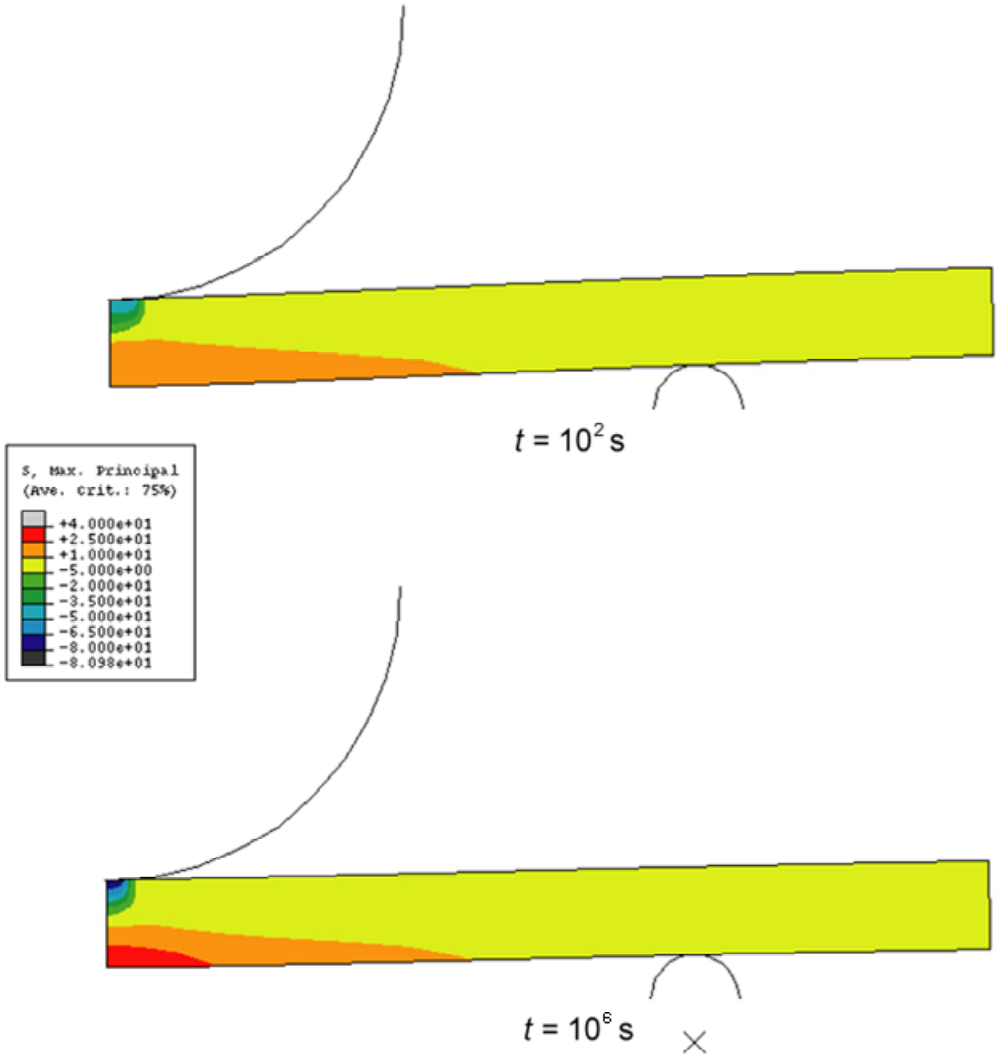

b)

Key

t time, s

NOTE The stress scale is in megapascals.

Figure A.14 —Calculated increase in central deflection d of plate with creep time t (a) and change in the distribution of the maximum principal stress with creep time (b)

Dimensions in millimetres

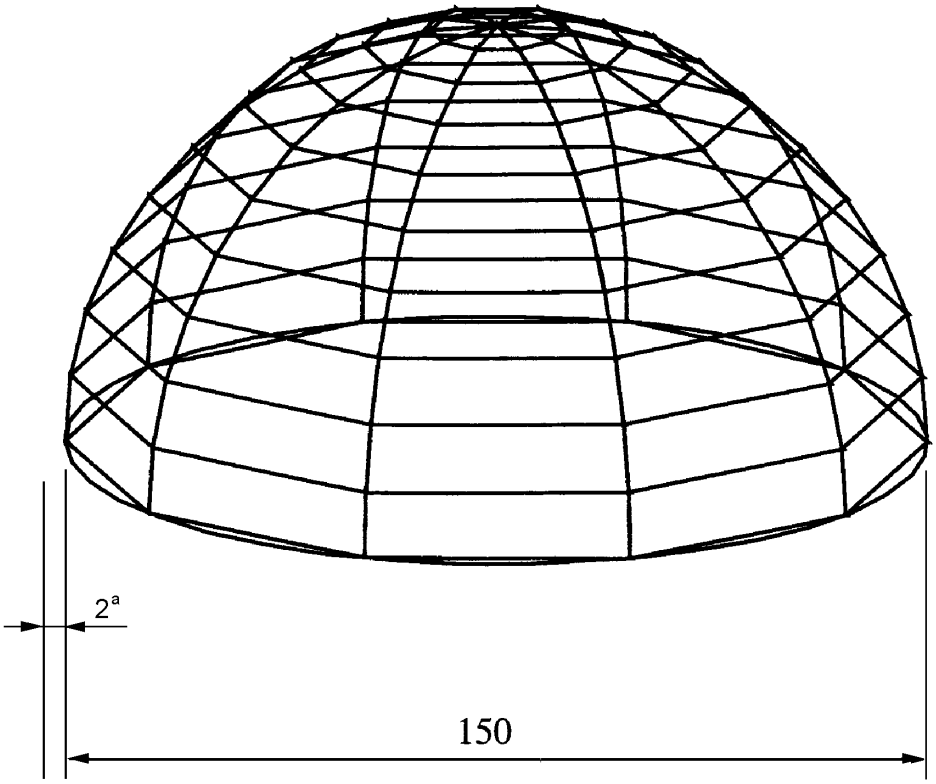

a Wall thickness.

Figure A.15 — Finite element mesh and dimensions used for calculating resonance frequencies of hemispherical shell of viscoelastic material

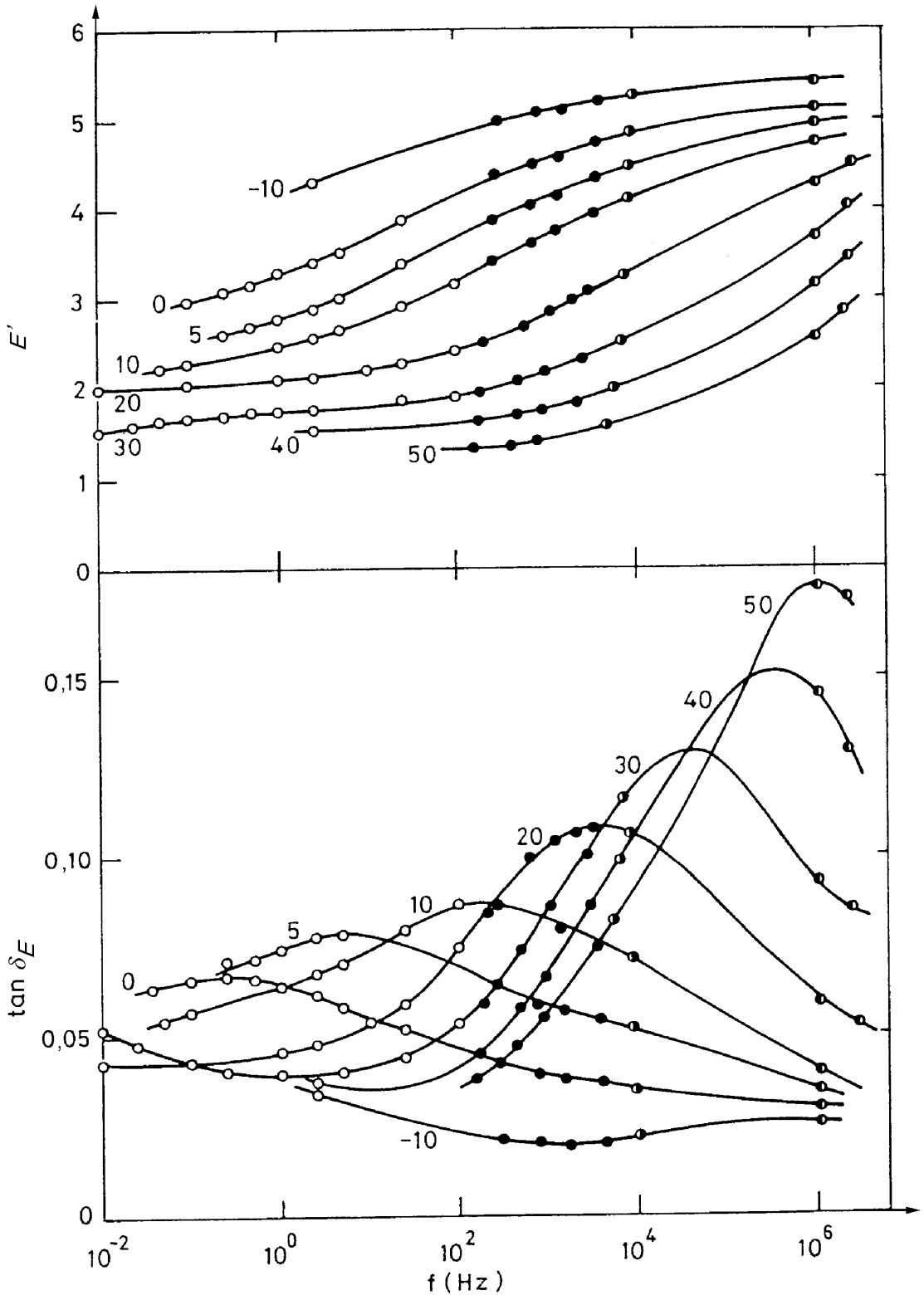

Key

○	tensile nonresonance method	f	frequency, Hz
●	flexural resonance	E'	tensile storage modulus, GPa
◑	ultrasonic pulse technique	tan σ_E	tensile loss factor
◐	longitudinal resonance		

Figure A.16 — Frequency dependence of E' and tan δ_E for polypropylene at temperatures (°C) on each curve

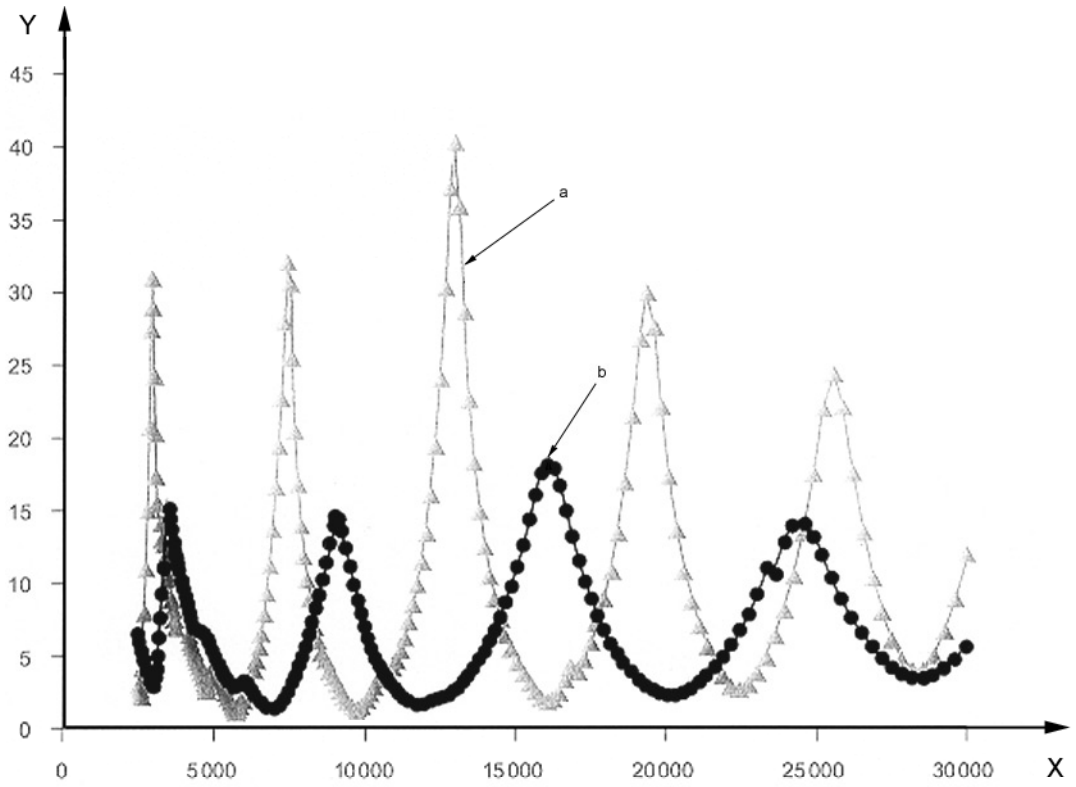

Key

X frequency, Hz

Y velocity amplitude, mm/s

a Base node velocity, data at single frequency: the curve was obtained using dynamic property data from Figure A.16 at a single frequency of 10 Hz.

b Base node velocity, frequency-dependent data: the curve was obtained using data over the whole frequency range.

Figure A.17 — Velocity amplitudes and frequencies of resonant modes of hemispherical shell shown in Figure A.15

Dimensions in millimetres

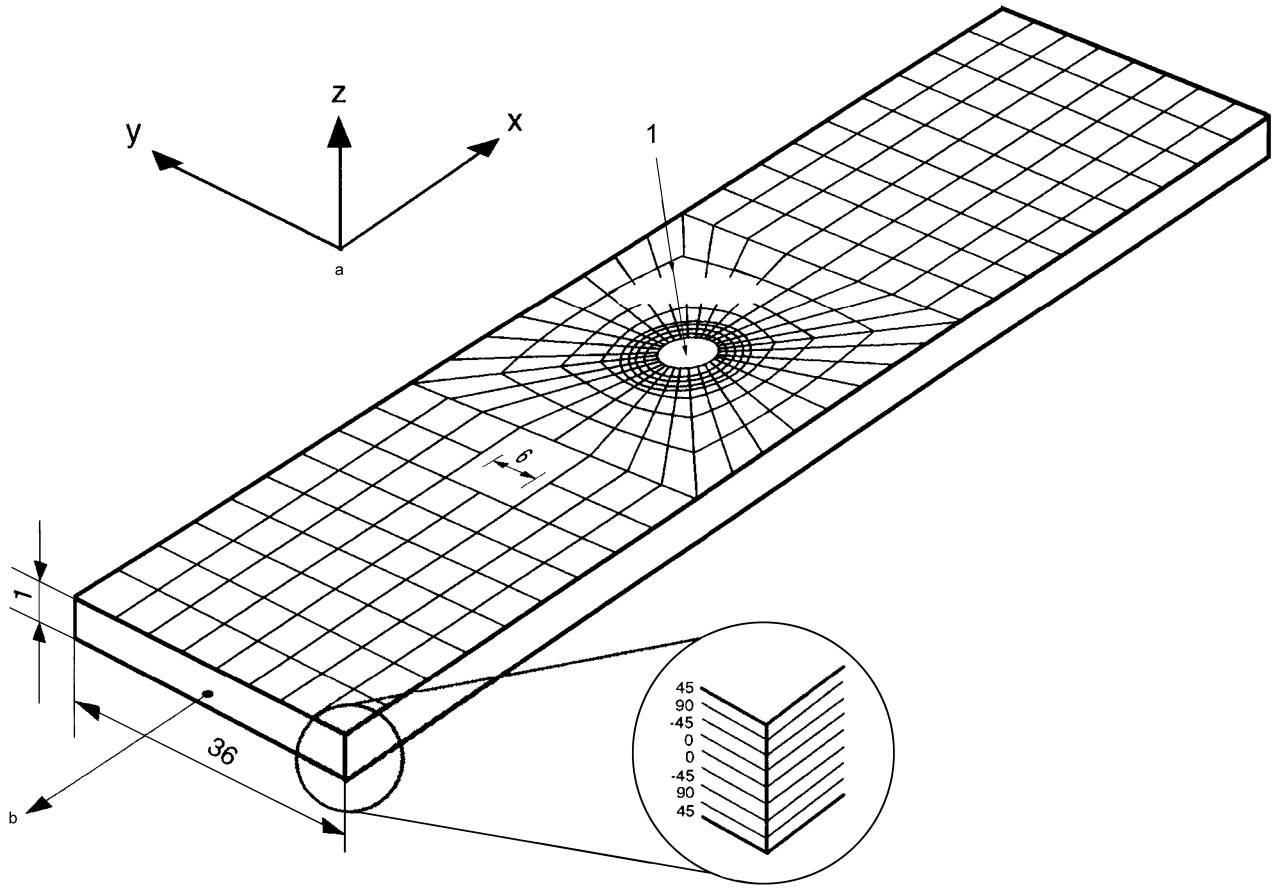

Key

1 central hole

a Laminate axes.

b Applied stress.

Figure A.18 — Schematic diagram of laminate showing configuration of layers and mesh used for finite element analysis

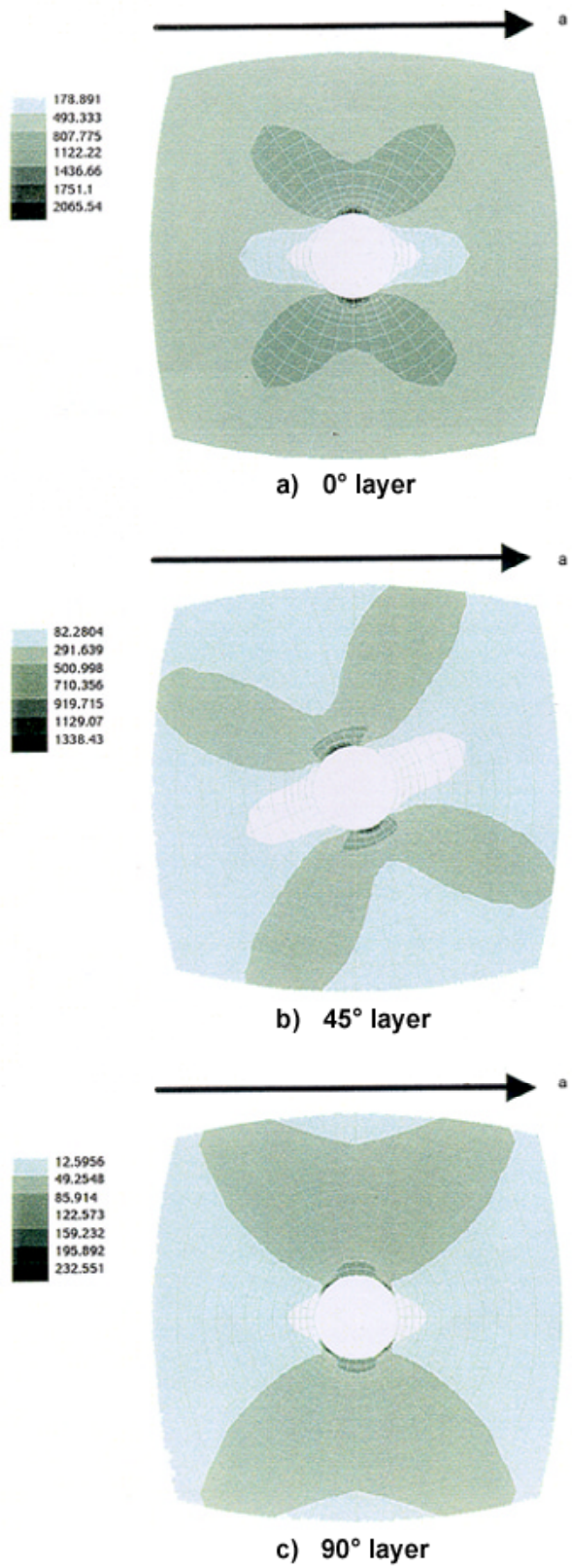

a Direction of applied stress.

Figure A.19 — Contours of maximum principal stress (MPa) in each layer produced by remote stress on laminate of 140 MPa

Annex B
(informative)

Application of processing simulation analysis for plastics

B.1 General

In this annex, the application of various processing simulation programs for plastics is illustrated to demonstrate the use of relevant material data identified in 4.3. The applications considered are shown in Table B.1.

Table B.1 — Applications of processing simulations

Clause	Processing method	Subclause	Analysis type
B.2	**Injection moulding**	B.2.1	Simple mould filling of thermoplastics
		B.2.2	Advanced mould filling, packing and cooling of thermoplastics
		B.2.3	Shrinkage/warpage analysis of thermoplastics
B.3	**Extrusion**	B.3.1	Polymer melting in the extruder
		B.3.2	Simulation of melt flow in a coat hanger die
		B.3.3	Simulation of melt flow in a profile die

It is important to note that the commercial processing simulation programs allow selection of a wide variety of viscosity models to describe the flow behaviour of polymer melt. Often, the format, especially the symbols for variables and model coefficients used in these viscosity models, can appear little different than those that one might find in well-known reference sources. Typically, each software program also includes a module for determining the appropriate coefficients for the chosen viscosity model from the experimental melt shear viscosity data by a suitable curve fitting procedure.

The most common viscosity models employed in the injection moulding simulation programs are listed in Table B.2. The first-order model is commonly used in simple two-dimensional analysis. The actual input requirements for the viscosity data might vary depending on the software program. For example, in Moldflow software[1)], the input format for viscosity data for the first order model can either be in the form of three coefficients (viscosity factor, shear factor and temperature factor) or as three (3) data point sets

T_1, $\dot{\gamma}'_1$ and η_1

T_2, $\dot{\gamma}'_2$ and η_2

T_3, $\dot{\gamma}'_3$ and η_3

1) Moldflow is an example of a product available commercially. This information is given for the convenience of users of this International Standard and does not constitute an endorsement by ISO of this product.

from which the model coefficients A, B and C are calculated by the special curve fitting module in the software. Likewise, for the second-order model, the input format for viscosity data can either be in the form of a second-order viscosity matrix, as follows

Temperature (°C)	Shear rate (1/s)	Viscosity (Pa·s)
$T_m - 20$	1 000	η_1
T_m	100	η_2
T_m	1 000	η_3
T_m	10 000	η_4
$T_m + 20$	100	η_5
$T_m + 20$	1 000	η_6

or as a set of six (6) polynomial coefficients.

Table B.3 summarizes the most common viscosity models used in simulation programs for processes involving extrusion. In practice, the power law and log polynomial models are used for simple analysis while Carreau and Cross models are employed in advanced analyses. The simplified form of Carreau model assumes the viscosity (η_∞) to be zero when shear rate approaches infinity.

Table B.2 — Common viscosity models employed in injection moulding simulation programs

Model in simulation program	Viscosity model	Description of symbol
First-order model	$\eta = A\ \dot{y}^{B}\ e^{CT}$	A Viscosity factor B Shear rate factor C Temperature factor
Second-order model	$\ln \eta = A_1 + A_2 (\ln \dot{y}) + A_3 T + A_4 (\ln \dot{y})^2 + A_5 (\ln \dot{y}) T + A_6 T^2$	A_1 Model coefficient A_2 Model coefficient A_3 Model coefficient, 1/°C A_4 Model coefficient A_5 Model coefficient, 1/°C A_6 Model coefficient, 1/(°C)^2
Cross/Arrhenius model	$\eta = \frac{Be^{T_b/T}\ e^{\beta p}}{1 + \left[\left(\eta_0 \dot{y}\right)/\tau^*\right]^{1-n}}$	η_o Zero shear viscosity, Pa·s n Power law exponent τ^* Shear stress level at which shear thinning begins to manifest itself, Pa T_b Temperature sensitivity factor, K B Constant relating to zero shear viscosity, Pa·s β Factor relating pressure dependence of η_o, 1/Pa p Pressure, Pa

Table B.2 (*continued*)

Cross/WLF model	$\eta = \frac{D_1 e^{\left\{-A_1(T-T_r)/\left[A_2+(T-T_r)\right]\right\}}}{1+\left[\left(\eta_0 \dot{y}\right)/\tau^*\right]^{1-n}}$ where $T_r = D_2 + D_3 p$	η_o	Zero shear viscosity, Pa·s
		n	Power law exponent
		τ^*	Shear stress level at which shear thinning begins to manifest itself, Pa
		T_r	Reference temperature, °C
		D_1	Constant, Pa·s
		D_2	Glass transition temperature at zero pressure, °C
		D_3	Pressure sensitivity factor, °C/Pa
		A_1	Temperature sensitivity factor of viscosity
		A_2	Constant, °C
		p	Pressure, Pa
For all models, η = viscosity, Pa·s; $\dot{y}$ = shear rate, 1/s; T = temperature, °C.			

Table B.3 — Most-common viscosity models employed in extrusion simulation programs

Model in simulation program	Viscosity model	Description of symbol	
Newtonian model	$\eta = Ae^{-b(T-T_r)}$	A	Constant, Pa·s
		b	Temperature sensitivity factor, 1/°C
		T_r	Reference temperature, °C
Power law model	$\eta = Ae^{-b(T-T_r)}\dot{y}^{n-1}$	A	Constant, Pa.s
		b	Temperature sensitivity factor, 1/°C
		T_r	Reference temperature, °C
		n	Power law exponent
Log polynomial model	$\ln \eta = a_1 + a_2 (\ln \dot{y}) + a_3 (\ln \dot{\gamma})^2 + a_4 (T-T_r) + a_5 (T-T_r)^2 + + a_6 (T-T_r)(\ln \dot{y})$	T_r	Reference temperature, °C
		a_1	Model coefficient
		a_2	Model coefficient
		a_3	Model coefficient
		a_4	Model coefficient, 1/°C
		a_5	Model coefficient, 1/(°C)^2
		a_6	Model coefficient, 1/°C

Table B.3 (*continued*)

Cross model	$\eta = \dfrac{\eta_0}{1+\left[\left(\eta_0 \dot{y}\right)/\tau^*\right]^{1-n}}$	η_o	Zero shear viscosity, Pa·s
		τ^*	Shear stress level at which shear thinning begins to manifest itself, Pa
		n	Power law exponent
Carreau model	$\eta = \dfrac{Ae^{-b(T-T_r)}}{\left[1+\left(re^{-b(T-T_r)}\dot{y}\right)^a\right]^{(1-n)/a}}$	η_o	Zero shear viscosity, Pa·s
		A	Model constant, Pa·s
		b	Temperature sensitivity factor, 1/°C
		T_r	Reference temperature, °C
		a	Constant
Simplified form	$\eta = \dfrac{\eta_0}{\left[1+\left(\lambda \dot{y}\right)^2\right]^{(1-n)/2}}$	r	Constant, s
		n	Power law exponent
		λ	Parameter relating to the shear rate for the onset of shear thinning, s
For all models, η = viscosity, Pa·s; $\dot{\gamma}$ = shear rate, 1/s; T = temperature, °C.			

To describe the pvT behaviour for advanced mould filling, packing and cooling analysis, the injection moulding simulation programs employ well-known models. The models employed to fit the measured pvT data in the simulation programs are illustrated in Table B.4. The common input format for the pvT data in Moldflow[2)] simulation program is a set of 13 standard points to describe the pvT behaviour of the material. For a semicrystalline material, seven (7) of these standard points are chosen in the lower temperature region, and four (4) standard points in the upper temperature region with the two (2) remaining standard points relating to boundary points. For an amorphous material, on the other hand, a set of only ten (10) standard points are utilized — four (4) standard points each in the lower and upper temperature region with the two (2) remaining standard points relating to boundary points. These 13 standard points are determined from the best fit of the measured pvT data over a suitable range of temperature and pressure (in accordance with ISO 17744) with the two-region model equations.

2) Moldflow is an example of a product available commercially. This information is given for the convenience of users of this International Standard and does not constitute an endorsement by ISO of this product.

Table B.4 — Common pvT models employed in injection-moulding simulation programs

Model in simulation programs	PvT model	Description of symbol
Two-domain Tait model [employed by C-mould [3] software]	$v(T,p) = v_0(T)\{1 - 0{,}0894 \ln[1 + p/B(T)]\} + v_t(T,p)$ where, if $T > T_t(p)$, $v_0 = b_{1m} + b_{2m}(T - b_5)$ $B(T) = b_{3m} e^{-b_{4m}(T - b_5)}$ $v_t(T,p) = 0$ and, if $T < T_t(p)$, $v_0 = b_{1s} + b_{2s}(T - b_5)$ $B(T) = b_{3s} e^{-b_{4s}(T - b_5)}$ $v_t(T,p) = b_7 e^{b_8(T - b_5) - b_9 p}$	v Specific volume, m^3/kg T Temperature, °C p Pressure, Pa $T_t(p)$ Transition temperature, °C = $b_5 + b_6 p$ b_{1m}, b_{1s} Tait coefficients, m^3/kg b_{2m}, b_{2s} Tait coefficients, $m^3/kg{\cdot}K$ b_{3m}, b_{3s} Tait coefficients, Pa b_{4m}, b_{4s} Tait coefficients, 1/K b_5 Tait coefficient, K b_6 Tait coefficient, K/Pa b_7 Tait coefficient, m^3/kg b_8 Tait coefficient, 1/K b_9 Tait coefficient, 1/Pa
Two-region model [employed by Moldflow [3] software] Semicrystalline material: in the lower temperature region (below T_g) in the upper temperature region (above T_g) and boundary equation Amorphous material: in the lower temperature region (below T_g) in the upper temperature region (above T_g)	$v = \frac{a_1}{a_4 + P} + \frac{a_2 T}{a_3 + P} + a_5 e^{a_6 T - a_7 p}$ $v = \frac{b_1}{b_4 + P} + \frac{b_2 T}{b_3 + P}$ $P = c_1 + c_2 T$ $v = \frac{a_1}{a_4 + P} + \frac{a_2 T}{a_3 + P}$ $v = \frac{b_1}{b_4 + P} + \frac{b_2 T}{b_3 + P}$	a_i = Tait coefficients b_i = Tait coefficients c_i = Tait coefficients

3) C-mould and Moldflow are examples product available commercially. This information is given for the convenience of users of this International Standard and does not constitute an endorsement by ISO of these products.

B.2 Simulation of the injection moulding process

To illustrate the influence of material data for processing simulation, it is important to consider each scenario discussed in 4.3.2, separately.

B.2.1 Illustration of simple mould filling analysis of thermoplastics

To illustrate the use of the material data in simple mould filling analysis of thermoplastics, a single component geometry — an automotive door panel — as shown in Figure B.1, is chosen. The part dimensions and the runner system in the illustration correspond closely to the actual dimensions of the component on a vehicle today. In particular, the thickness of the part is 2,25 mm and the runner system consists of a hot runner with a diameter of 16 mm, tapered sprue having a diameter ranging from 10 mm to 5 mm and fan gate thickness varying from an initial thickness of 4 mm to a junction thickness of 1,5 mm.

The finite element mesh of the part and the runner system is created using shell and beam elements (see Figure B.2). The material selected for this automotive door panel is an unfilled Polypropylene (PP). The material data input needed for the simple mould filling analysis (see Table 5) for this PP material is as follows:

ρ_m = 728 kg/m^3

c_{pm} = 3 400 J/kg °C

k_m = 0,169 W/m °C

T_r = 130 °C

NOTE The C-mould program used in this illustration calls for transition temperature T_r instead of T_s and T_{ej}.

The melt shear viscosity data is measured in accordance with ISO 11443 and material viscosity is represented by the Cross/Arrhenius model.

Simple mould filling simulations are carried out using the C-mould[4)] simulation program. The three cases considered correspond to using apparent viscosity data without any corrections, with Rabinowitsch correction only (correction for the non-Newtonian behaviour) and with both Rabinowitsch and Bagley corrections (for the juncture losses).

The Cross/Arrhenius model coefficients for viscosity data are as follows:

Case i Apparent viscosity data n = 0,251 22

τ^* = 51 845 Pa

B = 0,012 998 Pa·s

T_b = 5 498,5 K

β = 0 Pa^{-1}

Case ii With Rabinowitsch correction n = 0,252 08

only τ^* = 43 216 Pa

B = 0,014 934 Pa·s

4) C-mould is an example of a product available commercially. This information is given for the convenience of users of this International Standard and does not constitute an endorsement by ISO of this product.

T_b = 5 396,3 K

β = 0 Pa^{-1}

Case iii With Rabinowitsch and Bagley n = 0,226 98

corrections τ^* = 45 319 Pa

B = 0,009 970 8 Pa·s

Tb = 5 549,7 K

β = 0 Pa^{-1}

Figure B.3 shows the viscosity versus shear rate data at different temperatures for the three cases.

The following process conditions are used for the filling stage simulation.

— Melt temperature: 240 °C

— Mould temperature: 30 °C

— Fill time: 4 s

The relative injection speed profile is kept constant during filling and the Filling/Packing switch over was set at 97 % volume.

A comparison between the experimental observation of melt front advancement from a series of short shots and the result of the numerical simulation in the case without any corrections, as shown in Figure B.4, demonstrates a good correlation between numerical simulation and experiment in term of melt front description.

The influence of the corrections on pressure distribution for the three cases are shown in Figures B.5 to B.7. The differences in terms of maximum pressure (important for the determination of the machine size as well as the appearance and mechanical quality of the final part) are worth noting. The 17 % difference in maximum pressure observed between Case i (without correction) and Case iii (with complete corrections) clearly illustrates the importance of taking into consideration the corrections to viscosity data on the final results of moulding simulation and, consequently, on the prediction of the final part properties.

B.2.2 Illustration of advanced mould filling, packing and cooling analysis of thermoplastics

Use of the material data in advanced mould filling, packing and cooling analysis of thermoplastics is illustrated with the example of an automotive rocker cover (see Figure B.8). The part size corresponds to a total volume of 953,5 cm^3. The part dimensions are 500 mm × 250 mm × 100 mm and a global thickness of 3,0 mm, while the local thicknesses range between 1,5 mm (at the ribs) and 2,5 mm (at the flange).

For the advanced mould filling simulation, the MF/flow module of the Moldflow[5)] simulation program is selected. The material selected for the rocker cover is Minlon[6)] EFE6053, a PA 66 grade containing 24 % glass fibre and 16 % mineral filler. The material data input required for the advanced filling, packing and cooling analysis (see Table 6) is as follows:

5) Moldflow is an example of a product available commercially. This information is given for the convenience of users of this International Standard and does not constitute an endorsement by ISO of this product.

6) Minlon® is the trade name of a product supplied by DuPont. This information is given for the convenience of users of this International Standard and does not constitute an endorsement by ISO of the product named. Equivalent products may be used if they can be shown to lead to the same results.

c_{pm} = 2 554 J/kg °C

k_m = 0,271 4 W/m °C

NOTE Although the input for c_p and k in advanced filling analysis generally requires these values as a function of temperature (Table 6), for simplification, single values corresponding to the melt state are used for this illustration.

T_s = 235 °C

T_{ej} = 203 °C

The melt shear viscosity data are measured in accordance with ISO 11443 and a second-order model is chosen to represent the material viscosity. The second order viscosity matrix input values for this material are:

Temperature (°C)	Shear Rate (1/s)	Viscosity (Pa·s)
275	1 000	285,6
295	100	279,8
295	1 000	147,6
295	10 000	48,3
315	100	130,2
315	1 000	76,8

For the pvT data needed to account for melt compressibility in the packing phase, the 13 standard data point input values are:

Temperature (°C)	Pressure (MPa)	Specific volume (m3/kg)
0,0	0	0,000 667 25
0,0	160	0,000 654 27
20,0	0	0,000 671 84
20,0	160	0,000 656 71
245,2	0	0,000 733 82
252,1	80	0,000 713 06
256,3	160	0,000 697 84
261,0	0	0,000 759 58
269,9	160	0,000 715 00
270,0	0	0,000 762 97
270,0	160	0,000 715 01
310,0	0	0,000 778 03
310,0	160	0,000 724 09

The processing conditions used in the simulation are the following.

Melt temperature: 295 °C

Mould temperature: 90 °C

Injection time: 2,5 s

Flow rate: 377 cm^3/s

At 82 % filling, an injection pressure of 100 MPa is reached. At this stage the injection pressure is kept constant, which leads to a reduced flow-rate of 32,5 % at 100 % filling after 3,0 s.

Figures B.9 to B.12 show the results of the filling analysis for a balanced runner system with two gates each having identical dimensions of 2,0 mm diameter and 2,0 mm length. The initial pressure drop over the runners and gates was computed to be 20 MPa. Due to shear heating the flow-front temperatures increase from 295 °C (melt temperature) to 302,8 °C (see also Figure B.11) — a temperature increase of almost 8 °C. Employing a slower injection rate looks like an obvious option, however, the amount of frozen layer thickness will increase in that case much higher than the 72 % obtained with 3,0 s injection time (see Figure B.12). Proper packing of the areas with the highest amounts of frozen layer can then become difficult.

For the packing analysis, the packing pressure was decreased linearly from 100 MPa at the end of filling to 60 MPa in 4 s and reduced to 0 MPa, in the next 1 s, accounting for a total packing time of 5 s. The computed results are shown in Figures B.13 and B.14. Figure B.13 shows the pressure distribution in each of the elements of the model during the 5 s packing interval while Figure B.14 shows the amount of frozen layer thickness at the end of packing, in %. Though some thick elements still contain molten material in their central layer, it is obvious that after 5 s further packing makes less sense because some cover sections are almost completely frozen. Such results are useful in determining when to remove packing pressure.

The cooling analysis is based on the results of the filling analysis assuming a packing time of 5 s, a cooling time of 25 s and a clamp-open time of 5 s. Figure B.8 shows the three (3) cooling circuits, (diameter of 10 mm), designed for this part. The cooling circuits are assumed to be placed in a cavity made out of P20 steel, or a material with a similar thermal conductivity. In each of the circuits a flow rate of 10 l/min of water is assumed, with an inlet temperature of 80 °C compared with estimated mean cavity temperature of 90 °C. Figure B.15 shows the maximum temperatures close to the central layers of the elements. It can be seen that the 12 mm and 8 mm thick runners clearly have the highest temperatures. After 25 s, the maximum temperature in the cover is still about 220 °C, at the 5 mm thick rings in the four (4) holes in the cover. In order to avoid too much deformation of the cover due to ejection forces (which, of course, are dependent on the placement of the ejector pins), a longer cooling time might be appropriate. Figure B.16 shows the average temperatures over the thickness after 25 s cooling time and Figure B.17 shows the temperature difference between the top and bottom surfaces of the elements of the model. In Figure 17, the red elements have a much hotter top surface and the blue elements a much hotter bottom surface. Better cooling of these spots may not only result in a reduced cycle time, but also in less warpage because of more uniform temperatures at ejection.

B.2.3 Illustration of shrinkage/warpage analysis

The use of material data in shrinkage/warpage analysis will be illustrated with the same automotive rocker cover part as described in B.2.2 using the shrinkage/warpage analysis modules MF/shrink and MF/warp of the Moldflow [7)] simulation program.

The MF/shrink module uses shrinkage coefficients as measured by Moldflow in a designed experiment involving 40 combinations of the key moulding variables such as melt temperature, mould temperature, injection speed, and cavity pressure at hold. From the measured shrinkage values, the shrinkage coefficients are determined using the relationships which account for contributions from each of the main factors that influence the shrinkage of the material as the melt cools in the mould:

7) Moldflow is an example of a product available commercially. This information is given for the convenience of users of this International Standard and does not constitute an endorsement by ISO of this product.

$S_{Mp} = a_1 M (S_{pvT}) + a_2 M$ (crystallization) + $a_3 M$ (mould restraints) + $a_4 M$ (orientation) + a_5

$S_{Mn} = b_1 M (S_{pvT}) + b_2 M$ (crystallization) + $b_3 M$ (mould restraints) + $b_4 M$ (orientation) + b_5

where

S_{Mp}, S_{Mn} are components of shrinkage parallel and normal to the material orientation direction;

S_{pvT} is the volumetric shrinkage due to material pvT characteristics;

M_i are functions describing shrinkage due to indicated factors;

a_i, b_i are shrinkage coefficients in the parallel and normal shrinkage models.

For the material used in this illustration, Minlon EFE6053[8] — PA 66 grade containing 24 % glass fibre and 16 % mineral filler — the material data input for the shrinkage/warpage analysis (see Table 8) is as follows:

E_p = 8 250 MPa

E_n = 6 000 MPa

ν_{pn} = 0,35

ν_{nt} = 0,48 (computed from E_p, E_n and ν_{pn} values by the program)

G_p = 2 472 MPa (computed from E_p, E_n and ν_{pn} values by the program)

a_5 = 0,003 4 (corresponding to S_{Mp} = 0.34 %)

b_5 = 0,011 (corresponding to S_{Mn} = 1.1 %)

In view of the significantly larger influence of orientation on shrinkage for a highly filled material such as compared to other factors, all other shrinkage coefficients related to volumetric changes due to pressure and temperature changes during solidification of the melt, crystallization or mould restraints are set to 0,0. It is further assumed that the cavity has uniform surface temperature at ejection.

For the definition of the reference planes for the computed deformations (zero deformations, boundary conditions), the following constraints were set:

— for X-deformations (i.e. shrinkage in length direction), one corner point near gate at long, straight edge;

— for Y-deformations (i.e. shrinkage in width direction), two corner points at long, straight edge;

— for Z-deformations (i.e. warpage of seal face), three corner points at long, straight edge and at short edge of gates.

The results of the shrinkage/warpage analysis are presented in Figures B.18 and B.19. From Figure B.18, the computed shrinkage for the rocker cover over the long straight edge is shown to be equal to 0,46 % compared with a shrinkage of 0,34 % parallel to flow. From Figure B.19, it follows that the computed warpage is 3,2 mm (displacement of Corner 4 versus other 3 corners, which are fixed).

8) Minlon® is the trade name of a product supplied by DuPont. This information is given for the convenience of users of this International Standard and does not constitute an endorsement by ISO of the product named. Equivalent products may be used if they can be shown to lead to the same results.

B.3 Simulation of the extrusion process

The illustrations in this section are intended to demonstrate the use of relevant material data in the simulation of polymer melt flow in two different types of dies: a coat hanger die commonly used in sheet extrusion and a profile die typically used in the extrusion of plastic profile shapes.

B.3.1 Illustration of analysis of polymer melting in the extruder

Independent of the extruded shape itself — sheet, film or profile — the first step involved is the analysis of polymer melting in the extruder. The analysis involves three steps:

a) transport of the solid particles of polymer by drag induced flow with isothermal heat transfer;

b) melting of the polymer particles;

c) isothermal incompressible flow of the homogeneous melt.

To illustrate the analysis of polymer melting in the extruder, a conventional screw geometry with a 90 mm diameter screw (an L/D of 24 consisting of three (3) zones and constant single flight) and a 90 mm diameter smooth barrel is chosen. The material selected is a PE-LD resin. The material input temperature is set at 30 °C and screw revolutions per minute are set at 80. For the simulation, EXTRUCAD[9)] 3.0 software was used.

The material data input required for the analysis (see Table 9) is as follows:

T_m = 110 °C

ΔH_f = 12 978 5 J/kg

ρ_b = 595 kg/m^3

ρ_s = 919 kg/m^3

ρ_m = 775 kg/m^3

c_{pm} = 2 600 J/kg °C

c_{ps} = 2 595 J/kg °C

k_m = 0,18 W/m °C

μ_b = 0,3 (assuming a smooth barrel)

μ_s = 0,25 (assuming a smooth screw surface)

NOTE The dynamic friction coefficients μ_b and μ_s are generally difficult to measure. Very often, the roughness of the barrel and screw surface is accounted for in the value of these parameters. For μ_b, a common practice is to use a value of 0,3 for a smooth barrel, 0,45 for a rough barrel and 1,00 for a grooved barrel. Similarly, a value of 0,25 for a smooth screw surface and 0,35 for a corroded screw surface is used as default value for μ_s.

The melt shear viscosity, $\eta(T, \dot{y})$ is represented by the Carreau model, which does not take into account extensional flow contributions. The Carreau coefficients for this PE-LD resin are as follows:

A = 6 500 Pa·s

9) EXTRUCAD is the trade name of a product supplied by PolyDynamics. This information is given for the convenience of users of this International Standard and does not constitute an endorsement by ISO of the product named. Equivalent products may be used if they can be shown to lead to the same results.

b = 0,018 1/°C

r = 1 s

a = 2

n = 0,48

T_r = 180 °C

The flow analysis involves finite difference computations allowing estimation of bulk temperature, distributions of pressure and shear stress, and the energy flux between the barrel and the material along the extruder length for a given mass flow rate. Figure B.20 illustrates the computed bulk temperature along the screw length, while the distributions of average pressure and shear stress along the screw length are shown in Figures B.21 and B.22 respectively. Figure B.23 illustrates the distribution of computed total energy flux between the barrel and the material.

B.3.2 Illustration of the analysis of sheet extrusion process — Polymer melt flow in a coat hanger die

The analysis of a sheet extrusion process is illustrated with the same PE-LD material used above in B.3.1. The polymer melting analysis in the extruder is the same as described in B.3.1. A coat hanger die is chosen for the simulation of polymer melt flow in the die. For the simulation, the FLATCAD[10)] 3.0 software is selected.

Finite difference computations in the die allow estimation of bulk temperature, pressure and average residence time distributions in the die for a given mass flow rate. The results are shown in Figures B.24 to B.26.

B.3.3 Illustration of the analysis of profile extrusion process — polymer melt flow in a profile die

The analysis of a profile extrusion process is illustrated with a simple T-shaped profile using PROFILECAD[12)] 3.0 software. A conventional screw geometry with a 90 mm diameter screw (an L/D of 24 consisting of 3 zones and constant single flight) and a 90 mm diameter smooth barrel is chosen. The material selected is a PVC resin. The material input temperature is set at 30 °C and screw revolutions per minute is set at 100. The material data inputs required for the polymer melting analysis in the extruder (see Table 9) are as follows:

T_m = 190 °C

ΔH_f = 0°J/kg (amorphous material)

ρ_b = 530 kg/m^3

ρ_s = 1 340 kg/m^3

ρ_m = 1 050 kg/m^3

c_{pm} = 2 200 J/kg °C

c_{ps} = 2 320 J/kg °C

k_m = 0,182 W/m °C

10) FLATCAD and PROFILECAD are the trade names of products supplied by PolyDynamics. This information is given for the convenience of users of this International Standard and does not constitute an endorsement by ISO of the products named. Equivalent products may be used if they can be shown to lead to the same results.

μ_b = 0,3 (assuming a smooth barrel)

μ_s = 0,25 (assuming a smooth screw surface)

NOTE Very often, the roughness of the barrel and screw surface is accounted for in the value of the parameters μ_b and μ_s. For μ_b, a common practice is to use a value of 0,3 for a smooth barrel, 0,45 for a rough barrel and 1,00 for a grooved barrel. Similarly, a value of 0,25 for a smooth screw surface and 0,35 for a corroded screw surface is used as default value for μ_s.

Using a log polynomial viscosity model for PVC, the data input for the model coefficients is as follows:

a_1 = 11,784

a_2 = – 0,6391

a_3 = – 1,127 44 E-02

a_4 = – 1,834 49 E-02 °C^{-1}

a_5 = 8,784 48 E-06 °C^{-2}

a_6 = 9,665 12 E-04 °C^{-1}

T_r = 0 °C

Since polymer melting analysis has already been described in B.3.1, only the simulation of polymer melt flow in the profile die is presented here. Finite difference computations allow estimation of total stress, shear rate, and velocity distributions in the die for a given mass flow rate. The results are shown in Figures B.27 to B.29.

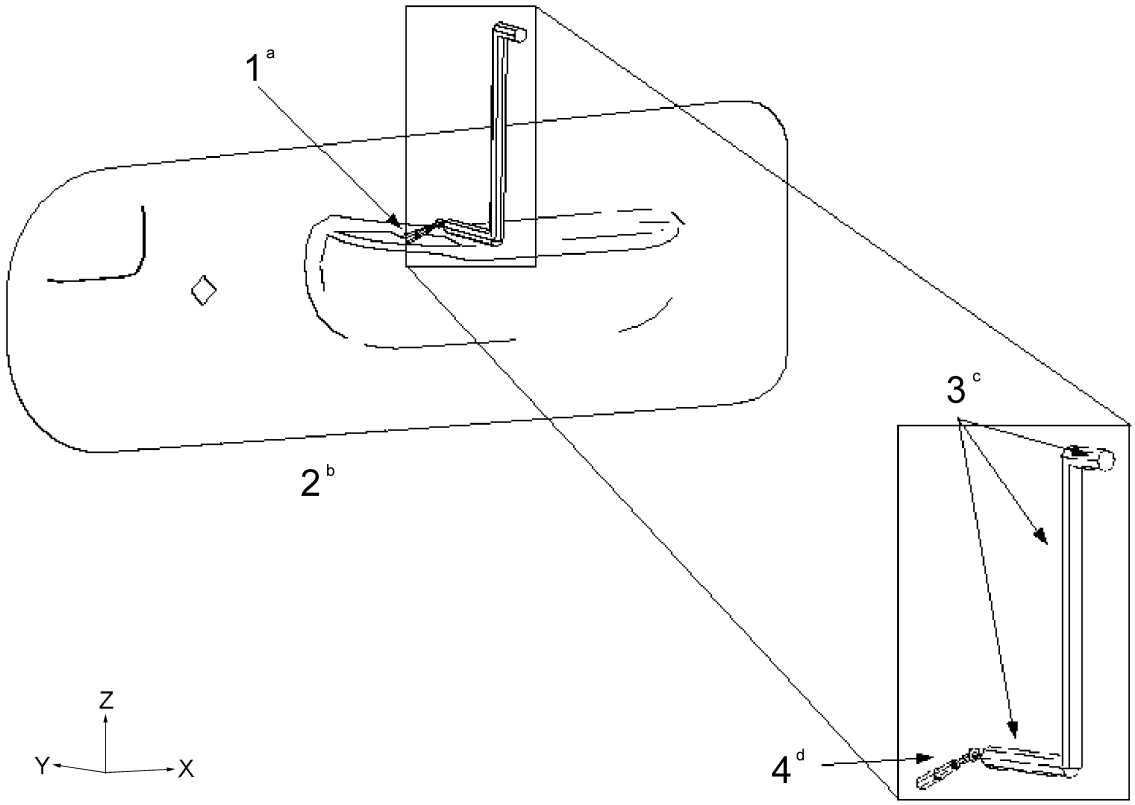

Key

1 fan gate
2 main part
3 hot runner
4 sprue
a Initial thickness = 4 mm; final thickness = 1,5 mm.
b Thickness = 2,25 mm.
c Diameter = 16 mm.
d Diameter = 5 to 10 mm.

Figure B.1 — Automotive door panel geometry and runner system

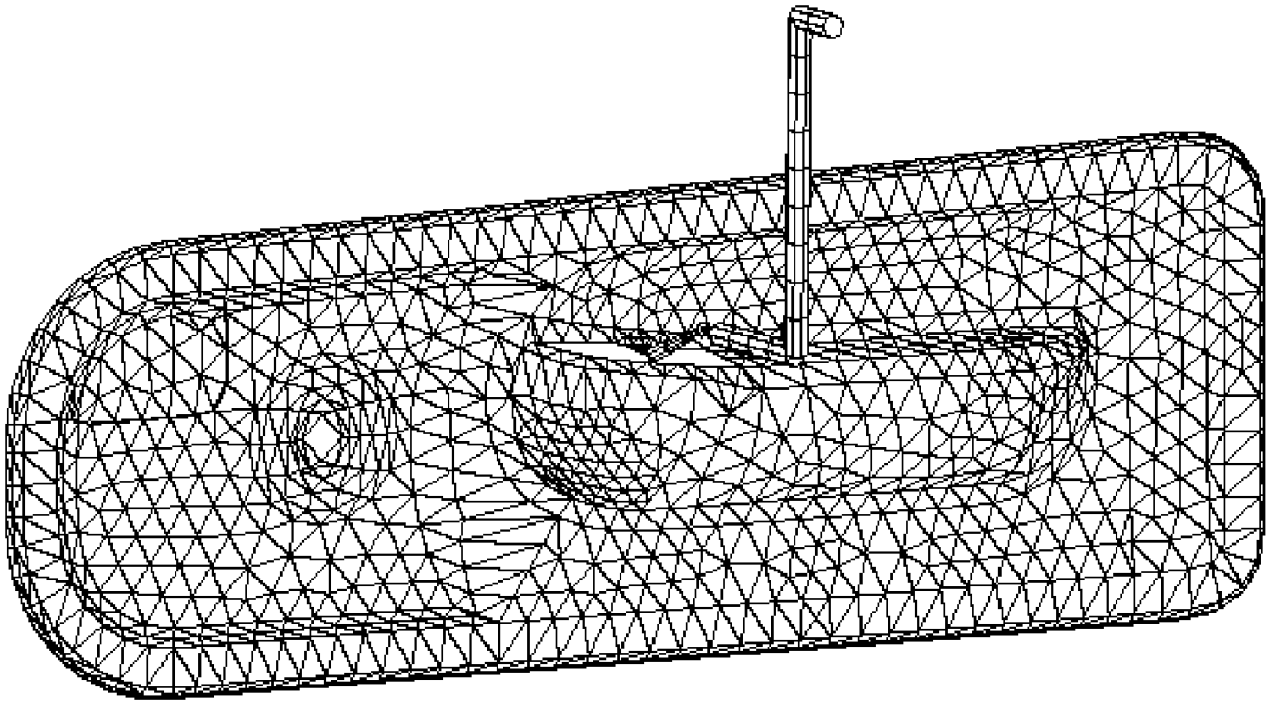

Figure B.2 — Finite element mesh used for the simple injection moulding simulation of the automotive door panel

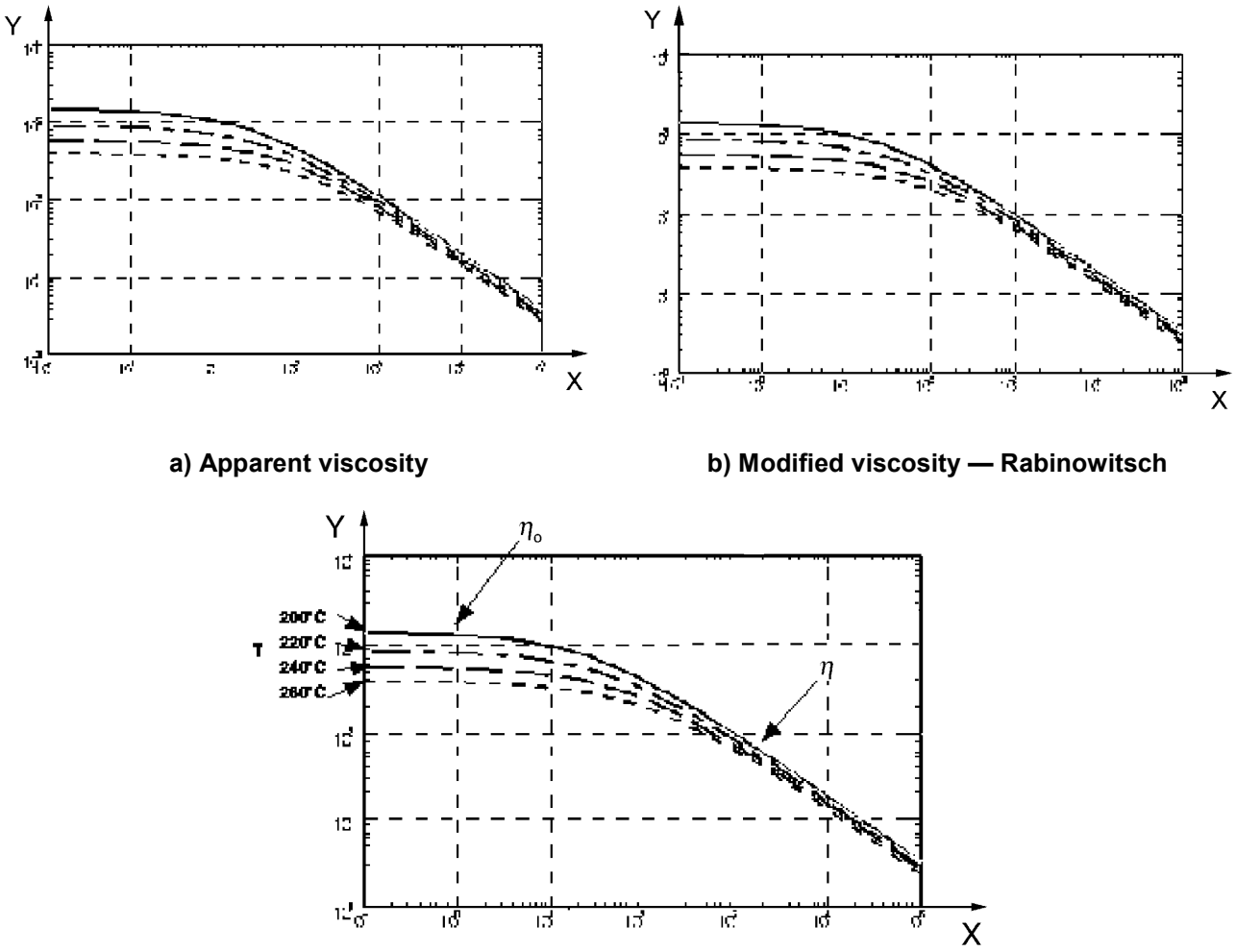

a) Apparent viscosity

b) Modified viscosity — Rabinowitsch

c) Modified viscosity — Rabinowitsch + Bagley

Key

X shear rate, 1/s

Y viscosity, Pa·s

η_o Newtonian value

η slope: shear rate dependency parameter

Figure B.3 — Representation of viscosity vs. shear rate data at different temperatures for the three cases

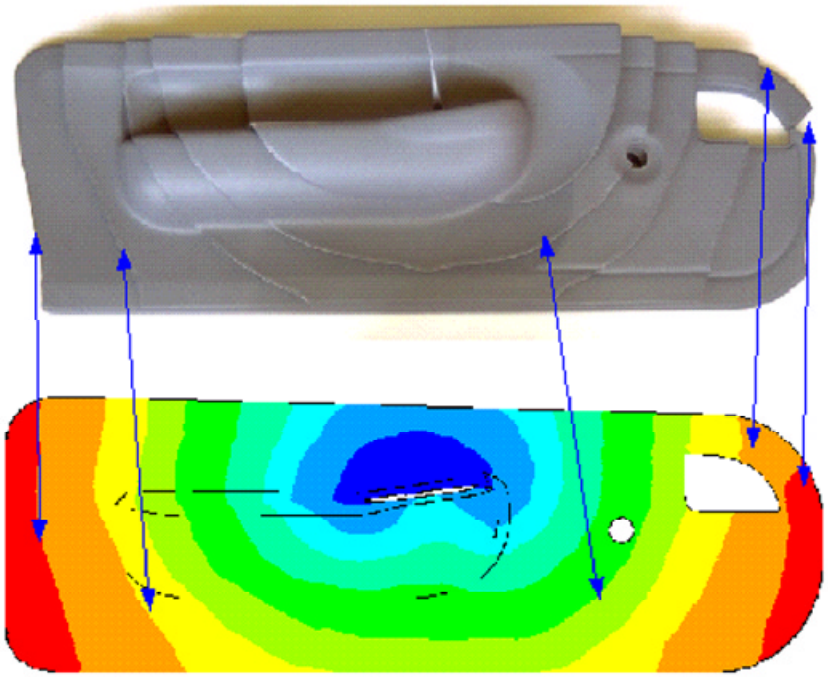

Figure B.4 — Comparison of the experimental short shots and the numerical simulation melt front advancement

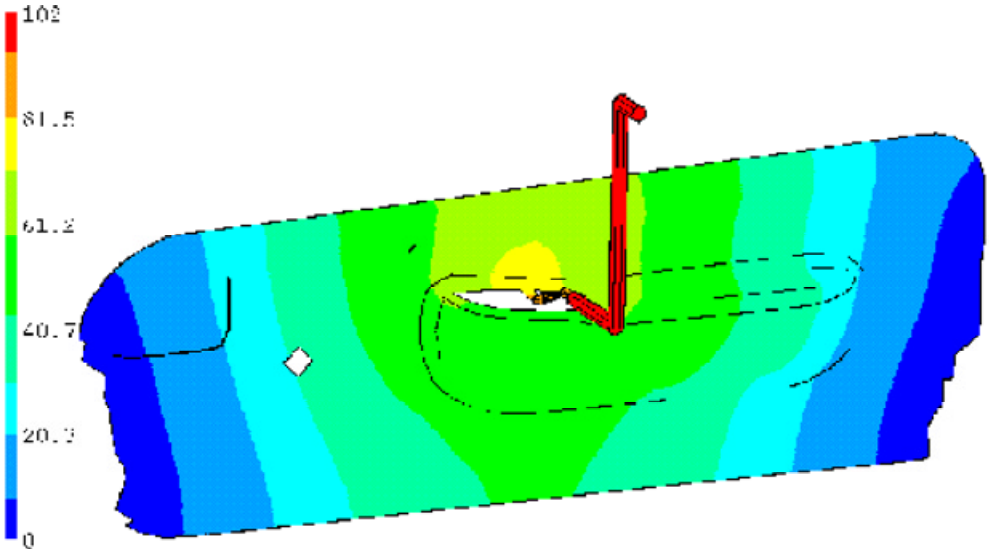

Apparent viscosity: P_{max} = 105 MPa

Figure B.5 — Pressure distribution at the end of filling stage for Case i (using the apparent viscosity)

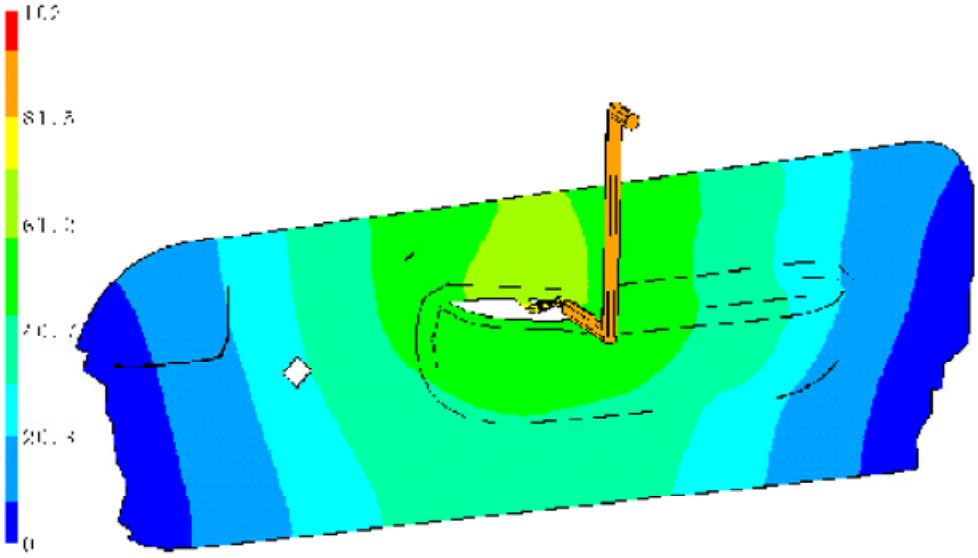

Modified viscosity — Rabinowitsch: P_{max} = 93 MPa (– 11 %)

Figure B.6 — Pressure distribution at the end of filling stage for Case ii (using the modified viscosity with Rabinowitsch correction only)

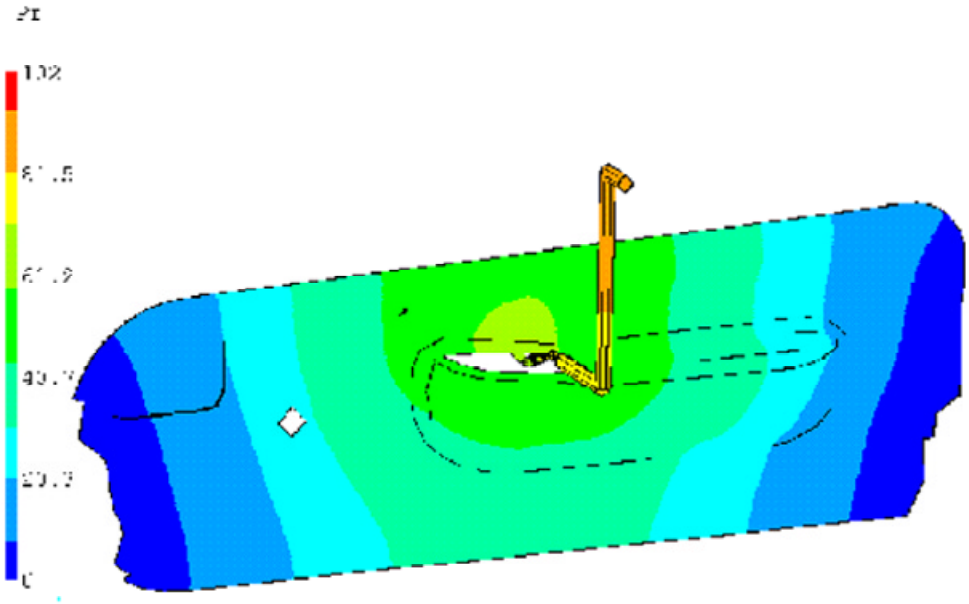

Modified viscosity — Rabinowitsch + Bagley: P_{max} = 87 MPa (– 17 %)

Figure B.7 — Pressure distribution at the end of filling stage for Case iii (using the modified viscosity with Rabinowitsch and Bagley corrections)

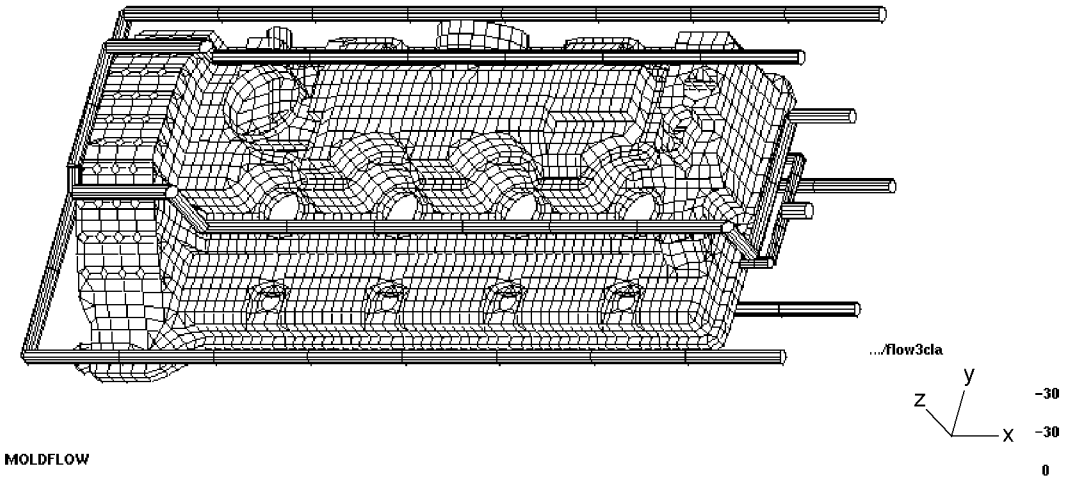

Figure B.8 — Model of the rocker cover illustrating the finite element mesh and cooling lines

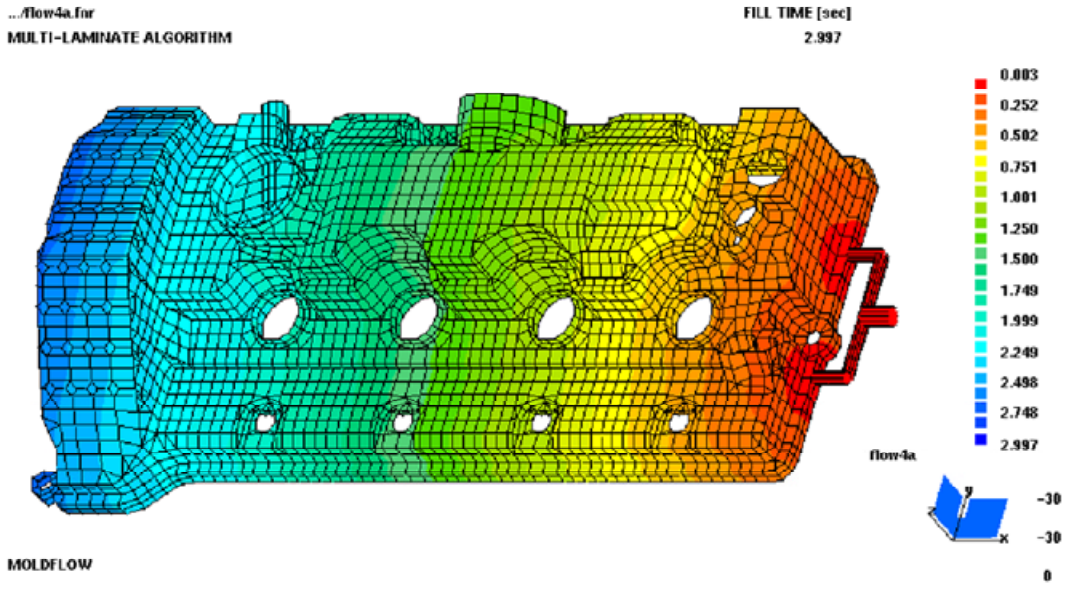

Figure B.9 — Computed melt front position versus time for the rocker cover

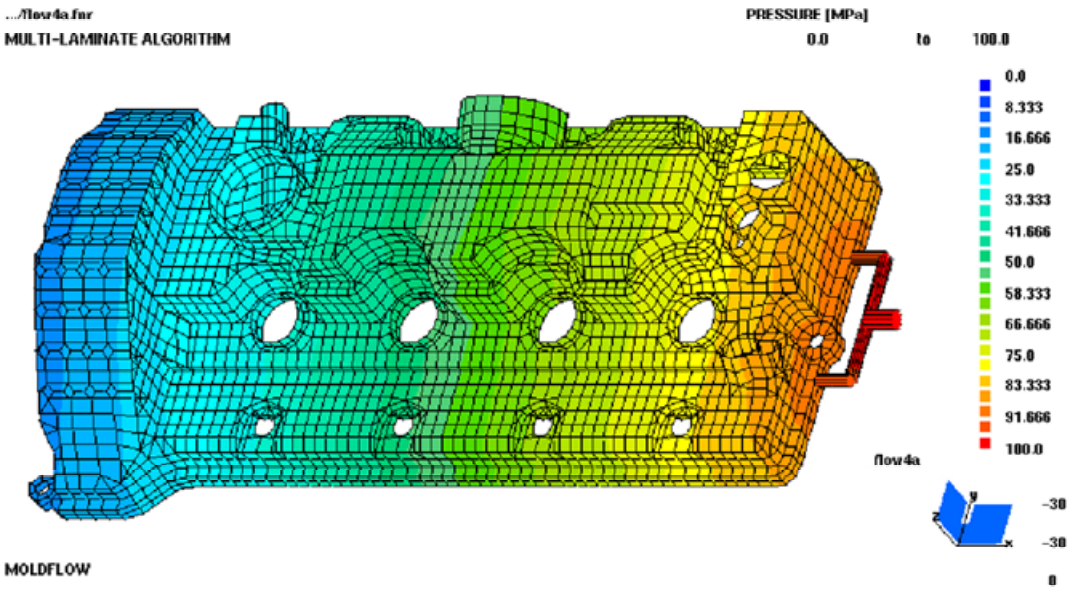

Figure B.10 — Pressure distribution at the end of filling (i.e. start of packing)

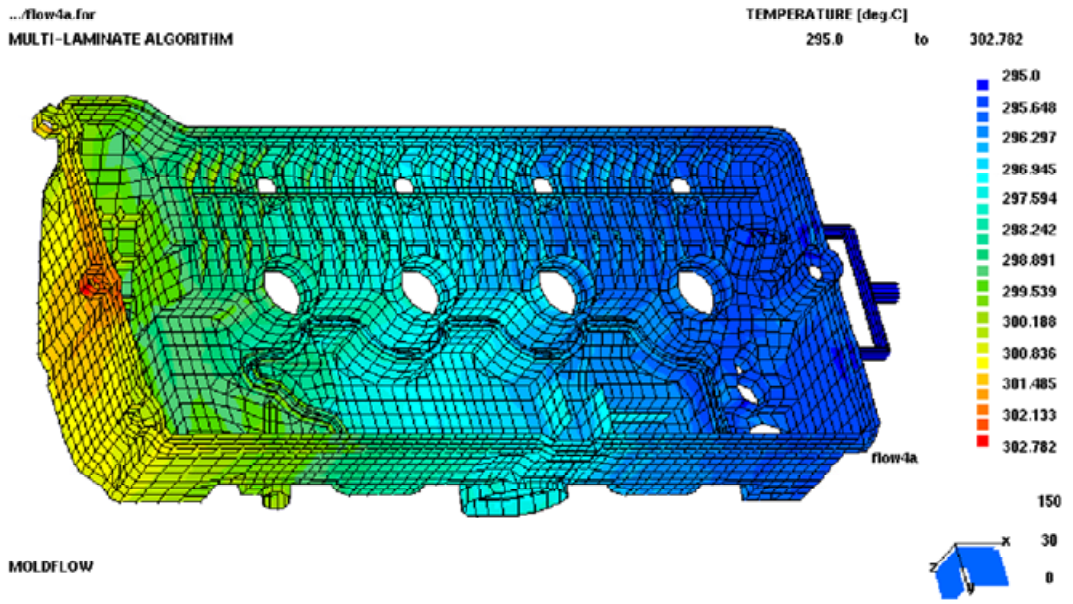

Figure B.11 — Computed temperatures for the melt flow-front, when passing through the cover

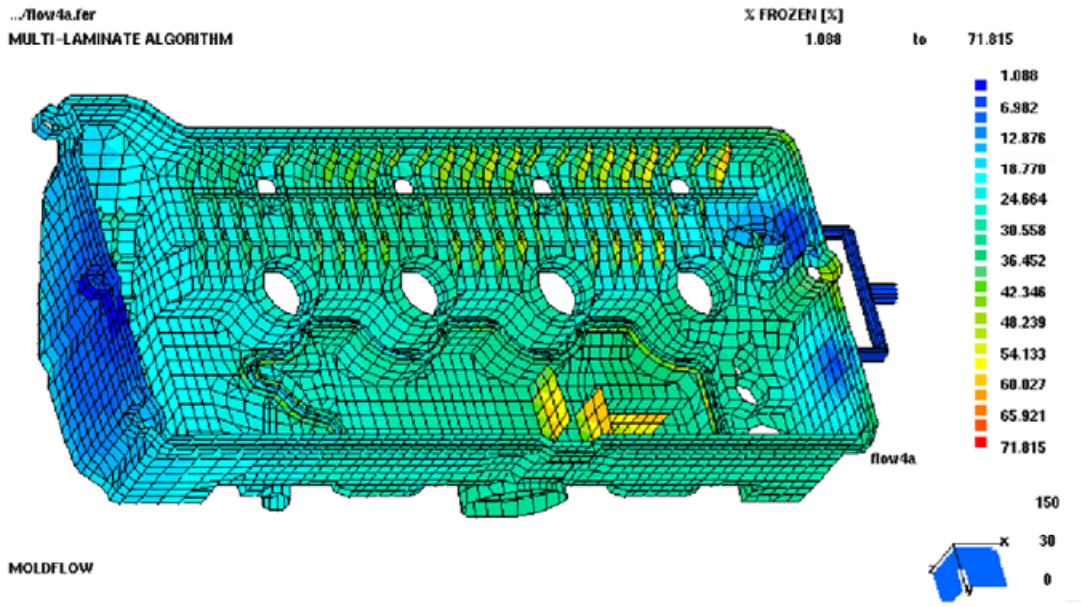

Figure B.12 — Computed frozen layer thickness (%) at the end of filling

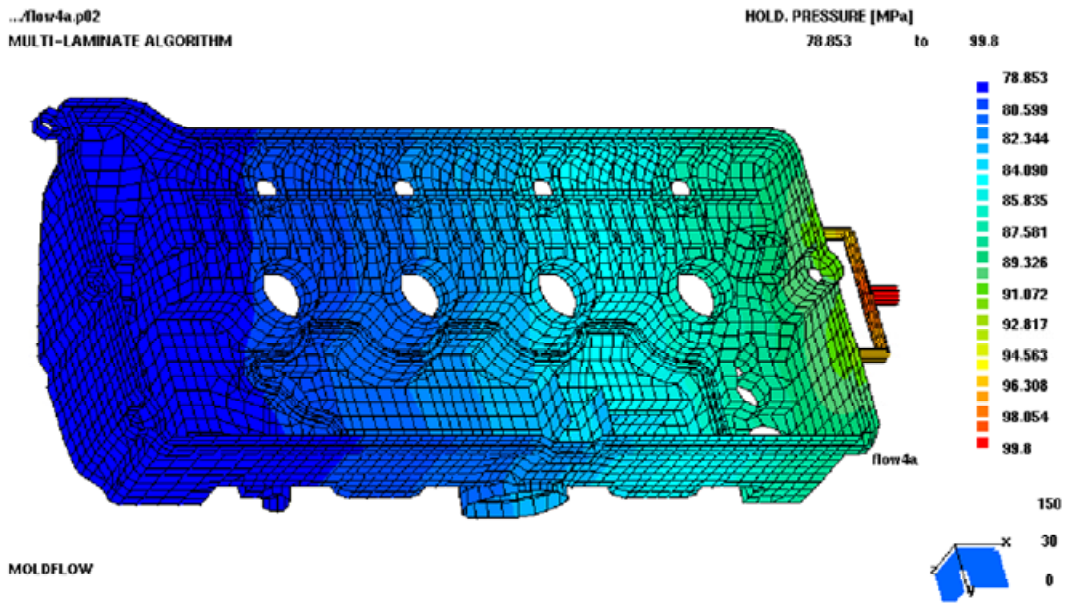

Figure B.13 — Computed (maximum) pressure during packing

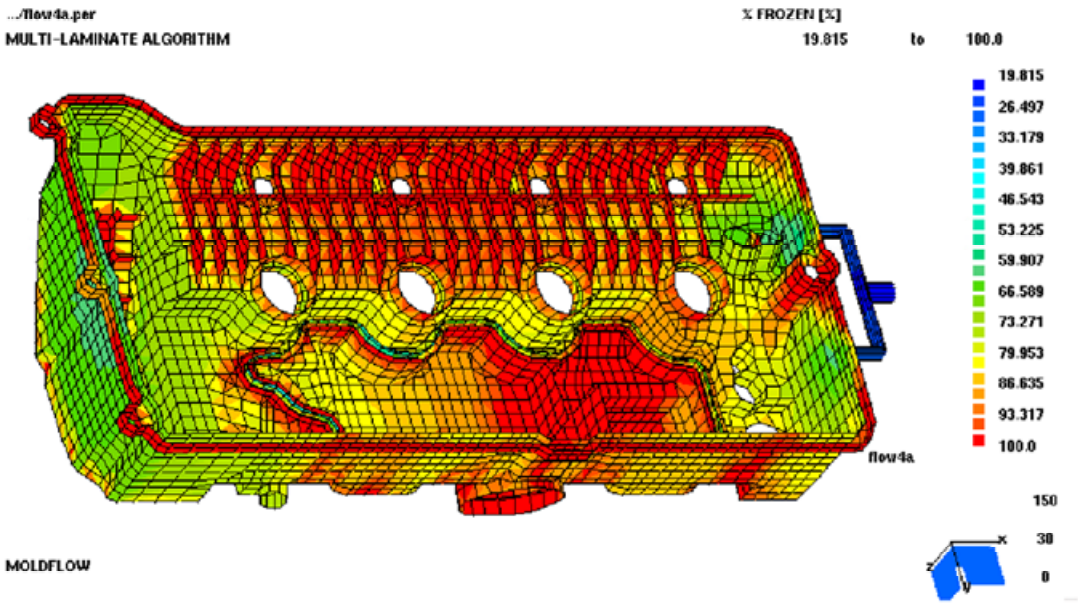

Figure B.14 — Computed frozen layer thickness % at the end of (5 s) packing

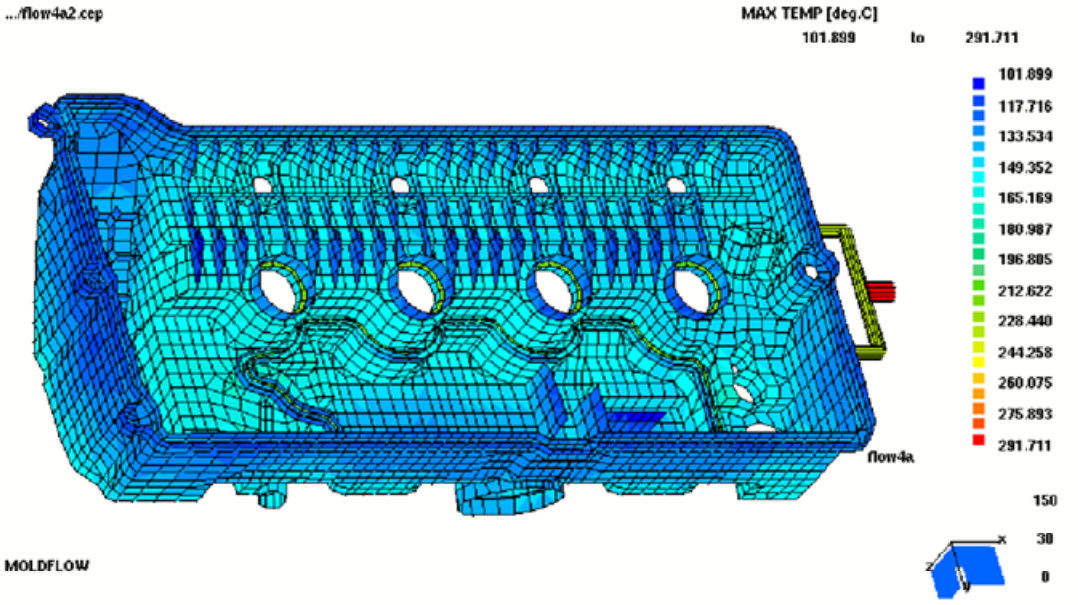

Figure B.15 — Computed maximum temperatures over thickness after 25 s cooling

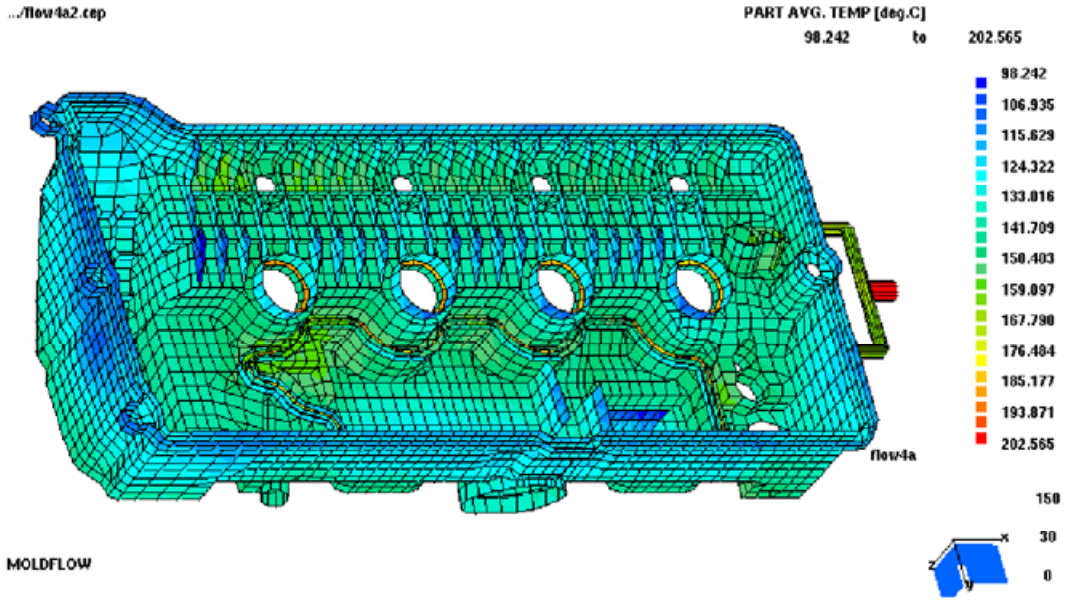

Figure B.16 — Computed average temperature over thickness after 25 s cooling

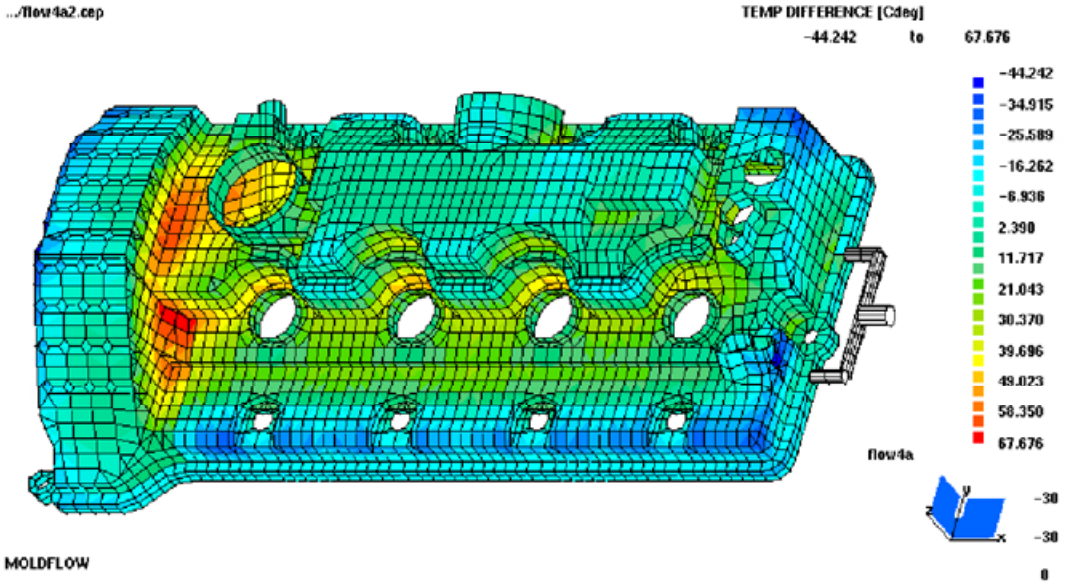

Figure B.17 — Computed temperature difference (top-bottom) after 25 s cooling

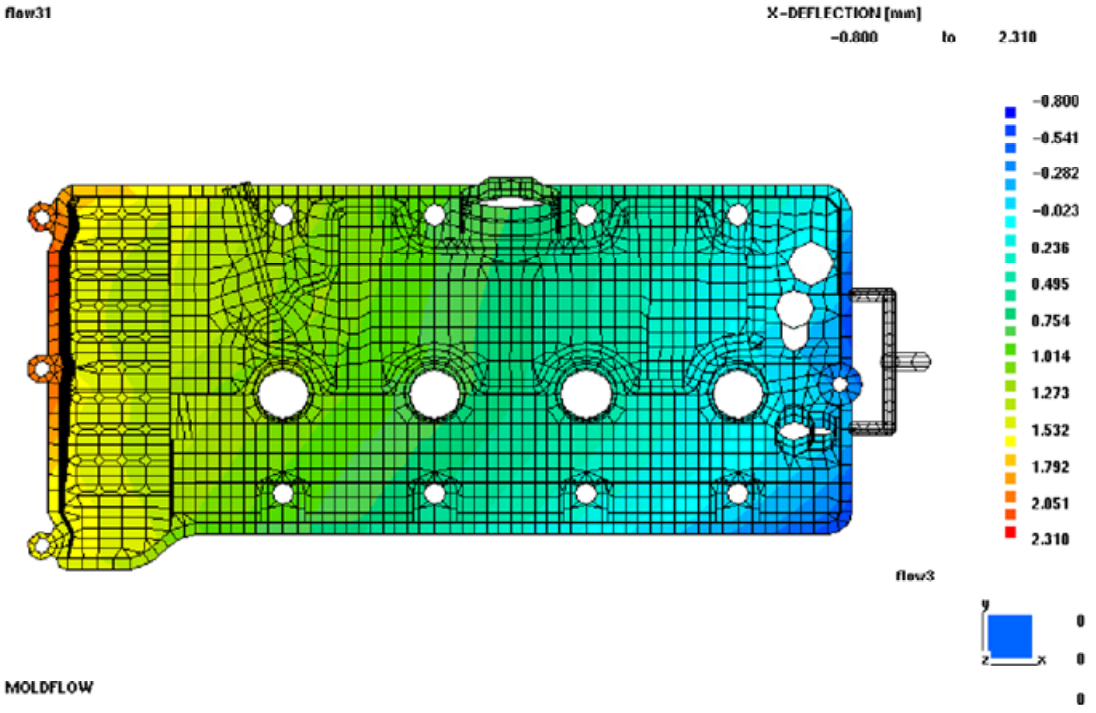

Figure B.18 — Computed deformations in X-direction for the rocker cover

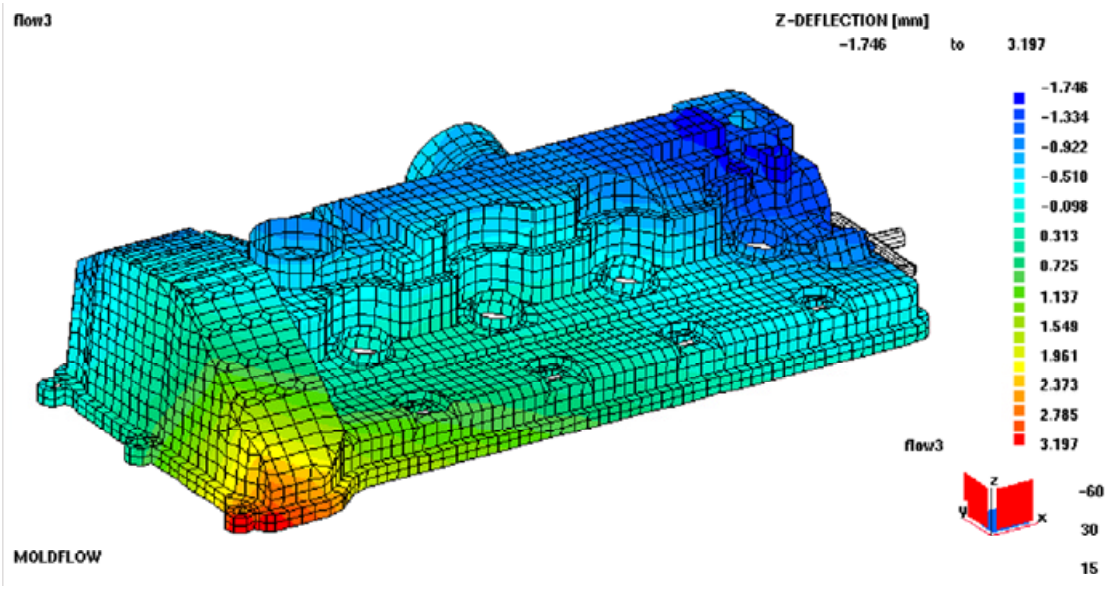

Figure B.19 —Computed deformations in Z-direction (warpage) for the rocker cover

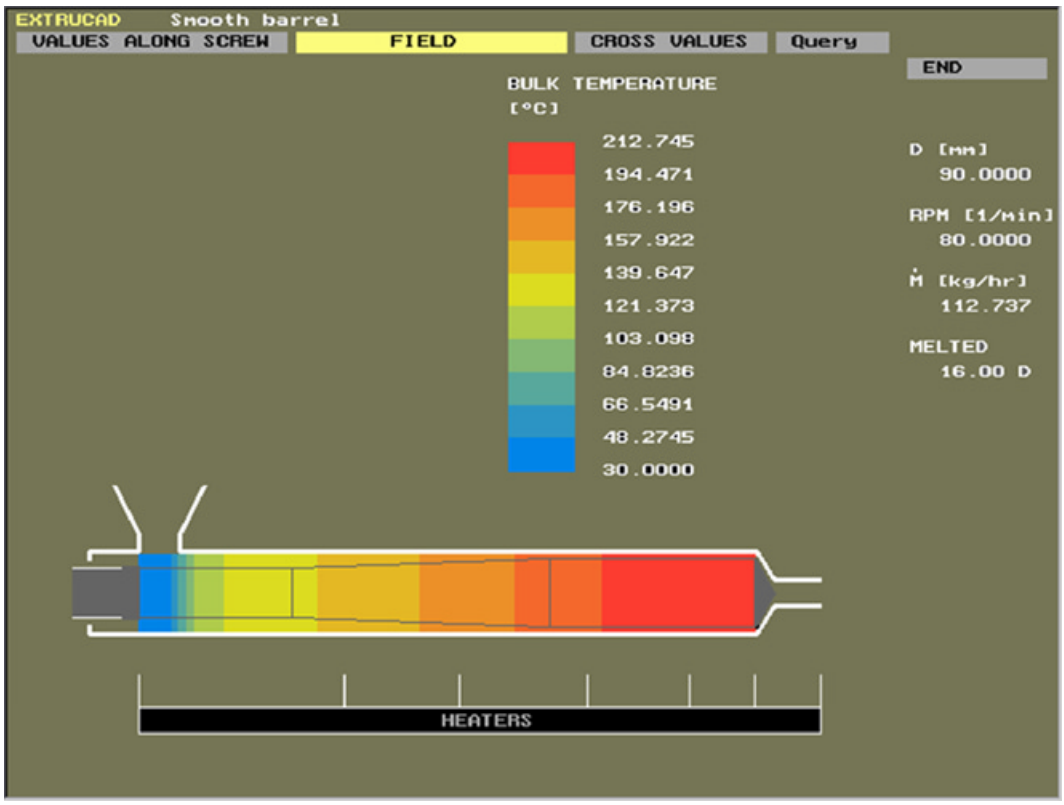

Figure B.20 — Computed bulk temperature distribution along the screw length

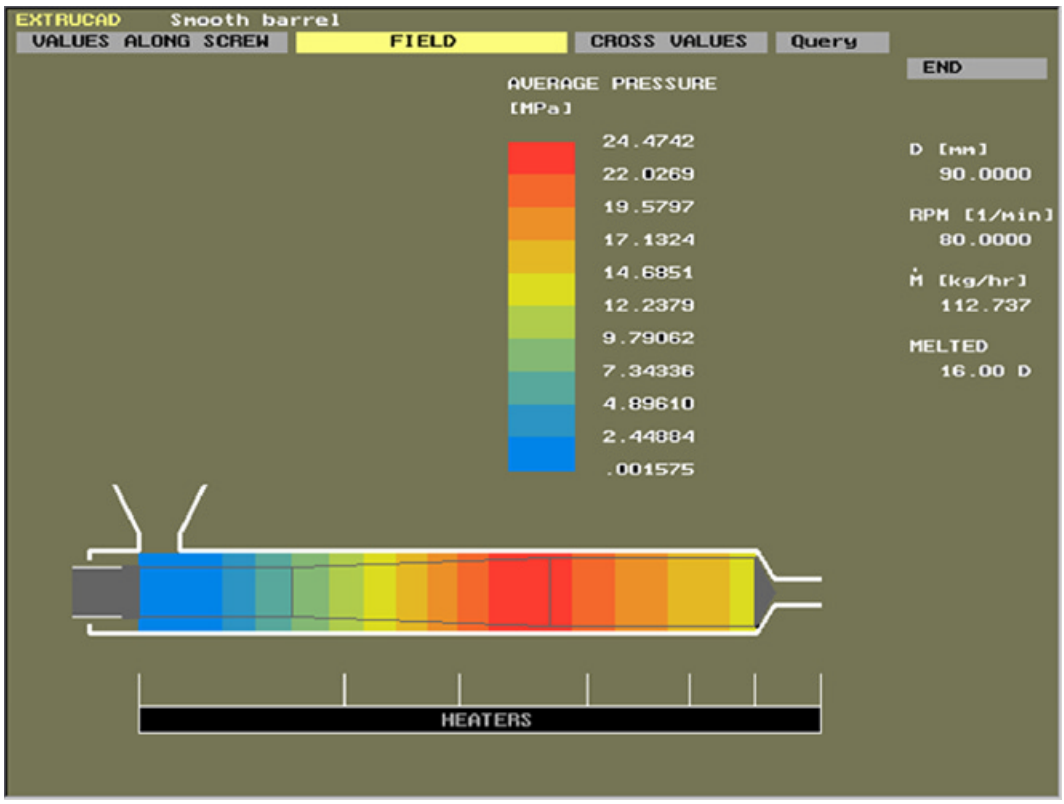

Figure B.21 — Computed average pressure distribution along the screw length

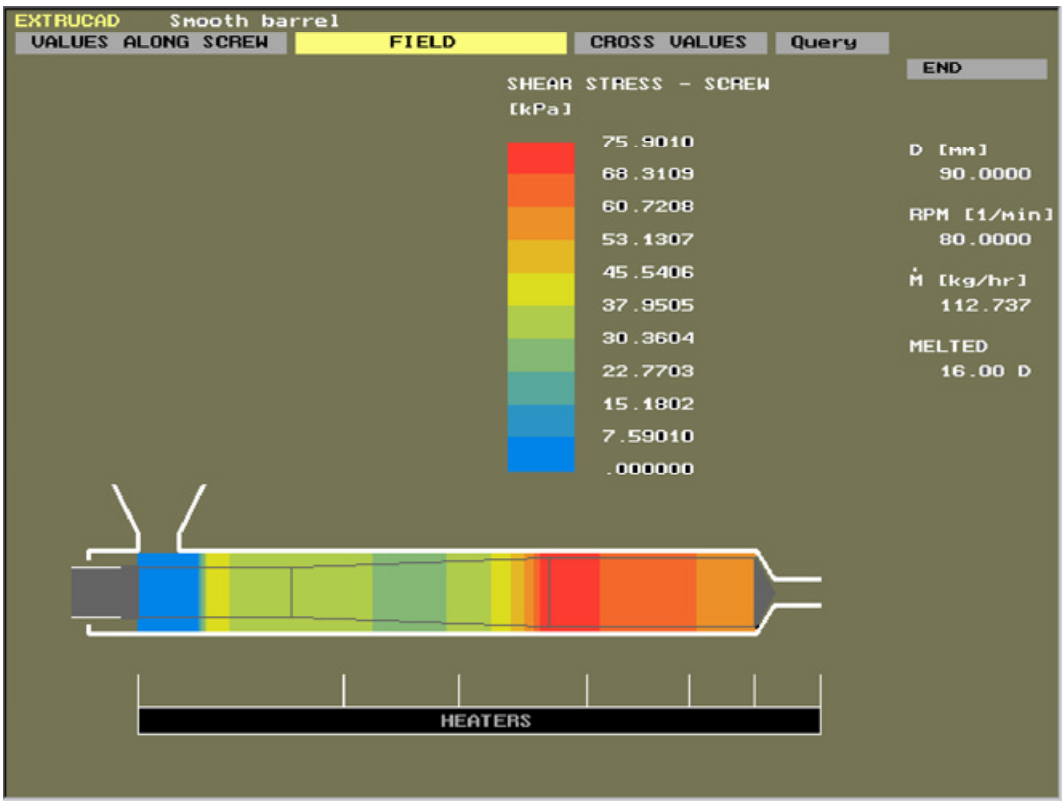

Figure B.22 — Computed distribution of shear stress at the screw surface along the screw length

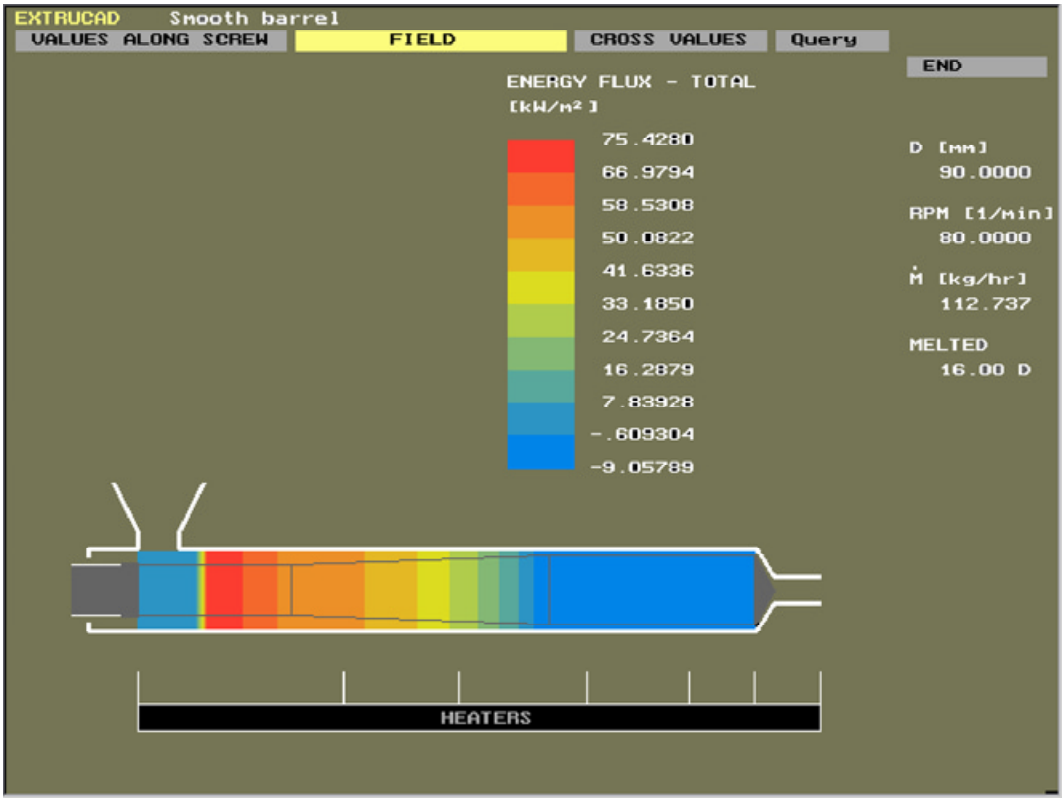

Figure B.23 — Computed distribution of total energy flux between the barrel and the material along the screw length

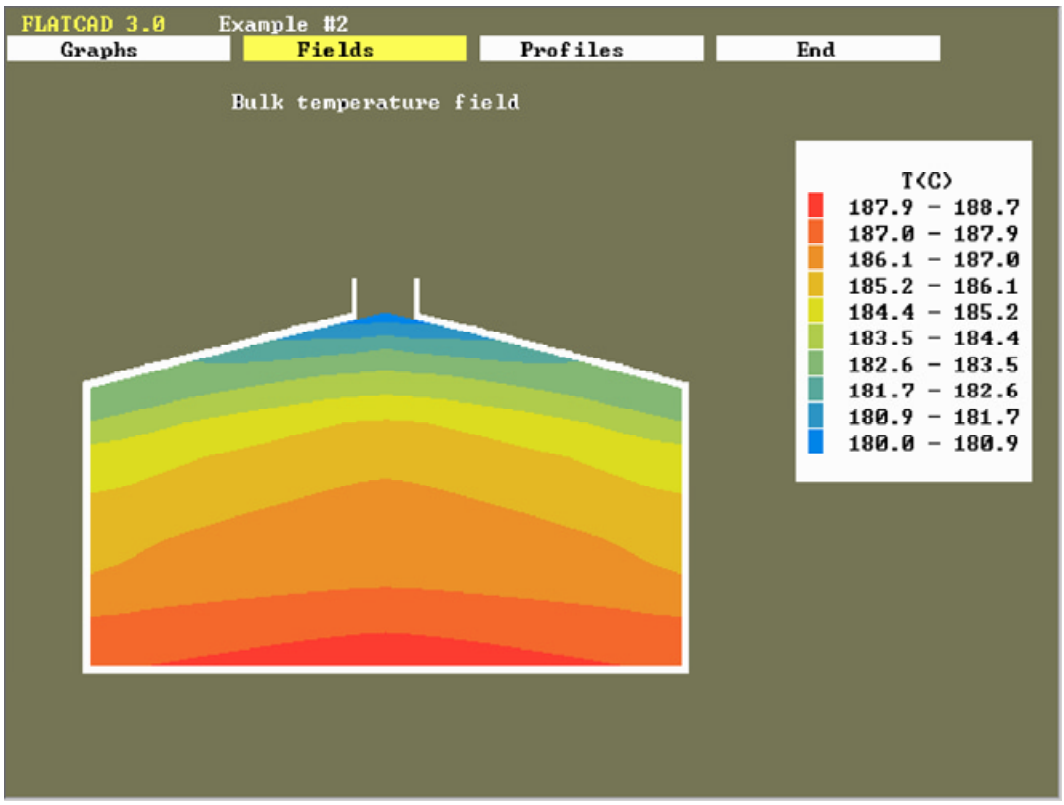

Figure B.24 — Computed bulk temperature distribution in the coat hanger die

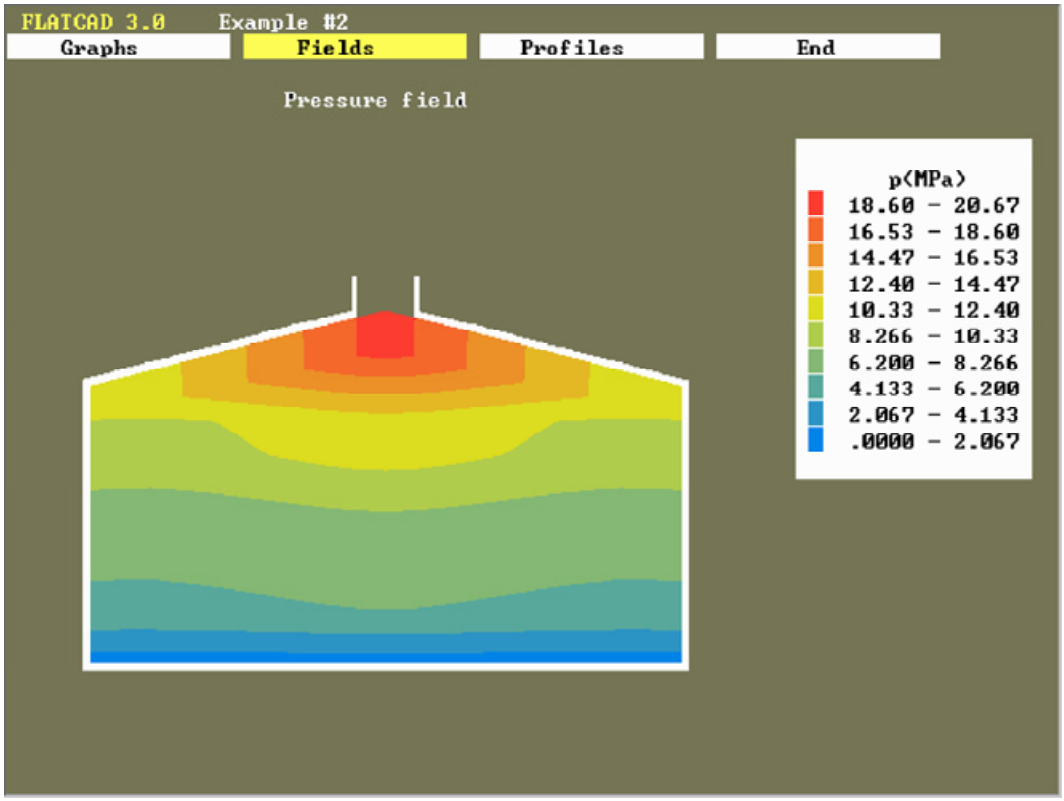

Figure B.25 — Computed pressure distribution in the coat hanger die

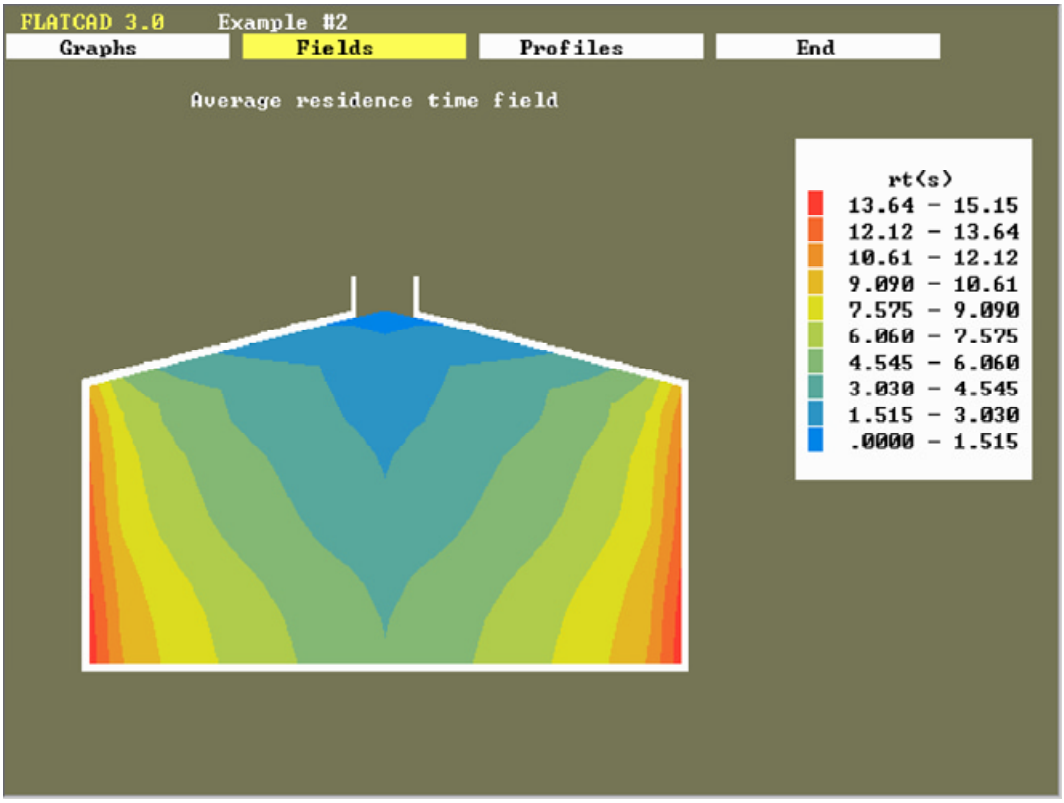

Figure B.26 — Computed average residence time distribution in the coat hanger die

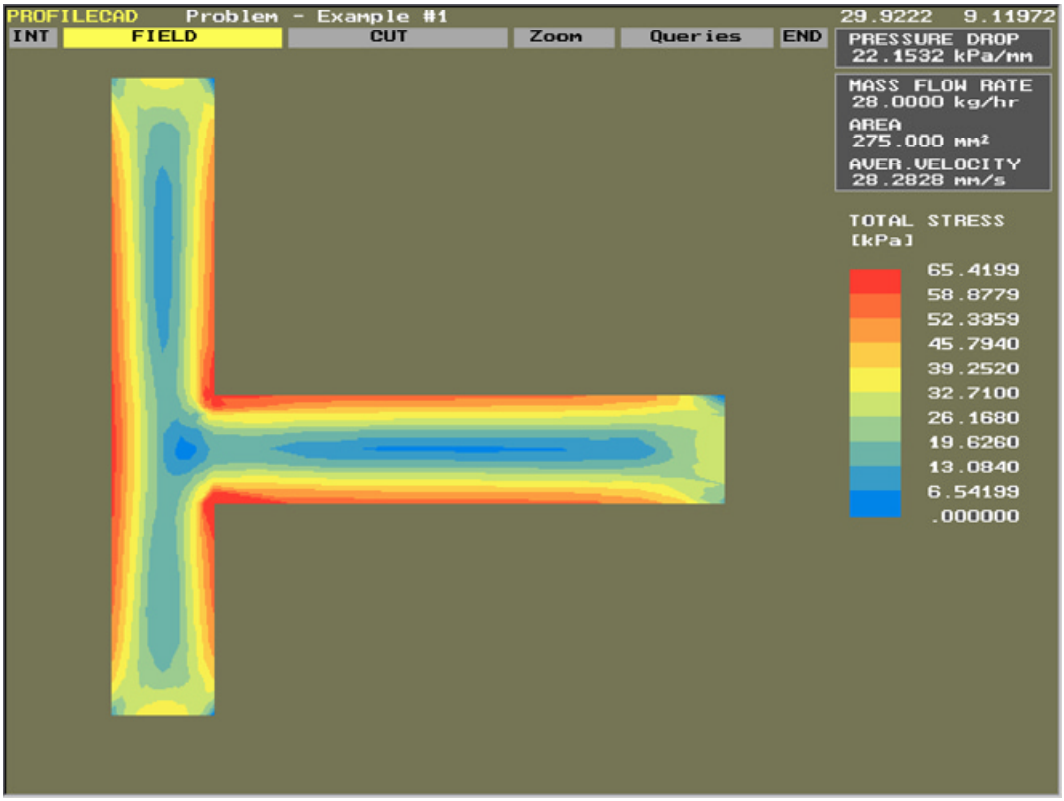

Figure B.27 — Computed total stress distribution in the profile die

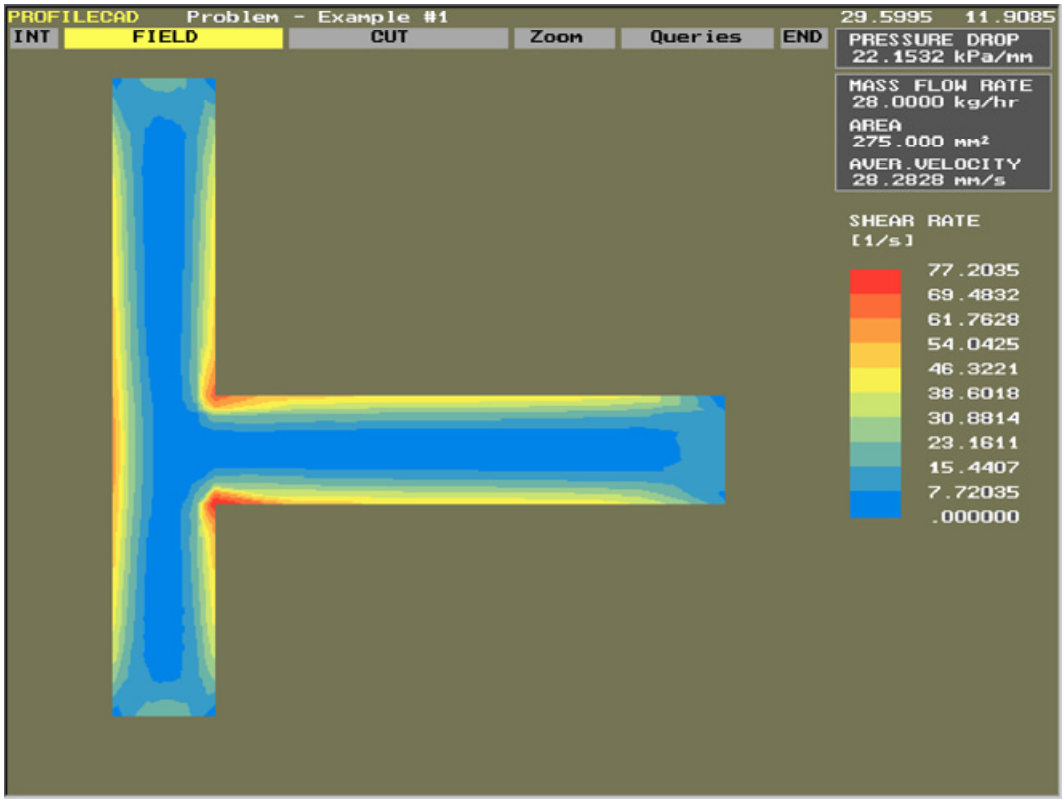

Figure B.28 — Computed shear rate distribution in the profile die

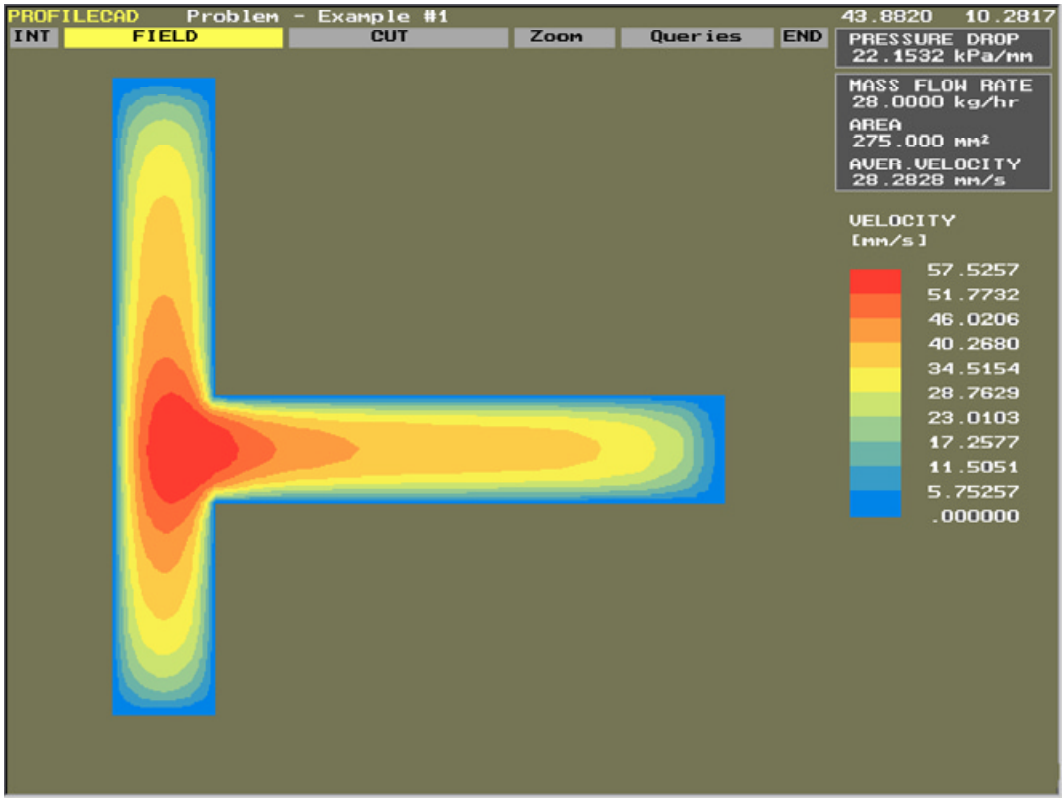

Figure B.29 — Computed velocity distribution in the profile die

ICS 83.080.01

Price based on 76 pages